Design and Analysis of

Mechanically Laminated Timber Beams

Using Shear Keys

By

Joseph F. Miller

A Dissertation

Submitted in partial fulfillment

of the requirements for the degree of

Doctor of Philosophy

in Civil Engineering

Michigan Technological University
2009

This dissertation, “Design and Analysis of Mechanically Laminated Timber Beams using Shear Keys,” is hereby approved in partial fulfillment of the requirements for the degree of Doctor of Philosophy in the field of Civil Engineering.

Department of Civil and Environmental Engineering

Signatures:

Dissertation Adviser _____

Dr. William Bulleit, PE

Department Chair _____

Dr. William Bulleit, PE

Date _____

Acknowledgements

My appreciation goes to Trillium Dell Timberworks (Knoxville, IL) for supplying the white oak key stock, and to Coldwater Veneer (Coldwater, MI) for supplying the clear yellow poplar timbers for the physical testing component of the research. I'd also like to thank Fastenmaser/OMG and Wurth Construction Specialty Supply for supplying the screws.

I'd like to thank my advisers for their help and support; in particular Dr. Bulleit, who, despite my jejune and somewhat contumelious attempts, ensured some pellucidity in my writing. Dr. Brungraber was also a guiding force throughout this process, providing invaluable and practical insights. I am moreover indebted to my wife for her patient support throughout this endeavor. *Prost*.

Abstract

Small timber layers can be mechanically laminated into a larger timber cross-section using shear keys to prevent slip between the layers. These mechanically laminated beams are commonly referred to as keyed beams, and their use has a strong historical precedence. Current building codes and design standards do not provide adequate guidelines for the analysis and design of keyed beams.

This project examined the applicability of an interlayer slip model to predict the partially composite behavior of the keyed beams. Solutions to the interlayer slip model for common loading configurations were developed, as were stiffness parameters for the semi-rigid wooden shear keys used to provide composite action.

Small scale testing was conducted on the wooden shear key components to verify the stiffness parameters. Full-scale testing of yellow poplar keyed beams using white oak and Parallam PSL shear keys was also performed to verify the interlayer slip model's ability to predict the strength and stiffness of specific specimens. A comparison to historical keyed beam test data was also conducted.

The interlayer stiffness model, as well as the analytical shear key stiffness parameters, was able to accurately predict both the behavior for the full-scale keyed beams tested specifically for this research as well as the historic keyed beam behavior. Shear key configuration, moisture content, and clamping connector stiffness all played significant roles in the actual keyed beam stiffness.

Table of Contents

1 Introduction 1
1.1 Background Information 1
1.2 Research Objectives 2
1.3 Literature Review 3
1.3.1 Historical Literature 3
1.3.2 Theoretical & Modern Literature 10
1.3.3 Design Literature 11
2 Theoretical Model 13
2.1 Partial Interlayer Slip Model Derivation 14
2.1.1 Beam Solution for n-Layers 15
2.1.2 Beam Solution for Two Layers 19
2.1.3 Beam Solution for Three Layers 20
2.2 Solutions for the Two Layer Model with Uniform Loading 22
2.2.1 Axial Force in Each Layer 22
2.2.2 Bounds on Uniformly Distributed Load Solution 23
2.3 Other Loading Conditions 25
2.3.1 Numerical Integration 25
2.3.2 Linear-Elasticity and Superpositioning 25
2.4 Stress Distribution 28
2.5 Shear Keys 30
2.5.1 Shear Key Stiffness 32
2.5.2 Shear Key Stiffness Coefficients 36
2.6 Beam Efficiency 39
3 Physical Testing Overview 42
3.1 Timber and Key Species 42
3.1.1 Timber Species Selection 42
3.1.2 Shear Key Species Selection 43
3.2 Key Configuration 45
3.2.1 Key Orientation 45
3.2.2 Grain Direction 46
3.2.3 Key Size 49
3.2.4 Wedge Slope 50
3.3 Clamping Connectors 51
3.3.1 Connector Type 51
3.3.2 Connector Placement 53
3.3.3 Connector Quantity 53
3.4 Beam Size 54
3.5 Loading Configuration 55
3.6 Key Layout in Keyed Beam 57
4 Small Scale Testing 60
4.1 Testing Apparatus 60
4.2 Modulus of Elasticity and Modulus of Rupture 61
4.2.1 Static Bending Test Procedure 61

4.2.2 Static Bending Test Results ... *62*
4.2.3 Adjustment of Modulus of Elasticity for Shear Deformation ... *64*
4.3 Screw Axial Stiffness and Withdrawal Capacity ... 65
4.3.1 Screw Withdrawal Test Procedure ... *66*
4.3.2 Screw Withdrawal Test Results ... *67*
4.4 Shear Key Stiffness ... 70
4.4.1 White Oak Shear Key Test Results ... *74*
4.4.2 Parallam PSL Shear Key Test Results ... *77*
4.4.3 Shear Key Test Comparison to Stiffness Model ... *81*
4.5 Screw Shear (Lateral) Stiffness ... 82
4.5.1 Screw Shear Test Procedure ... *83*
4.5.2 Screw Shear Specimen Test Results ... *83*
4.6 Moisture Content and Specific Gravity ... 86
4.6.1 Adjustments in Modulus of Elasticity Based on Moisture Content ... *86*
4.6.2 Adjustments in Modulus of Elasticity Based on Specific Gravity ... *87*
5 Full Scale Beam Testing ... 90
5.1 Beam Fabrication ... 90
5.2 Testing Apparatus ... 92
5.3 Test Results ... 94
5.3.1 Full and Stacked Beams ... *94*
5.3.2 Keyed Beams with White Oak Shear Keys ... *97*
5.3.3 Keyed Beams with Parallam PSL Shear Keys ... *101*
5.4 Adjustments to Test Results ... 103
5.4.1 Moisture Content and Specific Gravity ... *104*
5.4.2 Variations in Cross Section ... *106*
5.4.3 Test Frame Compliance ... *106*
6 Analysis of the Interlayer Slip Model using Full Scale Test Data ... 108
6.1 Comparison of Test Data ... 108
6.1.1 Interlayer Slip Model Input Parameters ... *108*
6.1.2 Analysis Results ... *112*
6.2 Shear Key Spacing Methodology ... 114
6.2.1 Simplified Approach ... *115*
6.2.2 Shear Stud / Composite Beam Approach ... *115*
6.2.3 Tributary Length Approach ... *117*
6.2.4 Recommended Spacing Calculation ... *118*
6.3 Material Parameter Sensitivity ... 119
6.3.1 Modulus of Elasticity of Timbers ... *120*
6.3.2 Cross-grain Modulus of Elasticity ... *121*
6.3.3 Clamping Connectors ... *123*
6.3.4 Key Size ... *125*
6.4 Comparison to Kidwell's Test Data ... 126
6.4.1 Determining Material Properties ... *127*
6.4.2 Brunel's Beam ... *129*
6.4.3 Joggled Beam ... *131*
6.4.4 Three Layer Beam ... *135*

6.4.5 Discussion of Results *138*
7 Ultimate Stress **139**
7.1 Predication of Failure Load 139
7.2 Comparison to Full Scale Testing 140
7.3 Comparison to Kidwell's Historical Testing 142
7.4 Discussion of Results 143
8 Design Procedure **145**
8.1 Shear Key and Clamping Connector Design 145
8.1.1 Shear Key and Timber Compressive Strength *146*
8.1.2 Shear Key Spacing *147*
8.1.3 Clamping Strength Requirements *150*
8.2 Full Design Procedure 151
8.2.1 Beam Bending Stress *151*
8.2.2 Beam Stiffness *153*
8.3 Simplified Design Procedure 153
9 Conclusions **156**
9.1 Summary 156
9.2 Qualified Recommendations 157
9.3 Future Research 160
10 References **164**
Appendix A – Solution for Two-Layer Beam with a Uniformly Distributed Load **169**
Appendix B – Solution for Two-Layer Beam with Point Load at any Point **170**
Appendix C – Solution for Two-Layer Beam with Symmetrically Placed Point Loads **176**
Appendix D – Calculations for Quantity of Clamping Connectors **182**
Appendix E – Longitudinal Modulus of Elasticity and Shear Modulus in Bending Tests **184**
E.1 Determination from Testing 184
E.2 Comparison of Full Depth and Simple Stacked Beam Deflection 186
Appendix F – Adjustment of Shear Keys Test Stiffness **188**
Appendix G – Calculation of Slip in a Simple Stacked Beam **189**
Appendix H – Interlayer Slip Calculations for Full-Scale Test Data **191**
H.1 Analysis of Test Data from this Research 191
H.2 Analysis of Test Data from Prior Research 195
Appendix I – Stress Calculations **200**

Table of Tables

Table 4-1 Static bending test results 63
Table 4-2 Screw withdrawal test results 68
Table 4-3 Results from white oak shear key tests 75
Table 4-4 Results from Parallam PSL shear key tests 78
Table 4-5 Key stiffnesses from physical tests as well as the theoretical model 81
Table 4-6 Results from screw shear tests 84
Table 5-1 Full-scale beam test results 96
Table 5-2 Adjusted stiffness values for full-scale beam tests 105
Table 5-3 Differences in stiffness from test frame compliance 107
Table 6-1 Physical data on keyed beam tests for use with the interlayer slip model 109
Table 6-2 Comparison of analytical and full-scale testing stiffnesses 112
Table 6-3 Comparison of various methods for determining shear key spacing 117
Table 6-4 Variations in stiffness with changes in timber modulus of elasticity 121
Table 6-5 Comparison of Brunel's beam stiffnesses to the interlayer slip model 130
Table 6-6 Comparison of joggled beam stiffnesses to interlayer slip model 133
Table 6-7 Comparison of joggled beam stiffnesses to interlayer slip model 135
Table 6-8 Comparison of three-layer beam stiffness to interlayer slip model 137
Table 7-1 Stress at maximum load for full-scale beam tests 140
Table 7-2 Stress at maximum load for Kidwell's beam tests 143

List of Figures

Figure 1-1 Two-layer keyed beam using wood shear keys to generate composite action.. 2
Figure 1-2 "Why wood bends, breaks, and stays stiff, and how to make it stiff." (Leupold, 1726). 4
Figure 1-3 - Tredgold's beams: (a) Keyed beam, (b) Joggled beam with cast iron wedge (Tredgold, 1820) 6
Figure 1-4 - Mahan's and Rankine's proposed beams, respectively (Mahan, 1886; Rankine, 1889) 7
Figure 1-5 - Derevyagin's beam which includes prestressing before installation of the shear keys (Karlsen, 1967). 9
Figure 2-1 Solid beam unloaded and subjected to positive bending moment 13
Figure 2-2 Simple stacked beam unloaded and subjected to positive bending moment .. 14
Figure 2-3 Section through an n-layer beam 16
Figure 2-4 Stress diagram for an n-layer beam 16
Figure 2-5 Superpositioning of pointloads 27
Figure 2-6 Normal stress diagrams for an arbitrary full depth (dashed line) and built up (solid line) beam 30
Figure 2-7 Side view of (a) square and (b) inclined shear keys along with (c) a top view showing the wedge shape of the shear keys 32
Figure 2-8 Inclined shear key 33
Figure 2-9 Deformed inclined key 33
Figure 2-10 Springs-in-series model of the shear key 34
Figure 2-11 Displacement components of a shear key 35
Figure 2-12 Shear flow in partially composite beams subjected to (a) two concentrated loads and (b) a uniformly distributed load. 40
Figure 3-1 2.5 inch thick shear key wedge dimensions 48
Figure 3-2 Solid sawn parallel-to-the-grain wedges are prone to splitting during installation 48
Figure 3-3 (a) Long and (b) short shear key configurations 50
Figure 3-4 Forces acting on a pair of wedges 51
Figure 3-5 Double threaded log screw 53
Figure 3-6 Key placement and screw location on keyed beams used in the full-scale testing 53
Figure 3-7 Loading configuration for full scale beam testing 56
Figure 3-8 Assumed shear stress distribution at shear key notch 58
Figure 4-1 Setup for static bending tests 62
Figure 4-2 Static bending test compression failure followed by a simple-tension failure 63
Figure 4-3 Load-displacement plots for static bending tests 64
Figure 4-4 Screw push-through (e.g. withdrawal) testing 67
Figure 4-5 Load-displacement plots for screw withdrawal tests 69
Figure 4-6 Screw withdrawal testing showing (a) entry of screw, (b) exit of screw, and (c) section through screw hole after screw had been removed. 70
Figure 4-7 8in long shear key test configuration 73
Figure 4-8 5in long shear key test configuration 74

Figure 4-9 Load-slip plots for white oak shear key tests 75
Figure 4-10 Load-spread plots of white oak shear key tests 77
Figure 4-11 Load-slip plots for Parallam PSL shear key tests 78
Figure 4-12 (a) 8 inch white oak key compressed uniformly, (b) 5 inch white oak key with uneven compression due to rolling, (c) compression of the timber end-grain when using Parallam PSL keys, (d) uniform spreading of side member and (e) uneven spreading with rolling of side member for Parallam PSL key tests. 80
Figure 4-13 Load-slip plots for screw shear specimen tests 84
Figure 4-14 Yielding of screw subjected to shear (lateral) loading 85
Figure 4-15 Localized crushing of wood fibers from screw subjected to shear (lateral) loading 85
Figure 4-16 Comparison of Wood Handbook MOE equations to test data (typical) 88
Figure 5-1 (a) Paired and notched timbers with checks on the horizontal faces and (b) clamping apparatus used when installing the screws 92
Figure 5-2 Full scale beam test configuration 93
Figure 5-3 Ring-shake and checking in the full depth beam 95
Figure 5-4 Load-deflection plots of full-scale beam tests 96
Figure 5-5 Keyed beam using white oak shear keys under load 98
Figure 5-6 Load-slip plots for white oak shear key tests 99
Figure 5-7 Cracked keyed beam using white oak shear keys 100
Figure 5-8 Crack propagating from re-entrant notch corner 100
Figure 5-9 Parallam PSL-keyed beam under load 103
Figure 6-1 Comparison of load-deflection plots and interlayer slip model solutions 113
Figure 6-2 Assumed shear key spacing using a composite beam approach 116
Figure 6-3 Assumed shear key spacing using tributary length approach 118
Figure 6-4 Relationship between elastic ratio and calculated beam stiffness for each beam test 122
Figure 6-5 Difference between test and model stiffness with varying elastic ratios 123
Figure 6-6 Relationship between the number of clamping screws and modeled beam stiffness 124
Figure 6-7 Relationship between key length and model stiffness 125
Figure 6-8 Key configuration in Brunel's beams (Kidwell, 1898) 129
Figure 6-9 Load-deflection plots for Brunel's beams (Kidwell, 1898) 130
Figure 6-10 Key configuration for joggled beam using white oak keys (Kidwell, 1898) 131
Figure 6-11 Key configuration for joggled beam using cast iron keys (Kidwell, 1898) 132
Figure 6-12 Load-deflection plots for joggled beams using white oak keys 133
Figure 6-13 Load-deflection plots for joggled beams using cast iron keys 134
Figure 6-14 Key configuration for three-layer beam using white oak keys (Kidwell, 1898) 136
Figure 6-15 Load-deflection plots for three-layer beam using white oak keys 137
Figure 8-1 Shear key spacing for a beam with (a) two concentrated point loads, and (b) a uniformly distributed load 149
Figure 8-2 Clamping connector geometry 151

1 Introduction

1.1 Background Information

There is a long standing historical precedent to build structures from large timbers. The use of timbers is due in part to wood's structural characteristics, workability, natural aesthetical appeal, as well as being a renewable resource. With the advent of balloon framing, reinforced concrete, and structural steel, along with new structural requirements, there was a logical progression away from building with heavy timber (Goldstein, 1999). However, none of the reasons that originally made building with timber popular have diminished. As the emphasis increases for use of renewable resources and materials with a natural aesthetic, timber again is increasing in popularity (Benson, 1999).

With this rebound in popularity, adapting the historical methods of using timber to meet more modern building requirements is essential to ensure its long term viability. Unlike more traditional buildings, modern timber structures are expected meet stringent building codes, which can result in longer spans, tighter deflection controls, and heavier loads. Likewise, excessive pressure on a renewable resource can hinder the industry, thus better stewardship of the materials at hand is key.

For long or heavily loaded spans using solid sawn timber, high grade and large cross sections are required to adequately carry the load. Due to a limited number of large trees for harvesting, the price, and availability, if available at all, of the required timber size can be quite prohibitive. The use of glue-laminated timbers (glulams), where small dimensional lumber is glued together to create a high grade composite cross section,

addresses these availability concerns. However, glulams do not have strong aesthetic appeal to most heavy timber enthusiasts, and others have concerns about the adhesives used in fabrication.

An alternative to the large solid sawn timber cross sections and glulams is to use mechanically laminated timbers. A common example, and one that is the focus of this research, is often referred to as a "keyed beam" because of the shear keys between layers. Timbers of smaller cross section (which come from smaller, more readily available trees) are used to generate a composite cross section. The interaction between timbers is generated using a series of shear keys. One method is to use wooden wedges for the shear keys, which are typically left exposed on the sides and help provide a visual appeal that many find attractive. Figure 1-1 shows a keyed beam with a common configuration of wooden shear keys. Currently there are no design procedures to directly address the analysis and design of these beams.

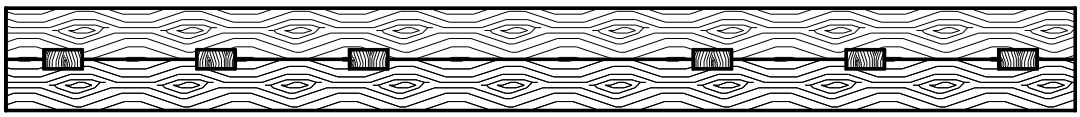

Figure 1-1 Two-layer keyed beam using wood shear keys to generate composite action

1.2 Research Objectives

The goal of this study is to develop an accurate behavioral model for mechanically laminated timber beams that provide partial interaction through the use of wood shear keys. The behavioral model will be compared against physical testing to verify its performance.

The objectives of this research are broken into four separate stages. These stages include:

1. Developing a n-ply solution to the classical interlayer slip model, coupled with specific solutions for common loading configurations for the two-layer solution.
2. Formulating stiffness models for inclusion into the interlayer slip model that accurately represent common wooden shear key configurations.
3. Determining experimentally the strength and stiffness of full sized keyed beams as well as individual key and screw components.
4. Developing a procedure than can be readily implemented by practicing engineers for the design and analysis of keyed beams.

1.3 Literature Review

The concept of mechanically joining timbers for the purpose of generating a larger composite bending section is not new. Limited availability of large timber in Europe before the invention of reliable adhesives necessitated their use.

1.3.1 Historical Literature

The earliest documentation that was found during this research, suggesting the use of shear keys to increase the depth of beams, was an article by Jacob Leupold, published in Leipzig, Germany (Leupold, 1726). The author's main focus was on bridge construction and he suggested the use of keyed beams as bridge girders as shown in Figure 1-2.

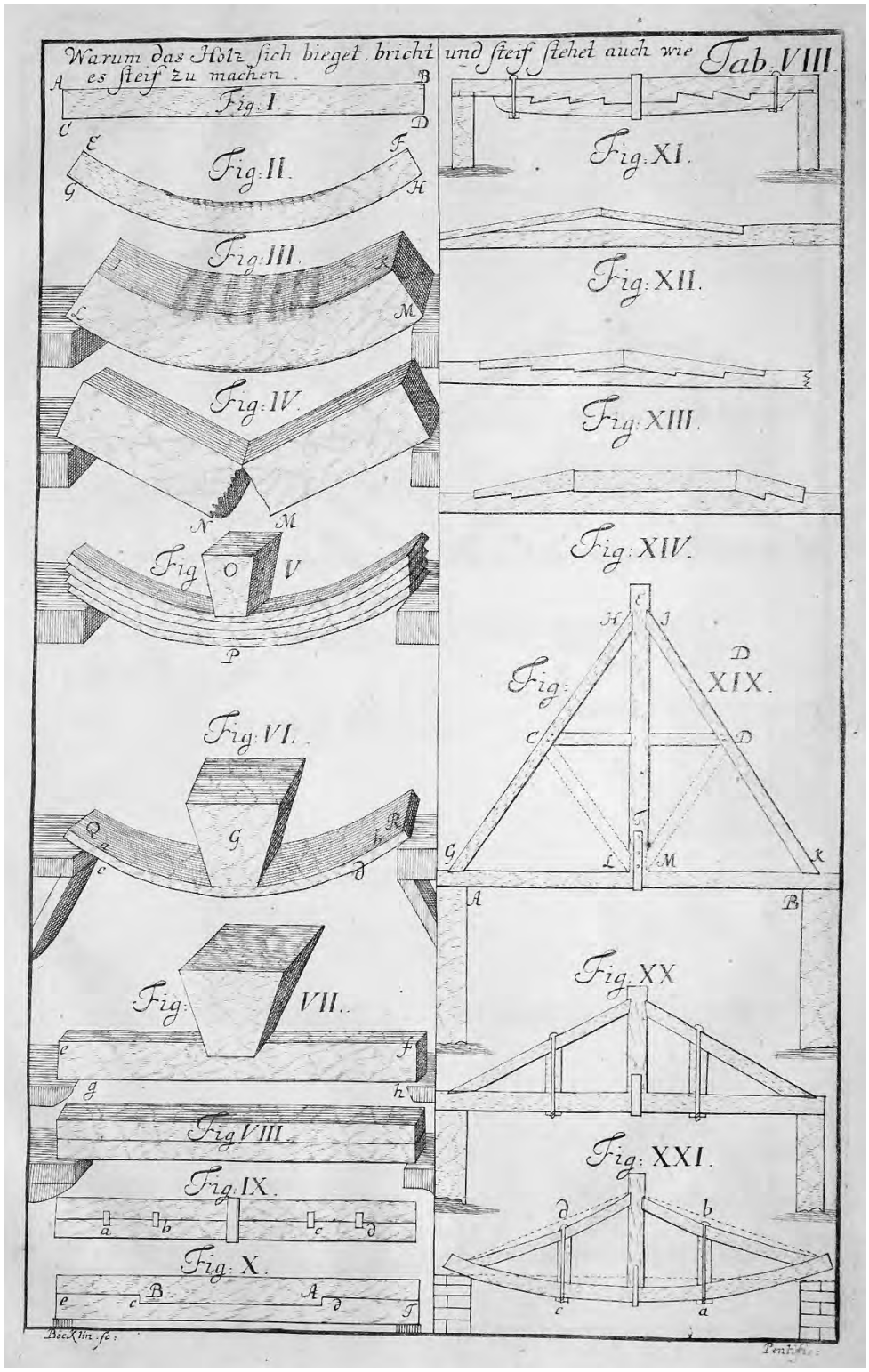

Figure 1-2 "Why wood bends, breaks, and stays stiff, and how to make it stiff." (Leupold, 1726).

The first notable technical documentation, at least in English, was published in England in 1820 by Thomas Tredgold, an outspoken civil engineer (Tredgold, 1820). He suggested the use of solid shear keys to limit interlayer slip. He also recommended tapering the upper beam, such that the ends of the beams where slightly shallower than the middle, so solid metal bands could be driven onto the ends to provide the clamping force, much in the same way metal bands are driven onto wooden barrels. Tredgold also indicated a strong preference for a joggled beam (mated saw tooth type indentations between layers) using a cast iron wedge to ensure tight bearing faces. These beams are shown in Figure 1-3. Of note are the incredible difficulties in fabricating Tredgold's beams. Procuring exact dimension metal straps to ensure proper clamping was also problematic. Also, the taper makes supporting a floor or flat roof difficult. Likewise, the fabrication tolerances required to make an appropriate joggled beam are extremely labor intensive, and the net depth of the members is reduced. Use of the cast iron wedge to ensure tight fitting faces was novel, but this will induce tensile stresses in the bottom member, which also has a hole drilled through it at the point of maximum stress. Once bending stress is applied, it will further increase the tensile stress in the bottom member, ensuring that the allowable capacity of this beam will be considerably lower than a fully composite beam.

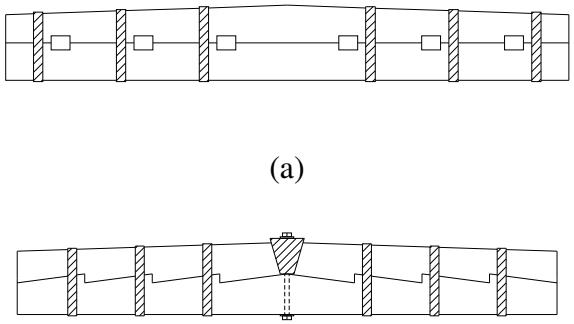

Figure 1-3 - Tredgold's beams: (a) Keyed beam, (b) Joggled beam with cast iron wedge (Tredgold, 1820)

Many other publications during the 19th century included similar descriptions or verbatim copies of built-up beams as those proposed by Tredgold (e.g., Trautwine, 1862). Other authors, such as Mahan (1886) and Rankine (1889), offered additional theoretical improvements to Tredgold's previously proposed beam. Mahan's addition was to use multiple layers of beams joggled together. He stated that to his knowledge no one had ever tried such a beam, and due to constructability concerns, no effort has probably ever been made since. Rankine suggested using through bolts, either square through the timbers, or preferably at an incline to provide the clamping force, rather than fitted metal bands. Mahan and Rankine's suggestions are shown in Figure 1-4.

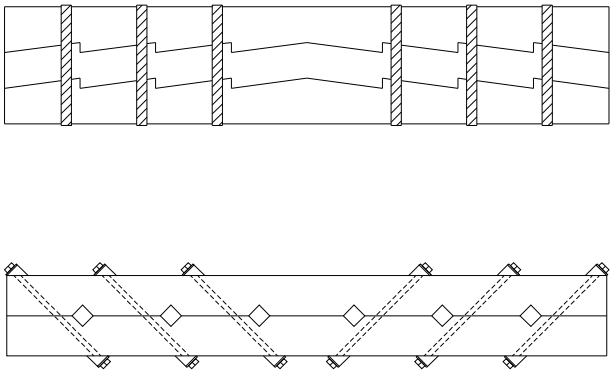

Figure 1-4 - Mahan's and Rankine's proposed beams, respectively (Mahan, 1886; Rankine, 1889)

During the mid 19th century, with the industrialization of the world, and in particular the development of vast systems of railroads, great demands were placed on regional and national timber supplies. These demands were caused not only by the inherent need for timber in the railroad industry for things such as railroad ties and bridge girders, but also for the development of industrial buildings and residential structures. Many railroads developed their own method for joining beams into deeper cross sections, typically with the use of cast iron and steel sections, for use as bridge girders. Of particular merit is an article by Snow (1895), of the Boston and Main Railroad, on the use of steel keys for built-up girders. His discussion includes guidance on required clamping forces as well as suggestions for spacing according to the "intensity of shearing strain." He also advocates using the full depth of the combined beam for determining stresses (full composite action).

Railroad bridge construction was not limited to the United States, however. Many railroad bridges were built throughout continental Europe, in particular Germany and Austria, that used *zusammengesetzte Balkenträger* (composite girders) along with *verdübelten Trägern* (keyed beams). A text by a Finnish professor, Michael Strukel,

documents many types of railroad bridges, some of which used keyed beams (Strukel, 1900).

Academic research was conducted by Prof. Dr. Forchheimer in Aachen, Germany on the use of keyed and built-up beams (Forchheimer, 1892). He investigated several types of keyed and built-up beams, and provided some guidance on the proper size and orientation of the keys. Forchheimer observed that the rotation of the keys, either caused by improper key sizing or insufficient clamping action, greatly reduced the capacity of the beam. He also noted that the grain orientation of the keys plays a significant role in the efficiency of the beam.

But, perhaps Edgar Kidwell, a professor at the Michigan College of Mines, has the most complete and academically rigorous review of keyed beams (Kidwell, 1898). The declining availability of locally available timber coupled with an increasing demand for timber use in mining was the catalyst for Kidwell's testing of full sized specimens with various wooden key configurations, as well as beams using iron and steel keys.

Kidwell (1898) concluded that indeed most of the published contemporary information available on keyed beams was of little practical merit. He also concluded: (1) cast iron keys will result in greater stiffness than wooden keys; (2) loosening of clamping bolts from timber shrinkage has a substantial impact on stiffness; (3) inclined keys are less desirable than square keys; and (4) keyed beams can achieve approximately 90% of the capacity of the a full depth, solid beam.

Shortly after Kidwell's research, steel and concrete became popular as structural materials, and little else was published on the topic for 70 years. What little was published included little new information (Warren, 1910). Others just repeated the

conclusions of those before them in a concise and easy to follow format, but without offering any new insights (Durm and Esselborn, 1908; Jacoby, 1909).

In 1967, Karlsen published an inclusive text on timber engineering, translated from Russian, that included several sections on keyed beams. Karlsen provides design recommendations for shear key sizes, correction factors for the beam stiffness, and a strong preference for inclined keys. Karlsen also makes a reference to Derevyagin's beams, which are keyed beams precambered and connected with wooden plates, rather than shear keys. The fabrication of this beam can be seen in Figure 1-5. Unfortunately no additional information about the Derevyagin's beam was provided for further investigation.

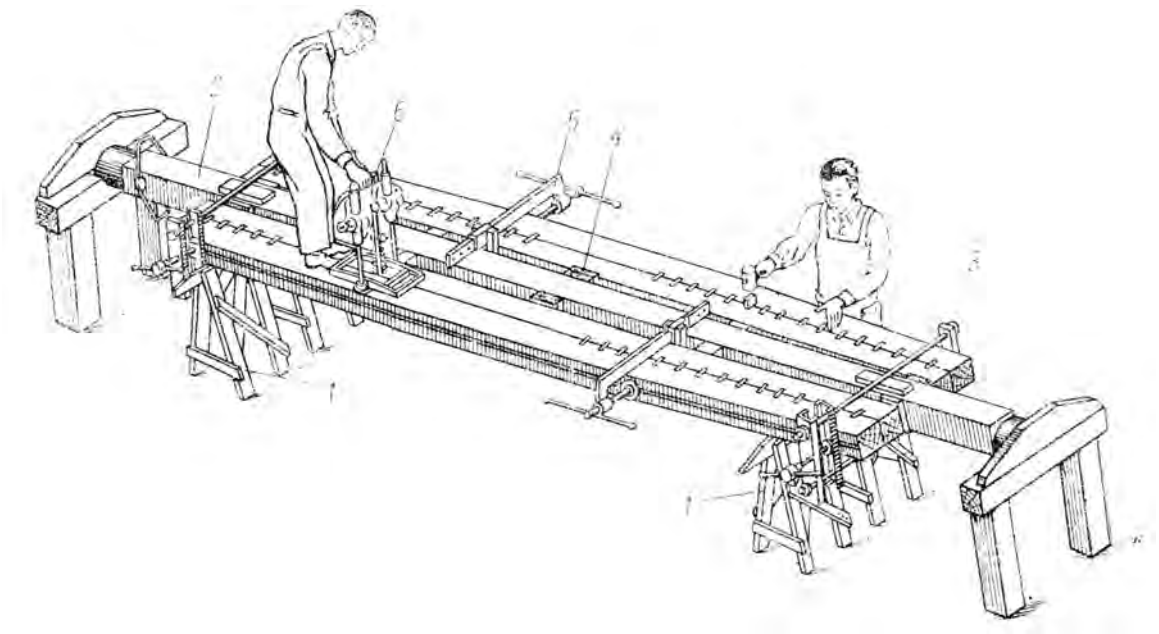

Figure 1-5 - Derevyagin's beam which includes prestressing before installation of the shear keys (Karlsen, 1967).

1.3.2 Theoretical & Modern Literature

From a theoretical standpoint, Newmark, Seiss, and Viest (1951), commonly referred to as Newmark's approach, developed a relationship for stacked beams that have partial interaction between the layers. While their development was intended for steel/concrete T-beams, it applies in general to any geometric and material configurations. The linear-elastic theory allows for some slip between the two layers by solving a series of differential equations relating the rate of change of slip and strains in the two layers. Since the rate of slip and strains are load dependent, solving the system of equations requires a separate solution for each loading condition. Coincidentally, at the same time as their development (Newmark et al., 1951), others in Russia (Pleshkov, 1952) and Sweden (Granholm, 1949) independently developed similar approaches. Only abstracts of these two sources could be found translated into English, so the full body of their work has not been reviewed.

Goodman (1967) expanded on Newmark's development for nail laminated dimensional lumber with two and three plies. A comparison between the approaches of Newmark (1951), Pleshkov (1952), and Granholm (1949) was also made. Goodman went on to expand his research and co-authored additional papers verifying his mathematical model (e.g. Goodman & Popov, 1968).

Additional authors have expanded on Newmark and Goodman for various specific problems. Wheat and Calixto (1994) investigated the effect of non-linear connectors at the interface using energy methods. Shear deformation was addressed by Schnabl et al. (2007), who showed that it has substantial influence on the vertical deflection of partially-composite beams. Not surprisingly, shear deformation had a higher contribution

to the overall deflection as composite action approached that of a full depth beam, as well as with beams having small span to depth ratios.

In order to facilitate computer modeling of beams with interlayer slip, research has also been conducted on developing finite element models that exactly match the model developed by Newmark et al. (1951) (Faetlla et al., 2002). Depending on the stiffness of the shear connectors between layers, the finite element modeling approach did not appear to capture the true curvature of the elements, which requires additional investigation for proper a description (Dall'Asta & Zona, 2004).

Considerable interlayer slip research has been done recently by Ranzi and others at the University of Sydney. This research includes the development of both a six degree-of-freedom beam element as well as an eight degree-of-freedom frame element, using the direct stiffness method, that can take into account partial interaction between layers (Ranzi & Bradford, 2007). Six and eight degree-of-freedom beam and frame elements with time dependent behavior have also been developed (Ranzi & Bradford, 2006). Further, inclusion of transverse partial interaction into a 14 degree-of-freedom frame element is also discussed, which requires a numerically intensive iterative model to converge on a solution (Ranzi, Gara, & Ansourian, 2006).

1.3.3 Design Literature

Despite an abundance of technical research on beams with partial interaction, no explicit method for designing such a beam has been proposed. Karlsen suggests using adjustment factors to modify the moment of inertia. The adjustment factors "can be looked up in appropriate design standards," (Karlsen & Slitskouhov, 1989) but just what

the appropriate design standards were was not made clear. The Eurocode (2004) uses an design approximation based on an effective stiffness "EI" (modulus of elasticity multiplied by the moment of inertia), which is numerically convenient so long as the stiffness of the shear connectors is known. Thelandersson and Larsen (2003) also included a section in their text about the design of composite structures. They briefly discussed the theoretical developments of Newmark et al. (1951), and included an exact solution for a sinusoidal shaped distributed load. A sinusoidal load was used as it simplifies into a compact series of equations, and can be used with a Fourier series to model more complex loading configurations. These compact equations look quite similar to those included in the Eurocode.

Extensive research has also been conducted on material specific relationships, primarily for steel or wood girders with concrete decks acting as T-beams (Wang, 1998) (Frangi & Fontana, 2003). While this research is not directly applicable to keyed timber beams, it does show that the development of a model capturing interlayer slip behavior is possible.

2 Theoretical Model

When a solid beam, of depth d, is loaded to produce positive moment (moment that causes the top side of the beam to go into compression, while the bottom side is in tension), the beam deflects downwards. See Figure 2-1. The top side shortens as the bottom side lengthens. At the centroid (mid-height for a rectangular section), commonly called the neutral axis of a beam, the beam does not change length when subjected to small transverse deflections.

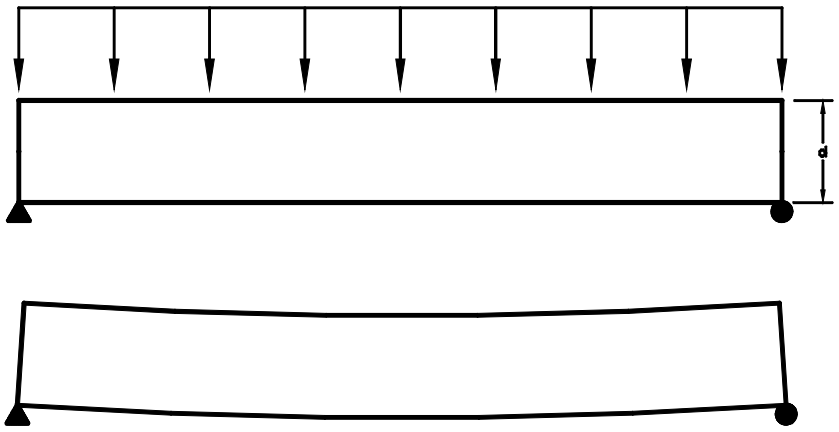

Figure 2-1 Solid beam unloaded and subjected to positive bending moment

When two beams, each of depth d/2, are stacked atop each other without being connected (no interaction between the two beams) and loaded to produce positive moment, each individual beam has both compression and tension components. The shortening of the top face of the bottom member, combined with the lengthening of the bottom face of the top member, results in substantial slippage between these two layers. See Figure 2-2.

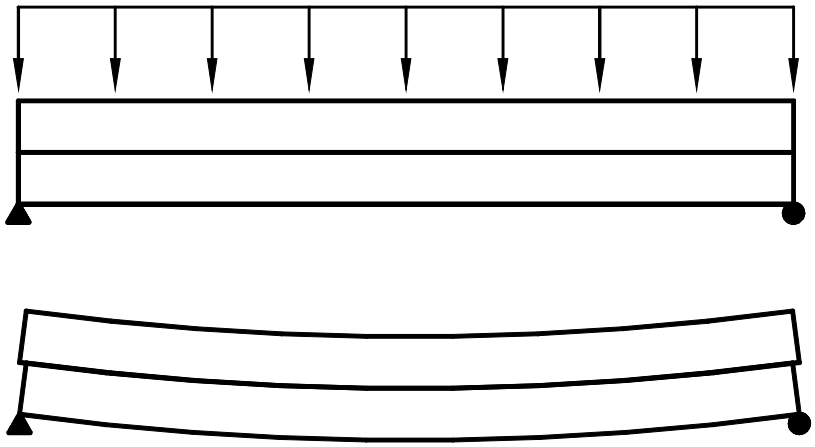

Figure 2-2 Simple stacked beam unloaded and subjected to positive bending moment

With the full depth beam as a lower bound on deflection (no interlayer slip), and the simple stacked beam as an upper bound (full interlayer slip), a mathematical model can be used to determine the partial interlayer slippage, and thus partial interaction.

2.1 Partial Interlayer Slip Model Derivation

The basic equations governing a keyed beam with interlayer slip are based on the following assumptions, which are discussed in more detail later:

- Friction effects between the layers are relatively small and can be ignored.
- Each shear key behaves in a linear fashion and carries load proportional to its stiffness.
- Each layer has the same curvature when under load.
- Faces that are in contact remain in contact.

2.1.1 Beam Solution for n-Layers

Given the section of an n-ply beam shown in Figure 2-3, equilibrium requires

$$\sum_{i=1}^{n} F_i = 0 \tag{2-1}$$

$$M = \sum_{i=1}^{n} M_i + \sum_{i=1}^{n} F_i c_i \tag{2-2}$$

where F_i and M_i are the forces and moments acting on the i th layer of a n -layer beam, while M is the total moment on the beam. A positive F value is tension, with negative values representing compression. The values for $M_1, M_2, \cdots M_n$ are the internal moments that act on a simple stacked beam (with no interaction). These moments remain constant throughout the analysis, with additional moment capacity being accounted for with the axial forces in each layer. The stress diagram for an n-layer beam, which consists of components from both moments M_i and axial forces F_i, is shown in Figure 2-4, where C is compressive stress and T is tensile stress. The c_i term in equation (2-2), which represents the distance from the neutral axis to the center of the i th layer, is calculated as

$$c_i = \frac{1}{2}\sum_{k=1}^{n} h_k - \sum_{k=1}^{i} h_k + \frac{h_i}{2} \tag{2-3}$$

where h_k and h_i are the depth of the k th and i th layer, respectively. Also note, c_i for locations above mid-depth will be negative and $\frac{d}{2} = \frac{1}{2}\sum_{k=1}^{n} h_k$.

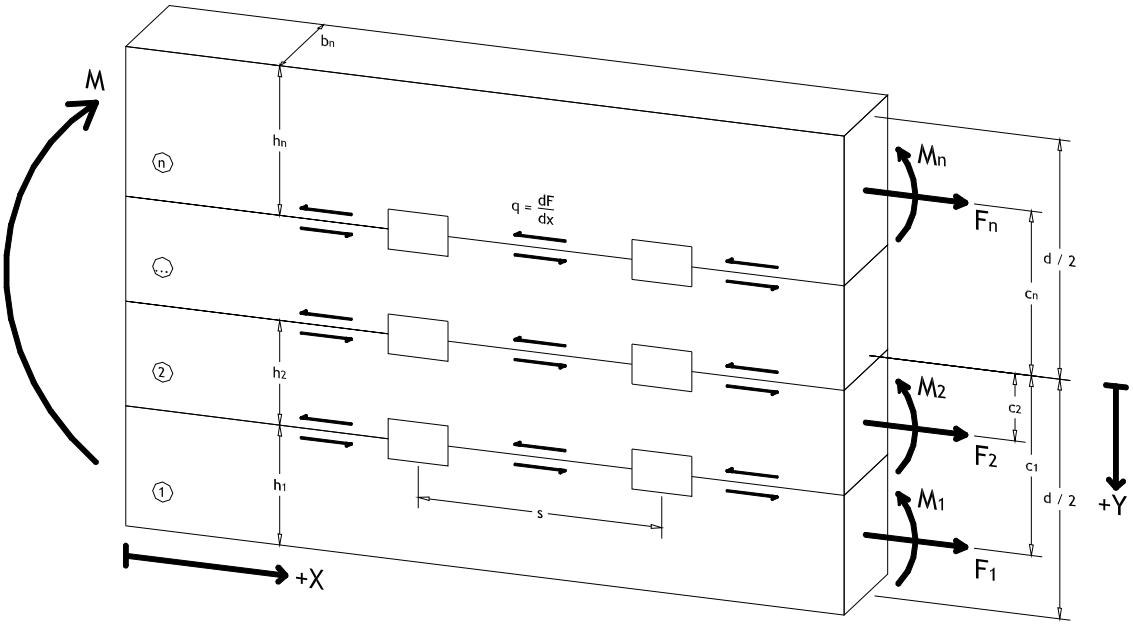

Figure 2-3 Section through an n-layer beam

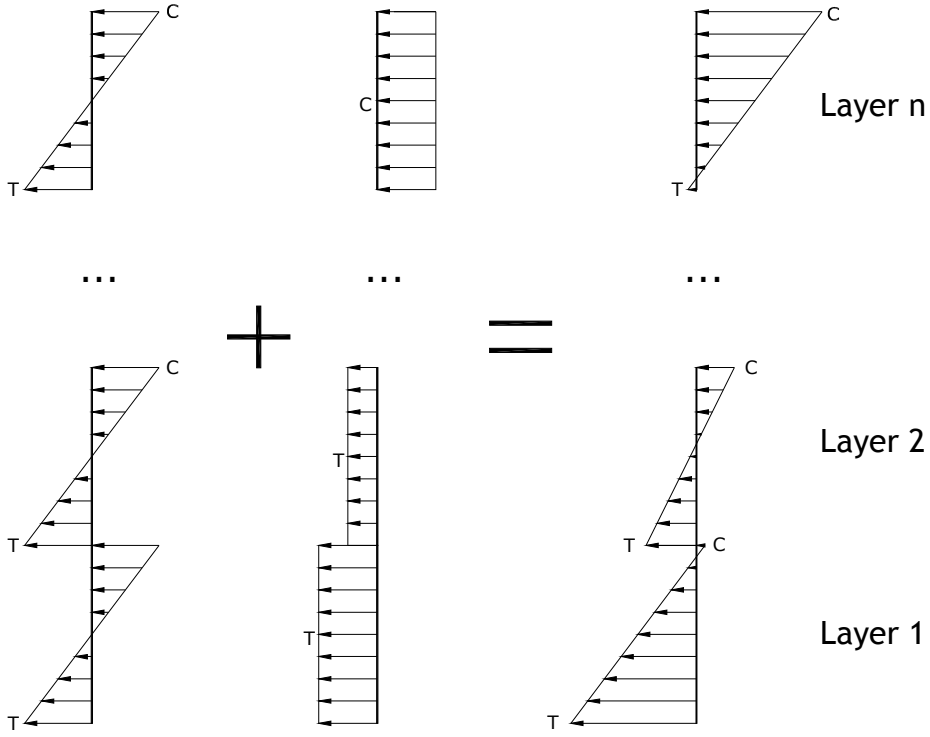

Figure 2-4 Stress diagram for an n-layer beam

Combining Hooke's law and a bending stress relationship

$$\sigma = E\varepsilon \tag{2-4}$$

$$\sigma = \frac{My}{I} \tag{2-5}$$

the bending strain is

$$\varepsilon = \frac{My}{EI} \tag{2-6}$$

and where E is the modulus of elasticity, M is an arbitrary moment, y is the depth from the beam neutral axis to the point of interest, and I is the moment of inertia. Therefore, we can describe the strain in layer i at the interface between layers i and j as

$$\varepsilon_{i,j} = \kappa\left[\frac{M_i c_i}{E_i I_i} - \frac{F_i}{A_i E_i}\right] \tag{2-7}$$

where

$$\begin{array}{lll} \kappa = -1 & & j = i+1 \\ \kappa = +1 & \text{when} & j = i-1 \\ \kappa = 0 & & j \neq i \pm 1 \end{array}$$

for $0 < j \leq n$ and c_i is the distance from the centroid of the ith layer to the interface of interest.

Any change in strain in two layers at an interface is assumed to be due to slip

$$\frac{d\alpha_{i,i+1}}{dx} = \varepsilon_{i+1,i} - \varepsilon_{i,i+1} \tag{2-8}$$

for $i+1 \leq n$. The slip between two layers, $\alpha_{i,i+1}$, can be described by

$$\alpha_{i,i+1} = \frac{1}{\sum_{l=1}^{m} \frac{K_{i,l}}{s_{i,l}}} \frac{dF}{dx} \tag{2-9}$$

$$\frac{d\alpha_{i,i+1}}{dx} = \frac{1}{\sum_{l=1}^{m} \frac{K_{i,l}}{s_{i,l}}} \frac{d^2F}{dx^2} \tag{2-10}$$

where $K_{i,l}$ and $s_{i,l}$ are the stiffness and spacing of the lth connector or shear key on the top side of the ith layer, and m is the total number of shear keys between two layers. Combining the equations (2-7) and (2-10)

$$\frac{1}{\sum_{l=1}^{m} \frac{K_{i,l}}{s_{i,l}}} \frac{d^2F}{dx^2} = -\left[\frac{M_{i+1}c_{i+1}}{E_{i+1}I_{i+1}} - \frac{F_{i+1}}{A_{i+1}E_{i+1}}\right] - \left[\frac{M_i c_i}{E_i I_i} - \frac{F_i}{A_i E_i}\right] \tag{2-11}$$

If we assume all plies have the same curvature, then we can describe the curvature as

$$\frac{M_i}{E_i I_i} = \frac{M_{i+1}}{E_{i+1}I_{i+1}} = \frac{M - \sum_{i=1}^{n} F_i c_i}{\sum_{i=1}^{n} E_i I_i} \tag{2-12}$$

Combining equations (2-11) and (2-12), we obtain

$$\frac{1}{\sum_{l=1}^{m} \frac{K_{i,l}}{s_{i,l}}} \frac{d^2F}{dx^2} = \frac{F_{i+1}}{A_{i+1}E_{i+1}} + \frac{F_i}{A_i E_i} - \left(\frac{M - \sum_{i=1}^{n} F_i c_i}{\sum_{i=1}^{n} E_i I_i}\right)\left(c_i + c_{i+1}\right) \tag{2-13}$$

Given a beam with a specific geometry, a known function for the moment, and proper boundary conditions, we can solve the above system of $n-1$ differential equations for an exact solution for the forces, F_i, in each ply.

Since horizontal shear is the rate of change of the axial forces in a member, the shear flow at the interface between layers at any point along the length can be determined as

$$q = \frac{dF}{dx} \tag{2-14}$$

Likewise, deflections can be determined by recognizing that the curvature of a beam is the second derivative of the vertical deflection

$$\frac{d^2\Delta}{dx^2} = \frac{M - \sum_{i=1}^{n} F_i c_i}{\sum_{i=1}^{n} E_i I_i} \tag{2-15}$$

2.1.2 Beam Solution for Two Layers

Based on the above solution, it is possible to rewrite the governing differential equations for a composite beam consisting of only two layers. This research focuses mainly on beams fabricated from two layers, so this solution is provided for reference. Rewriting equation (2-13)

$$\frac{1}{\sum_{i=1}^{m} \frac{K_i}{s_i}} \frac{d^2F}{dx^2} = F\left(\frac{1}{A_B E_B} + \frac{1}{A_T E_T}\right) - \left(\frac{M - F\left(\frac{h_B}{2} + \frac{h_T}{2}\right)}{E_B I_B + E_T I_T}\right)\left(\frac{h_B}{2} + \frac{h_T}{2}\right) \tag{2-16}$$

where the ith layer is the B (bottom) layer and the $i+1$th layer is the T (top) layer. To meet horizontal equilibrium, the force in the top layer must equal the force in the bottom layer, such that

$$F = F_T = F_B \tag{2-17}$$

By recognizing that E, I, A, h, and $\sum \frac{K}{s}$ are constants for each layer, we can introduce two new constants that are similar in form to those proposed by Newmark, Seiss, and Viest (1951)

$$C_F = \sum_{i=1}^{m} \frac{K_i}{s_i} \left[\left(\frac{1}{A_B E_B} + \frac{1}{A_T E_T} \right) + \frac{\left(\frac{h_B}{2} + \frac{h_T}{2} \right)^2}{E_B I_B + E_T I_T} \right] \tag{2-18}$$

$$C_M = \sum_{i=1}^{m} \frac{K_i}{s_i} \left[\frac{\frac{h_B}{2} + \frac{h_T}{2}}{E_B I_B + E_T I_T} \right] \tag{2-19}$$

Therefore, we can rewrite equation (2-16) in a much simpler form

$$\frac{d^2 F}{dx^2} - C_F F = -C_M M \tag{2-20}$$

Since both F and M are functions of x, equation (2-20) is a standard ordinary differential equation. For a given loading (moment) function, along with material and section properties, a specific solution can be determined for the axial force F in the layers at any point. With the use of equation (2-15), it is also possible to directly solve for the displacement at any point along the length of the beam.

2.1.3 Beam Solution for Three Layers

The following calculations are based on a simplified three-layer beam, such that the modulus of elasticity, E, is identical in all three layers, as well as each layer has the same cross sectional properties (i.e., b and h are identical for each layer). The solution

of the interlayer slip for a three-layer beam with varying material or sectional properties could be found using the procedure discussed below.

With three identical layers in the built-up beam, the middle layer will not experience any cumulative axial force. Also, the forces in the top and bottom layers will be identical. With this in mind, it is possible to write equation (2-13)

as

$$\frac{1}{\sum_{l=1}^{m}\frac{K_{i,l}}{s_{i,l}}}\frac{d^2F}{dx^2}=\frac{F}{AE}-\left(\frac{M-2Fh}{3EI}\right)(h) \tag{2-21}$$

which is the governing differential equation describing the axial force, F at any point along the layer's length. Equation (2-21) can be simplified and rewritten as

$$\frac{d^2F}{dx^2}-C_{F3}F=-C_{M3}M \tag{2-22}$$

where C_{F3} and C_{M3} are constants that are calculated as

$$C_{F3}=\sum_{l=1}^{m}\frac{K_l}{s_l}\left(\frac{1}{AE}+\frac{2h^2}{3EI}\right) \tag{2-23}$$

$$C_{F3}=\sum_{l=1}^{m}\frac{K_l}{s_l}\left(\frac{2h}{3EI}\right) \tag{2-24}$$

Recognizing that both A and I can be written in terms of b and h, these constants simplify to

$$C_{F3}=\sum_{l=1}^{m}\frac{K_l}{s_l}\left(\frac{9}{bhE}\right) \tag{2-25}$$

$$C_{M3}=\sum_{l=1}^{m}\frac{K_l}{s_l}\left(\frac{4}{bh^2E}\right) \tag{2-26}$$

The deflection at any point along the beam can be found by using equation (2-15), which reduces to

$$\frac{d^2\Delta}{dx^2} = \frac{M - 2Fh}{3EI} \tag{2-27}$$

for a built-up beam consisting of three identical layers.

The solution of the differential equation for a three-layer beam, shown in equation (2-22), with a specific loading configuration (point loads at any point, symmetrically placed point loads, or a uniformly distributed load), will be identical to those developed for a two-layer beam. In order to use the two-layer solutions, C_{F3} and C_{M3} must be substituted for C_F and C_M, and the three-layer built-up beam must be made from three identical layers with identical shear key configurations.

2.2 Solutions for the Two Layer Model with Uniform Loading

2.2.1 Axial Force in Each Layer

For a uniformly distributed load w on a simply supported beam of length L, we can write the moment equation for any point along its length x as

$$M(x) = \frac{wx}{2}(L - x) \tag{2-28}$$

which can be substituted into equation (2-20). Solving for $F(x)$

$$F(x) = C_1 e^{-\sqrt{C_F}x} + C_2 e^{\sqrt{C_F}x} - \frac{wC_M(2 - xLC_F + x^2C_F)}{2C_F^{\,2}} \tag{2-29}$$

where C_1 and C_2 are integration constants. There cannot be an axial force in the layers at the ends of the beam, so $F(0) = 0$ and $F(L) = 0$. Using these boundary conditions, C_1 and C_2 can be determined as

$$C_1 = \frac{wC_M\left(1 - e^{\sqrt{C_F}L}\right)}{C_F{}^2\left(e^{-\sqrt{C_F}L} - e^{\sqrt{C_F}L}\right)}$$

$$C_2 = \frac{wC_M\left(e^{-\sqrt{C_F}L} - 1\right)}{C_F{}^2\left(e^{-\sqrt{C_F}L} - e^{\sqrt{C_F}L}\right)} \tag{2-30}$$

Substituting these integration constants back into equation (2-29) results in

$$F(x) = \frac{wC_M}{C_F{}^2}\left(\cosh\left(\sqrt{C_F}x\right) + \frac{\sinh\left(\sqrt{C_F}x\right)}{\sinh\left(\sqrt{C_F}L\right)}\left(1 - \cosh\left(\sqrt{C_F}L\right) - 1 + \frac{C_F x(L-x)}{2}\right)\right)$$

(2-31)

The shear flow at any point of the beam can be determined by solving equation (2-14). Likewise, determining the deflection at any point along the length can be found using equation (2-15), recognizing the boundary conditions of $\Delta(0) = 0$ and $\Delta(L) = 0$. Solutions for the shear flow and deflection at any point can be found in Appendix A.

2.2.2 Bounds on Uniformly Distributed Load Solution

The lower bound for the axial forces in each layer, caused by composite action in a beam with partial interaction, should be the same as a simple stacked non-composite beam. Likewise, the upper bound for the axial forces for a beam with partial interaction

should be the full depth beam with no interlayer slip. The amount of interaction between the two layers is directly proportional to the stiffness of the individual shear keys, K. The lower bound is thus

$$\lim_{k\to 0} F(x) = 0 \tag{2-32}$$

If we assume the top and bottom layers have the same breadth, the upper bound can be found to be

$$\lim_{k\to \infty} F(x) = \frac{3wx(L-x)}{8\left(\frac{h_B}{2}+\frac{h_T}{2}\right)} \tag{2-33}$$

At the midspan of the beam, $x = \frac{L}{2}$, which results in

$$F\left(\frac{L}{2}\right) = \frac{3wL^2}{32\left(\frac{h_B}{2}+\frac{h_T}{2}\right)} \tag{2-34}$$

The axial force in the top or bottom half of a full composite section of width b is

$$F(x) = \frac{Mc}{I}\left(\frac{bc}{2}\right) \tag{2-35}$$

where c is the distance from the neutral axis to the extreme fibers. We can rewrite equation (2-35) as

$$F(x) = \frac{\frac{wx}{2}(L-x)\left(\frac{h_B}{2}+\frac{h_T}{2}\right)}{\frac{b\left(\frac{h_B}{2}+\frac{h_T}{2}\right)^3}{12}}\left(\frac{b\left(\frac{h_B}{2}+\frac{h_T}{2}\right)}{2}\right) \tag{2-36}$$

Again looking at midspan where $x = \frac{L}{2}$

$$F\left(\frac{L}{2}\right) = \frac{3wL^2}{32\left(\frac{h_B}{2} + \frac{h_T}{2}\right)} \tag{2-37}$$

which is the same as equation (2-34). Thus, the solution for the axial force in a partially composite beam subjected to a uniformly distributed load matches the required bounds.

2.3 Other Loading Conditions

Solutions of the interlayer slip model for a single point load at any point on a simply supported beam were developed, as well as the solution for a pair of point loads symmetrically placed on a simple beam. These derivations and formulae can be found in Appendix B and Appendix C, respectively.

2.3.1 Numerical Integration

Solutions of the interlayer-slip equations become quite difficult when modeling complex distributed loadings, either those that vary linearly or by some varying rate along the length of the beam. The solution to a point load at any location, along with a numerical integration technique, such as Newmark's method (Newmark, 1959), makes it possible to accurately model the more complex distributed loads without additional solutions of the interlayer slip model.

2.3.2 Linear-Elasticity and Superpositioning

The development of the general interlayer slip theory was based on the assumption of linear-elastic behavior. With linear-elastic behavior, it is possible to use

superpositioning to model complex structures by adding the effects of individual loads. To show that this method indeed works for the interlayer slip model, the solution for a two-layer beam with two point loads symmetrically placed was developed. The solution can be found in Appendix C. The deflection of the two-point load condition was compared to a superimposed single-point load condition, as is shown in Figure 2-5.

In order to behave linear-elastically, the deflection at any location on a beam subjected to two point loads must be the same as the combination of the respective deflections caused by a single point load. An arbitrary beam and symmetric point loading configuration was analyzed, both using superposition of the single point load solutions as well as by using the two symmetrically placed point load solution. The resultant deflected shapes, as well as plots of axial force at any point along the length, were identical.

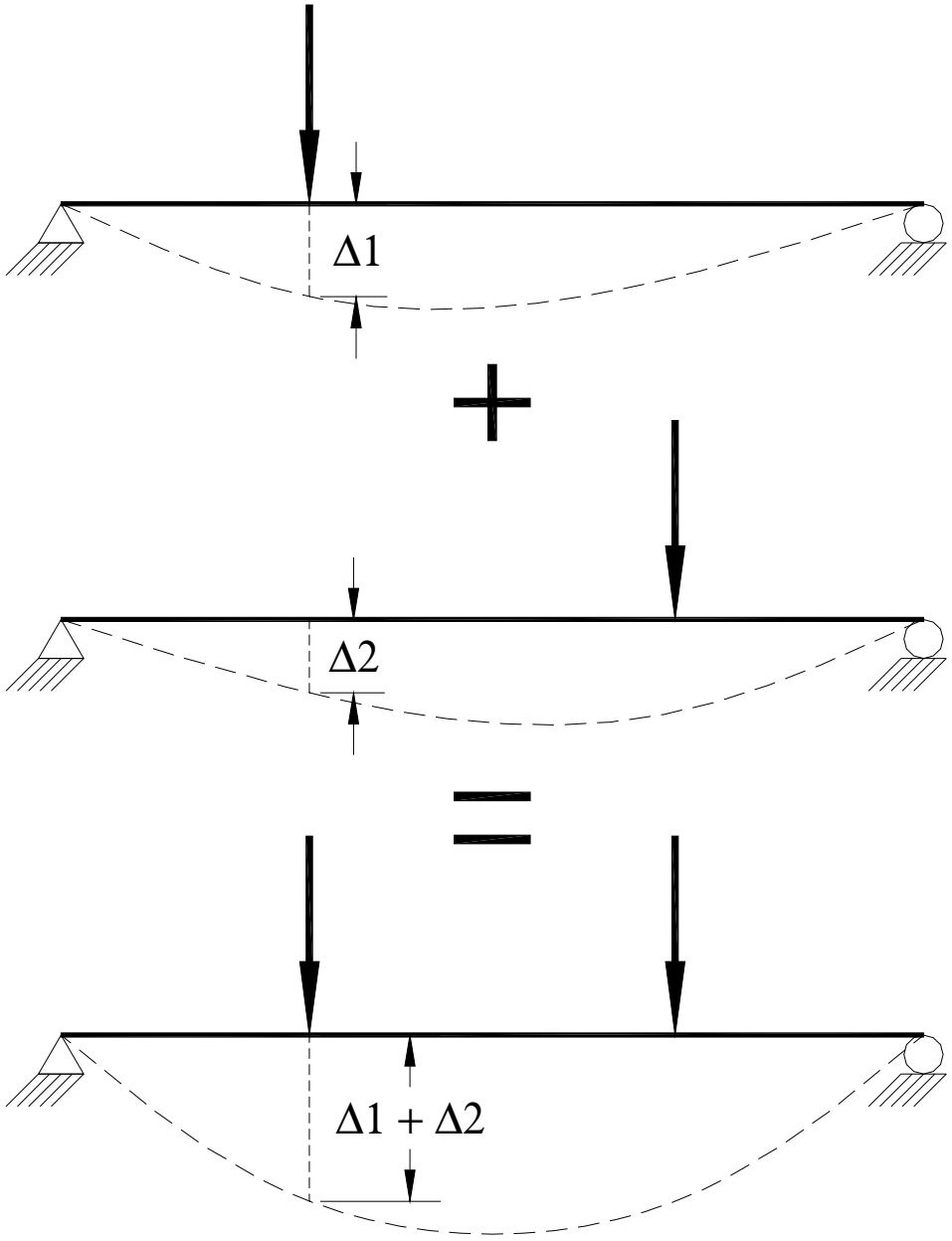

Figure 2-5 Superpositioning of pointloads

2.4 Stress Distribution

The strain distribution at any point in a layer of a two-layer partially composite beam, described in section 2.1.1 as equation (2-7), can be written as

$$\varepsilon_T = \frac{M_T z}{E_T I_T} - \frac{F_T}{A_T E_T} \tag{2-38}$$

$$\varepsilon_B = -\frac{M_B z}{E_B I_B} - \frac{F_B}{A_B E_B} \tag{2-39}$$

where the subscripts T and B represent the top and bottom layers, respectively, and z is the distance from the center of the layer to the point of interest. Using Hooke's law (equation (2-4)), the stress in each layer is

$$\sigma_T = \frac{M_T z}{I_T} - \frac{F}{A_T} \tag{2-40}$$

$$\sigma_B = -\frac{M_B z}{I_B} - \frac{F}{A_B} \tag{2-41}$$

where the first term represents the bending stress in the layer, and the second term represents the axial stress induced from the partial composite action. Again assuming the same curvature in both layers, as described by equation (2-12), the original moment in the top and bottom layers (M_T and M_B) can be related to the total applied moment M in the built-up beam as

$$\frac{M_T}{E_T I_T} = \frac{M_B}{E_B I_B} = \frac{M - Fc}{E_T I_T + E_B I_B} \tag{2-42}$$

This relationship can be used to write the stress equations (2-40) and (2-41) in terms of the total applied moment and the axial force in any layer, such that

$$\sigma_T = \frac{(M - Fc)E_T z}{E_T I_T + E_B I_B} - \frac{F}{A_T} \tag{2-43}$$

$$\sigma_B = -\frac{(M - Fc)E_B z}{E_T I_T + E_B I_B} + \frac{F}{A_B} \tag{2-44}$$

These stress equations can be evaluated for a beam with a specific loading configuration by solving the interlayer slip model, described in section 2.1, for the axial force in each layer.

The lower and upper bounds on the stress equations (2-43) and (2-44) must match the maximum stress in simple stacked and full depth beams, respectively. To verify these limits, the stress in an arbitrary beam with symmetrically placed point loads was analyzed. The amount of interaction between layers was varied from no interaction (full slip) to full interaction (no slip) by adjusting the stiffness of the shear key, K, shown in equations (2-18) and (2-19). As $K \to 0$, the calculated extreme fiber stress in the beam using the interlayer slip model approached the extreme fiber stresses in a pair of simple stacked beams with the same applied load. Likewise, as $K \to \infty$, the calculated extreme fiber stress in the beam using the interlayer slip model approached that of a full depth beam. For any specific applied load, the extreme fiber stress in a simple stacked beam will be exactly twice that of full depth beam.

The magnitude of maximum stress along the length of a beam may be different for a built-up beam with partial composite action than for a full depth or simple stacked beam, depending on the applied loading configuration. The stress in a full depth or simple stacked beam is a function of the moment and cross-sectional properties (distance to point of interest and the moment of inertia), and assuming a constant cross-section

along the length, the shape of the moment diagram is the shape of the extreme fiber bending stress diagram. For a built-up beam, the change in axial force in the layers due to partial interaction can result in localized points of maximum stress. Figure 2-6 shows the normal stress distribution at the beam face for an arbitrary built up beam with some interlayer slip (solid line) and a full depth solid beam (dashed line), subjected to two symmetrically placed point loads. Peaks in the stress diagram are noticeable in the built up beam at the points of applied load.

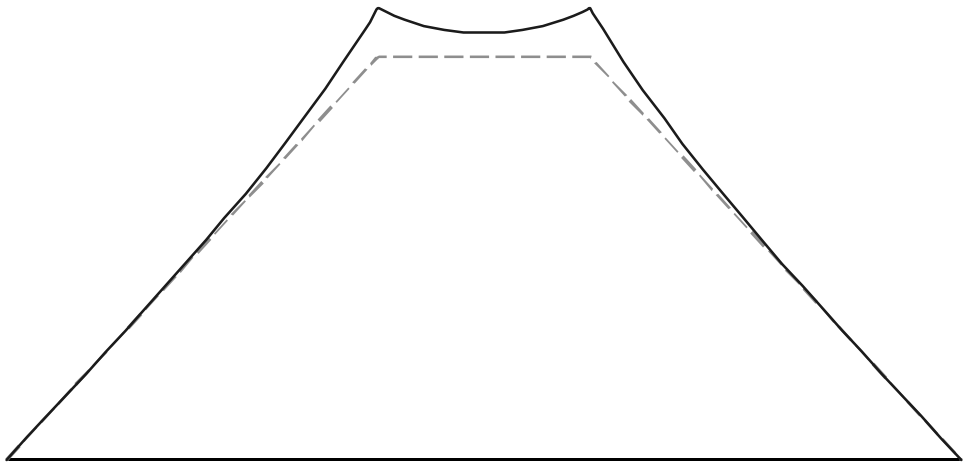

Figure 2-6 Normal stress diagrams for an arbitrary full depth (dashed line) and built up (solid line) beam

2.5 Shear Keys

The closed-form interlayer slip solutions previously developed require knowledge of the stiffness of each particular connector along the beam length (see Figure 2-7). These connector stiffnesses depend on the type and configuration of the shear key as well as the beam material properties. From this point onward, the term "shear key" includes the actual wood key along with the clamping connectors, behaving as an assembly.

Two configurations of shear keys are common in traditional timber design; one is a key inclined to the interface and the other is a key square to the interface. Both consist of a pair of wedges, driven in from opposite faces of the timber, to ensure a tight fitting joint. These wedges will form a shear key that will then be installed either square to the timber or at an incline. Fabricating the notch for the square shear keys requires slightly less effort, but parallel to grain shearing of the wedges will become a design concern. Notches for the inclined wedges may be slightly more difficult to cut, but the key will be almost entirely in compression, greatly reducing concerns about horizontal shearing of the keys. The inclined shear key reduces the angle to the grain of the re-entrant corner of the notch, which will likely have an effect at reducing the stress concentration at this point.

As force is transmitted through an inclined shear key, it will cause the shear key to rotate and thus open up a gap at the interface. A mechanical connector, either a through bolt, lag bolt, or other screw, is required to provide a clamping force. This connector will be loaded in shear at the interface as well, and thus can contribute to the overall stiffness of the interface. Axial stretching of the connector will likewise cause some movement of the shear key, and thus this stiffness also needs to be included in determining the stiffness of the interface. The square and inclined shear keys can be seen in Figure 2-7.

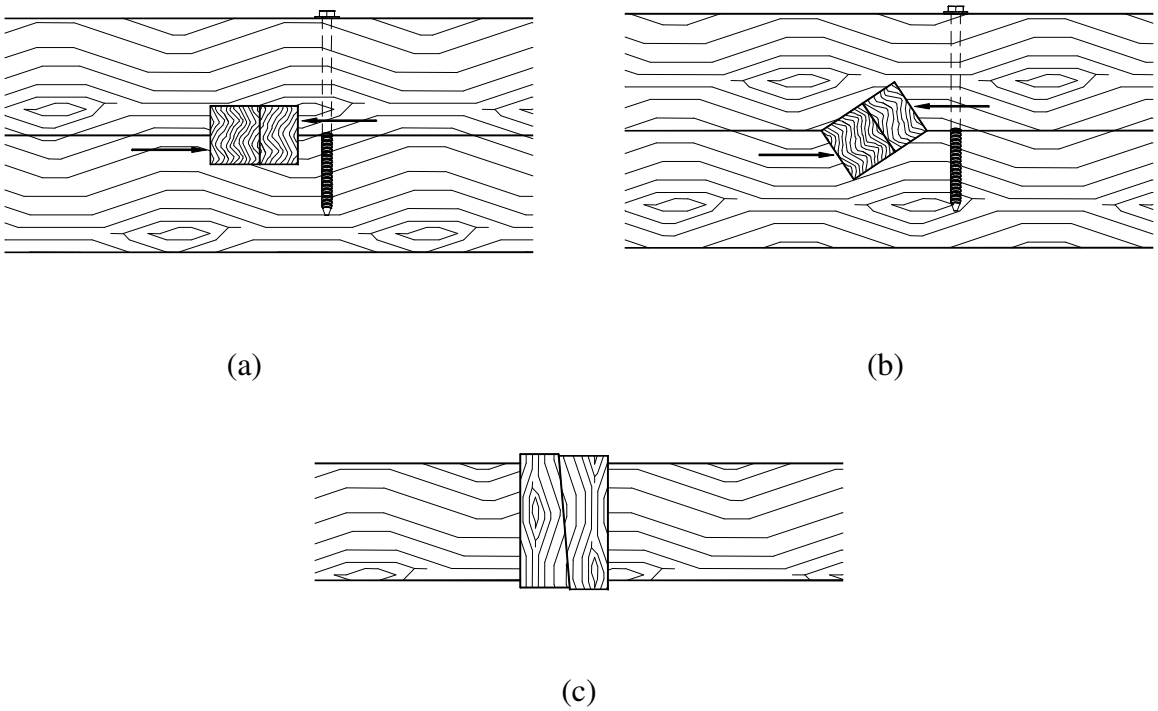

Figure 2-7 Side view of (a) square and (b) inclined shear keys along with (c) a top view showing the wedge shape of the shear keys

2.5.1 Shear Key Stiffness

Shear keys are used to inhibit slipping between the layers of a built up beam. Thus, the stiffness of the shear keys in this plane is of particular concern in determining the strength and efficiency of the built-up beam, where efficiency is defined as the percentage of a comparative solid-sawn beams horizontal shear that is resisted (see 2.6). We will start with an inclined shear key notched to a depth t into the individual layers and of length w, as shown in Figure 2-8. In Figure 2-8, N is the horizontal force that the shear key is resisting, and R is the clamping force required to counteract the rotation of the keys. P is the axial force, which is components of N and R, acting parallel to the shear key.

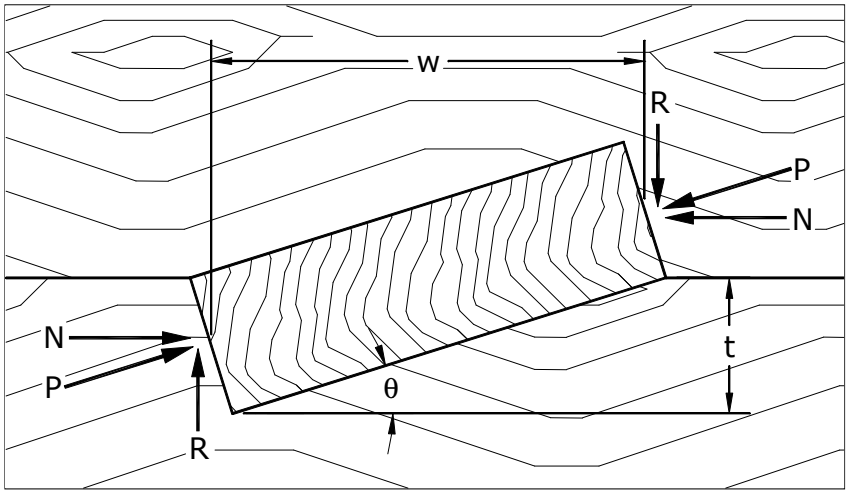

Figure 2-8 Inclined shear key

As axial force is developed in the individual layers, the shear key will deform as shown in Figure 2-9. As was already noted, the horizontal movement of the key is of primary concern. Contributions to this movement include compression of the timbers at the notches, axial shortening of the shear key, and the gap created as the key rotates.

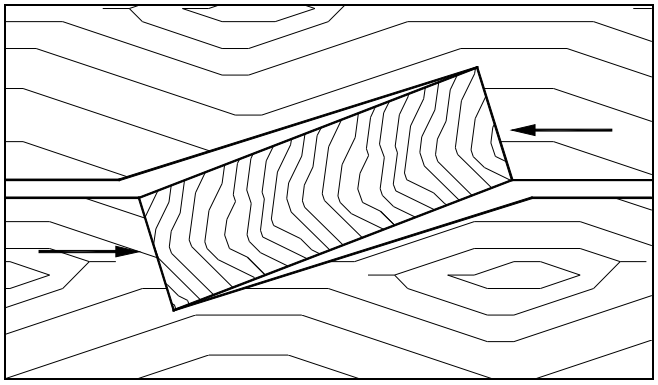

Figure 2-9 Deformed inclined key

In order to model the stiffness of the shear key, we can depict the shear key shown in Figure 2-8 as a series of three springs which are shown in Figure 2-10. The K_B and K_T

terms represent the stiffnesses in compression of the beams in the bottom and top members. The K_K term represents the axial stiffness of the shear key.

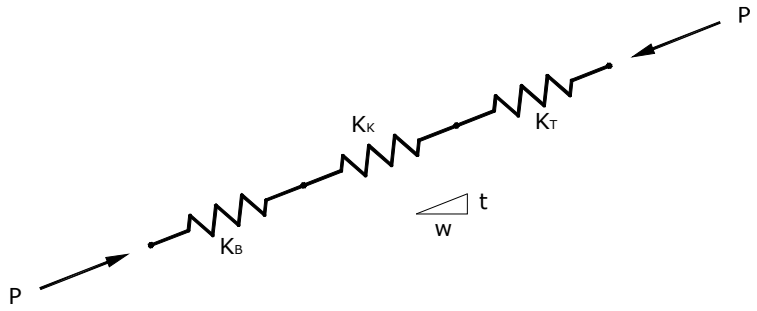

Figure 2-10 Springs-in-series model of the shear key

The effective stiffness of the shear key connection, K_{eff} is

$$\frac{1}{K_{eff}} = \frac{1}{K_B} + \frac{1}{K_K} + \frac{1}{K_T} \tag{2-45}$$

With the assumption that the top and bottom timbers are of similar properties, $K_T = K_B$, we can solve for the effective stiffness as

$$K_{eff} = \frac{K_K K_T}{2K_K + K_T} \tag{2-46}$$

The total compressive displacement of the keyed connection can be written as

$$\Delta_{comp} = \frac{P}{K_{eff}} \tag{2-47}$$

We are concerned with the displacement oriented parallel to the timbers, not oriented parallel to the keyed connection. From Figure 2-8, we can see P has a horizontal component N, and compressive displacement Δ_{comp} has a horizontal displacement Δ_{key}, which allows us to write

$$\Delta_{key} = \frac{N}{K_{eff}} \tag{2-48}$$

The axial stretching of the clamping connectors also contributes to the slipping between the layers, as it allows the key to rotate slightly. The axial displacement of the clamping connectors, $\Delta_{stretch}$, is written as

$$\Delta_{stretch} = \frac{R}{K_{clamp}} \tag{2-49}$$

where K_{clamp} is the axial stiffness of the clamping connector (see Figure 2-11). If multiple screws or bolts are used to provide the clamping force, K_{clamp} is the summation of the cumulative axial stiffnesses.

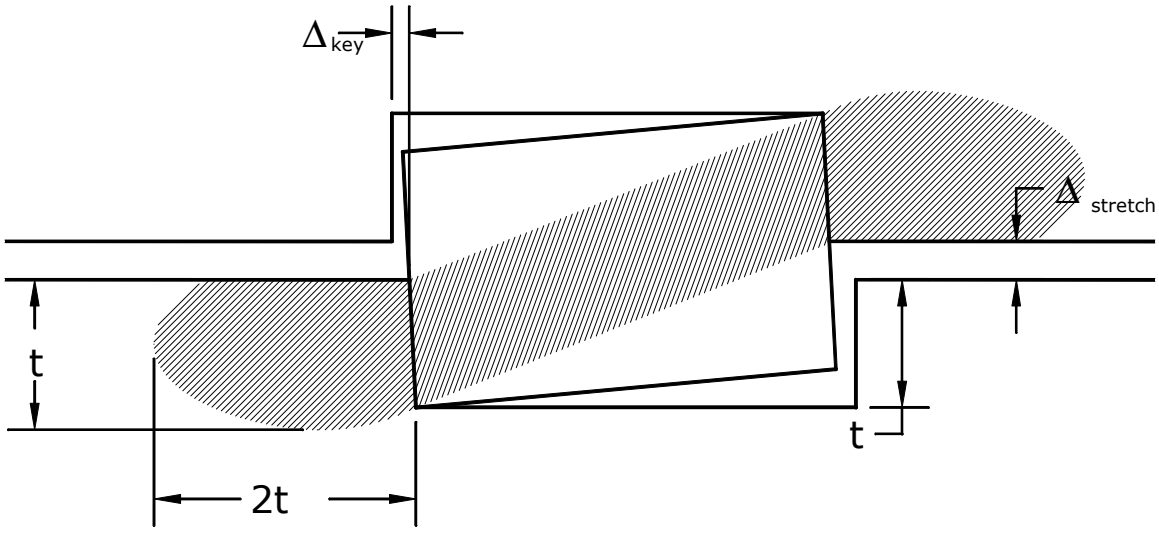

Figure 2-11 Displacement components of a shear key

Again from Figure 2-8, we can see the forces R and N are components of P, thus $R = N\tan\theta$. The horizontal slipping Δ_{clamp} caused by the axial stretching of the

clamping connector can also be written as $\Delta_{clamp} = \Delta_{stretch} \tan\theta$. The horizontal displacement caused by the axial stretching of the clamping connector can thus be written as

$$\Delta_{clamp} = \frac{N \tan^2 \theta}{K_{clamp}} \tag{2-50}$$

Combining the horizontal displacement from the axial compression of the key component as well as the horizontal displacement from the axial stretching of the clamping connector, we are able to write the stiffness for a single shear key as

$$K_{key} = \frac{N}{\Delta_{key} + \Delta_{clamp}} \tag{2-51}$$

Substituting equations (2-48) and (2-50) into equation (2-51), the stiffness of a shear key can be written as

$$K_{key} = \frac{K_{clamp} K_{eff}}{K_{clamp} + K_{eff} \tan^2 \theta} \tag{2-52}$$

The key stiffness shown in equation (2-52) ignored the stiffness contribution for the clamping connectors loading in shear. For most connectors, consisting of screws or bolts, the stiffness of a laterally loaded connection is assumed to be proportionally very low and is therefore ignored in this analysis. This assumption is later verified in section 4.5.

2.5.2 Shear Key Stiffness Coefficients

In order to calculate the shear key assembly stiffness for use in the interlayer slip model, the various stiffness components in equation (2-52) need to be calculated. With the width

of the timber beams being b, and the depth of influence in the compression zone of the timber L, being approximated as two times the key thickness t using a Boussinesq / soil pressure bulb analogy (Coduto, 2001) (see Figure 2-11), the stiffness of the timbers being compressed at the shear key interface is

$$K_T = \frac{AE_\theta}{L} = \frac{tbE_\theta}{2t} = \frac{bE_\theta}{2} \tag{2-53}$$

where E_θ is the modulus of elasticity of the timber at an angle θ to the grain, as shown in Figure 2-8. E_θ can be approximated by the use of Hankinson's formula, such that

$$E_\theta = \frac{E_\parallel E_\perp}{E_\parallel \sin^2\theta + E_\perp \cos^2\theta} \tag{2-54}$$

Published values for the modulus of elasticity for timber are values parallel to the grain. Perpendicular to the grain modulus values for wood are seldom measured or recorded. Instead, elastic ratios are commonly used that relate the longitudinal modulus (parallel to grain) to radial and tangential modulii (perpendicular to grain). The elastic ratios are published values relating one orthotropic material modulus to that of another. These elastic ratios vary widely depending on species and grain orientation, with tangential to longitudinal ratios as low as 0.02 and radial to longitudinal ratios as high as 0.197 (FPL, 1999). The elastic ratios have been shown to vary with a positive correlation to the longitudinal modulus of elasticity (Bodig and Jayne, 1982). Several authors suggest averaging the elastic ratio between the radial and tangential directions, as this grain orientation is seldom known at the time of design (Bodig and Jayne, 1982; Wangaard, 1981). These authors also suggest using an elastic ratio on the order of 1:20 (that is, $E_\parallel = 20E_\perp$). Their recommendation is based on the predominant use of softwoods in

design. For this research, and in common heavy timber construction practice, white oak keys were used, which has elastic ratios of 1:14 (longitudinal to tangential) and 1:6 (longitudinal to radial) (FPL, 1999). Yellow poplar has published ratios of 1:24 and 1:10, respectively. Based on these values, the elastic ratio of 1:12 was initially chosen to relate the longitudinal and perpendicular modulii ($E_{\parallel} = 12E_{\perp}$). We can rewrite equation (2-54) to include this as

$$E_{\theta} = \frac{E_{\parallel}}{12 - 11\cos^2\theta} \tag{2-55}$$

Including equation (2-55) into the timber stiffness equation (2-53) yields

$$K_T = \frac{bE_{\parallel_{TIMBER}}}{2(12 - 11\cos^2\theta)} \tag{2-56}$$

Likewise, the stiffness for the key portion is

$$K_k = \frac{AE}{L} = \frac{btE_{\parallel_{KEY}}}{(12 - 11\cos^2\varphi)w} \tag{2-57}$$

where φ is the orientation of the shear key grain with respect to the force P.

The stiffness of the clamping connectors may be able to be approximated using a mechanics based approach as above if a through-bolt or other similar type of connector is used. When screws are used, the axial stiffness will need to be verified from physical tests or manufacturer's data, as no method to calculate the axial withdrawal stiffness of a screw is known to exist.

2.6 Beam Efficiency

The efficiency of a built-up beam is directly related to the amount of interaction between the layers. The interaction results in axial forces in each layer (see Figure 2-3). A low efficiency beam has little interaction between the layers (acts like a simple-stacked beam) and small additional axial forces in each layer. A high efficiency beam has nearly rigid interaction between the layers (acts like a full-depth beam). The rate of change of the axial force in the layers is the shear flow (see equation (2-14)). The shear flow in a transversely loaded full depth solid beam is calculated as

$$q = \frac{VQ}{I} \tag{2-58}$$

where V is the vertical shear, Q is the first moment, and I is the moment of inertia. Plots of the shear flow in both an arbitrary built-up beam as well as a full depth beams are shown in Figure 2-12a and Figure 2-12b. The shape of the shear flow diagrams for a beam subjected to a uniformly distributed load appears quite similar regardless whether it is a full depth beam or a built-up beam. A beam subjected to a pair of concentrated points load exhibits substantial variation in the respective shear flow diagrams near the center of the span. In either loading case, the area under the built-up beam shear flow diagram is less than the area under the full-depth beam diagram.

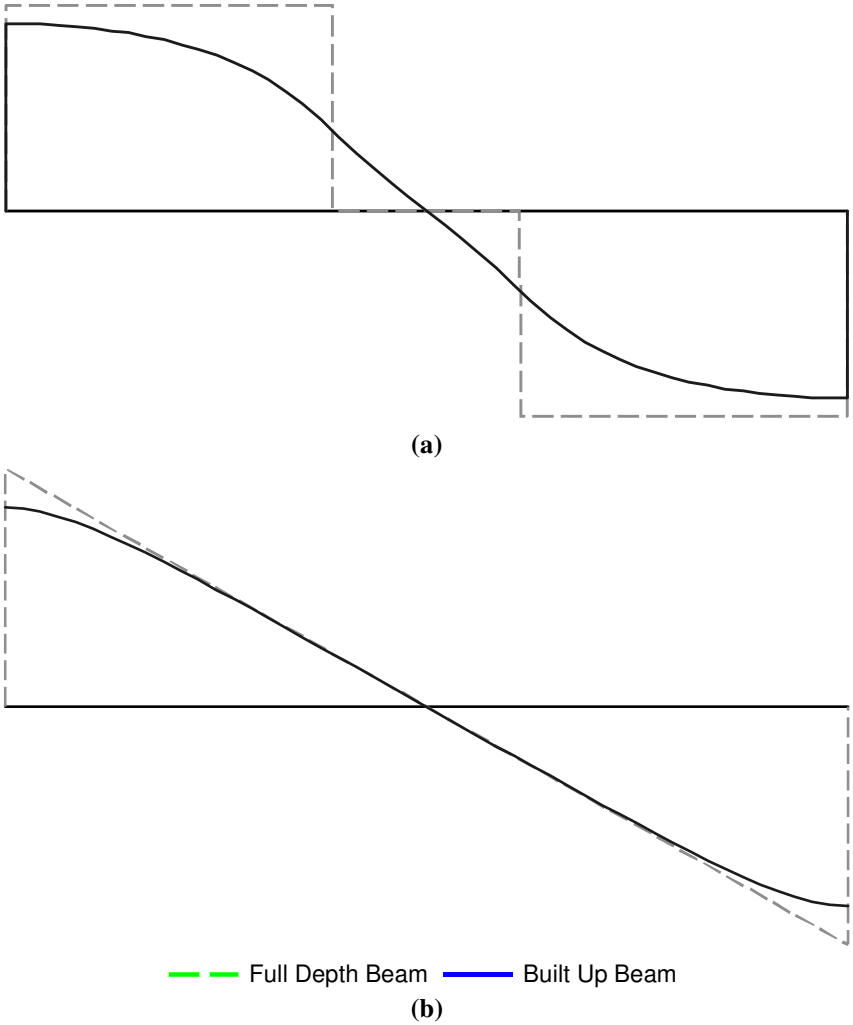

Figure 2-12 Shear flow in partially composite beams subjected to (a) two concentrated loads and (b) a uniformly distributed load.

The area under the shear flow diagrams is the axial force generated in each layer of the built-up beam. The ratio of the area under a built up beam shear flow diagram to the area under an equivalent full depth beam represents the beam efficiency λ, such that

$$\lambda = \frac{\int \frac{dF}{dx} dx}{\int \frac{VQ}{I} dx} \tag{2-59}$$

where the first moment Q and moment of inertia I are based on the full depth cross-section. The value of λ can range between zero and one.

3 Physical Testing Overview

In order to verify the interlayer slip model and shear key stiffness components developed in the previous section, physical testing was conducted on individual, small scale components as well as full sized beams. To best utilize the materials available for the testing, configurations that were similar to those being used in professional practice were used (Brungraber, 2008). These configurations are further described below.

3.1 Timber and Key Species

3.1.1 Timber Species Selection

According to the Timber Frame Business Council, there are several species commonly used in timber frame construction: Douglas fir, eastern white pine, southern yellow pine, and red oak (TFBC, 2009). While each of these common species have specific strong points, yellow poplar (*Liriodendron tulipifera*) was chosen for this research. Yellow poplar is a commonly available, inexpensive, fast-growing hardwood that has reasonable structural qualities. There is also a longstanding history of yellow poplar use in timber structures, including covered bridges and mill buildings (Forest Service, 1985).

Yellow poplar was selected primarily because of the availability of large, clear, straight grained specimens. Clear specimens were desired so that natural defects such as knots would not dominate behavior during the physical testing. Yellow poplar timbers were readily available from a sawmill within Michigan which further added to the appeal

of their use. An increasing availability of second-growth yellow poplar (Forest Service, 1985) was also a contributing factor in its selection.

3.1.2 Shear Key Species Selection

Traditional and contemporary sources suggest using hardwoods, in particular white oak (*Quercus alba*), for wedge stock (Kidwell, 1898; Karlsen, 1967). According to section 1.6.3 of the TFEC 1-07 Standard for Design of Timber Frame Structures and Commentary (TFEC, 2007):

> *Wood wedges used to secure through-tenons or scarf joints, or used for other structural applications shall be fabricated from clear, straight-grain, defect-free, hardwood stock. Wedges shall be fabricated to minimize slope of grain, but in no case shall slope of grain be greater than 1:6 relative to each face of the wedge. The specific gravity of the wedge stock shall not be less than that of the timber used in the connection, but in no case shall the oven-dry specific gravity of the wedge stock be less than 0.57.*

The shear keys are acting in a structural application and consist of a pair of wedges, therefore the requirements set forth in TFEC 1-07 above should directly apply. As there was substantial agreement between all of the investigated sources, white oak was chosen as the main shear key material.

A non-traditional manufactured shear key material was also desired for use with the key testing. Manufactured shear key material considered for possible use included glue-laminated timbers, laminated veneer lumber (LVL), and parallel strand lumber

(PSL). These manufactured wood products appeared to have several advantages over the white oak for use as shear keys, mainly that they:

- are thoroughly dried. Any shrinkage in a shear key would greatly reduce the efficiency of the keyed beam.
- have interwoven or discontinuous grain. Seasoning and growth defects are removed or broken up by the manufacturing process, decreasing the likelihood of damage during installation.
- have higher and more consistent modulus of elasticities than solid-sawn material. The manufacturing process culls low grade material from the final product, and adhesives used to bind the wood fibers increases the stiffness.

The main deterrents from using manufactured wood products for the shear key material are that they:

- can cost significantly more than solid-sawn pieces of white oak.
- are commonly available only in several species.
- use adhesives in the manufacturing process. One of the main contemporary uses of keyed beams is in places were adhesives are not desired.

Glulams, while thoroughly dried, still regularly use large pieces of continuous wood (although finger jointing allows for shorter pieces to be used), and are one of the building materials keyed beams are intended to replace. Laminated veneer lumber is commonly available only in narrow thicknesses (typically 1.75 inch or less), limiting the size of shear keys. Parallel strand lumber can be made into almost any size, and because

of the fabrication process, is considerably stiffer when loaded parallel to the grain than solid-sawn material.

Based on the above factors, parallel strand lumber was chosen as the manufactured wood product to be used as shear keys, specifically southern pine TrusJoist 2.0E Parallam PSL (Parallam). Parallam PSL is described as being "manufactured from strands of a single wood species, or species combinations, that are oriented parallel to the length of the member and coated with a phenol-formaldehyde adhesive." (ICC-ES, 2007).

3.2 Key Configuration

3.2.1 Key Orientation

Stiffness models were developed for both keys inclined to the interface of the timbers (inclined keys) and keys square with the interface (square keys). Kidwell (1898) argued that notches for the inclined keys were more difficult to cut and that the inclined keys were quite prone to roll and force the layers apart. He therefore recommended square keys. Karlsen (1967) instead argued that square keys are prone to shearing along the grain and thus preferred inclined keys which act primarily in compression.

With the availability of modern power tools, notching for an inclined key is no more difficult than notching for a square key. Likewise, the stiffness model for the keys includes rotation of the key, so any propensity of one key configuration to roll compared to the other can be directly accounted for. Shearing parallel-to-the-grain of the key is a legitimate concern with the square keys. Parallel-to-the-grain shear failures are a sudden and brittle failure.

An additional benefit of the inclined keys is they require removal of less material from the timbers than an equivalent capacity square key. An inclined key also results in a smaller stress concentration at the re-entrant corner of the notch, since the notch orientation is rotated slightly (Karlsen 1967). An inclined key's ability to resist only one-way shear (reversal of moment in the keyed beam can result in reversal of slip directions) can be seen as a deterrent for its use. However, the difficulty in fabricating a square key that can carry two-way shear without allowing some initial slipping makes this argument impractical. Based on these reasons, only inclined keys are investigated in this research's physical testing components.

3.2.2 Grain Direction

Physical behavior, which is also evident in the analytical model previously developed, shows the stiffness of the shear keys directly impacts the stiffness of the keyed beam. For wood shear keys, the parallel-to-the-grain modulus of elasticity is approximately ten to twenty times as stiff as the perpendicular-to-grain modulus of elasticity (FPL, 1999). Orienting the shear keys so that they are compressed parallel-to-the-grain would therefore result in a stiffer keyed beam.

Kidwell (1898) acknowledged wood is stiffer parallel-to-grain than perpendicular-to-grain, but still advocated that the wedge stock be installed so that it is loaded in the perpendicular-to-grain direction. "The writer does not believe that there is any solid foundation for the idea that the grain of the keys should be vertical. This would greatly increase the cost of making the keys, and probably result in causing many of them to split

while driving." (Kidwell, 1898). Kidwell went on to discount all wooden keys and suggested using only cast-iron ones because of their much higher modulus of elasticity.

Karlsen (1968) acknowledged that connections with keys loaded in compression perpendicular-to-the-grain are much easier to fabricate and install, but disliked their use because of their low stiffness. He claimed shear keys loaded in a parallel-to-the-grain fashion will be much stiffer, although they cannot be installed as wedges due to splitting during installation, and instead must be installed as solid pieces of wood. However, Karlsen also suggested parallel-to-grain shear keys end up having no greater capacity than perpendicular-to-the-grain keys. The failure to carry more load, despite being considerably stiffer, is purportedly because they cannot be made to carry load evenly due to fabrication tolerances. According to Karlsen, the uneven load carrying results in high stress concentrations at notch corners, which in turn cause some connections to fail before others even start to carry load (Karlsen, 1968).

An attempt was made to verify Kidwell's and Karlsen's comments about parallel-to-the-grain wedges splitting during installation. Three pairs of straight grained, unchecked, white oak wedges, 2.5 inches thick, 10 inches long, and 8 inches in combined depth were fabricated with the grain running approximately perpendicular to the wedge faces (Figure 3-1). The pairs of wedges were installed into a similar sized inclined notches in a keyed beam. The wedges were driven with a 3-lb drill hammer to fully engage both bearing faces. Of the three sets of wedges, one set was able to be installed fully with no splitting, while at least one wedge from the each of the other two sets split along the grain during the driving process (Figure 3-2).

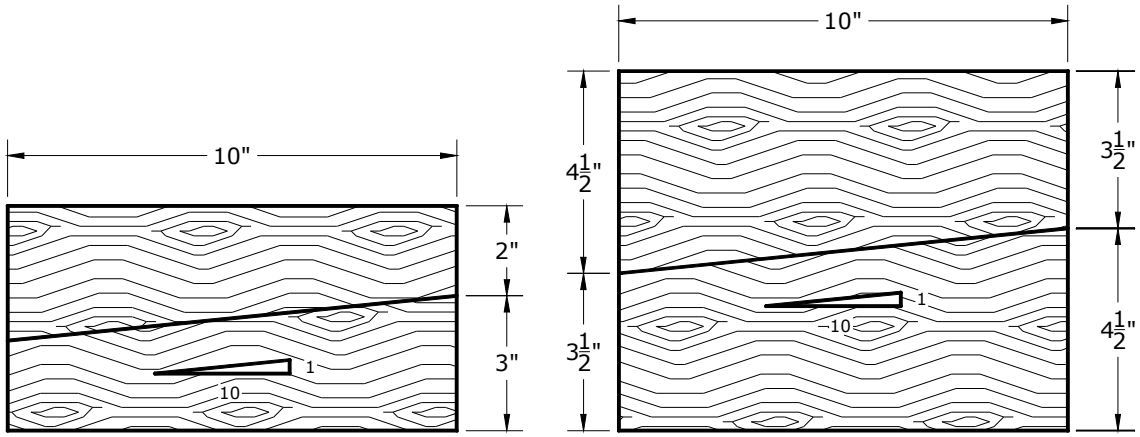

Figure 3-1 2.5 inch thick shear key wedge dimensions

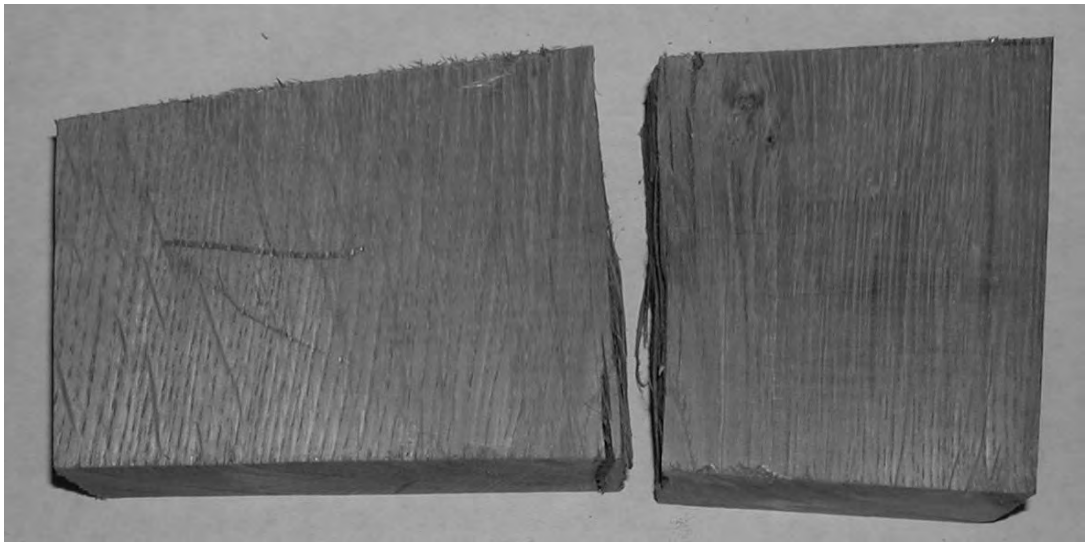

Figure 3-2 Solid sawn parallel-to-the-grain wedges are prone to splitting during installation

With convincing evidence that solid sawn parallel-to-grain wedges were not feasible, the research instead focuses on using white oak wedges as shear keys installed with the load orientated perpendicular to the shear key grain. Due to the fabrication process used in making Parallam PSL, the shear keys using this material were able to be installed as wedged shear keys with the grain running parallel to the load direction.

3.2.3 Key Size

Kidwell (1898) recommended shear keys with an aspect ratio of at least 2:1; that is, shear keys that are at least twice as long as they are thick. Karlsen (1967) instead recommended an aspect ratio of at least 5:1. Smaller aspect ratios would greatly increase the amount of clamping force required to keep the shear key from rotating. For a given key thickness, larger aspect ratios, when compared to smaller aspect ratios, increase the amount of material that has to be removed from the timbers, as well as increases the amount of material required for the shear keys. Karlsen and Kidwell both also suggested that the notches not exceed approximately $1/5^{th}$ of the beam depth, although they do not provide any specific reasoning for such a requirement. However, notches of excessive depth would certainly affect the bending capacity of the beam. For this research 2.5 inch thick keys were ultimately chosen based on the availability of the shear key material.

Two different lengths of shear keys were used. Shorter keys, with a length of 5 inch (aspect ratio of 2:1) were used as well as longer 8 inch keys (aspect ratio of 3.2:1). Each test involving shear keys, which are described in later sections, was conducted using both short and long keys fabricated from both white oak and Parallam PSL. The short and long key sizes can be seen in Figure 3-3.

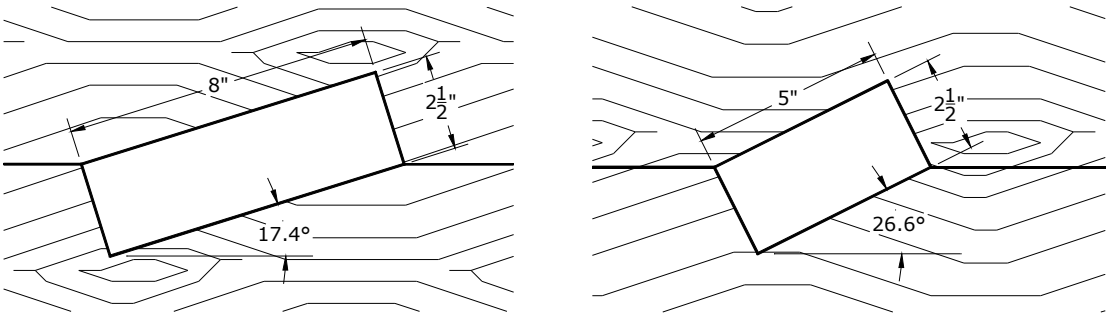

(a) **(b)**

Figure 3-3 (a) Long and (b) short shear key configurations

3.2.4 Wedge Slope

The shear keys used in this testing consisted of a pair of inclined wedges cut from a single piece of material. The incline allows the shear key (pair of wedges) length to be fine tuned, once installed into the notched timbers, to ensure full contact across all bearing faces. The axial force P being resisted by the shear key must be transferred across the interface between the wedges as a normal force P_N. A friction force P_F is thereby required to keep the wedges in place as they are loaded in compression (Figure 3-4). The static friction coefficient μ_S for wood varies based on moisture content, smoothness of the surfaces, species, and other variables, although the Wood Handbook lists a range $\mu_S = 0.3 - 0.5$ (FPL, 1999). These friction coefficients of 0.3 to 0.5 would permit any rise under 3 to 5 to maintain equilibrium. Per section 1.6.3 of the TFEC 1-07, which is shown above in section 3.1.2, the slope of a wedge must not exceed 1:6 (1.67:10). With this in mind, a conservative slope of 1:10 was chosen for the wedges used to form a shear key.

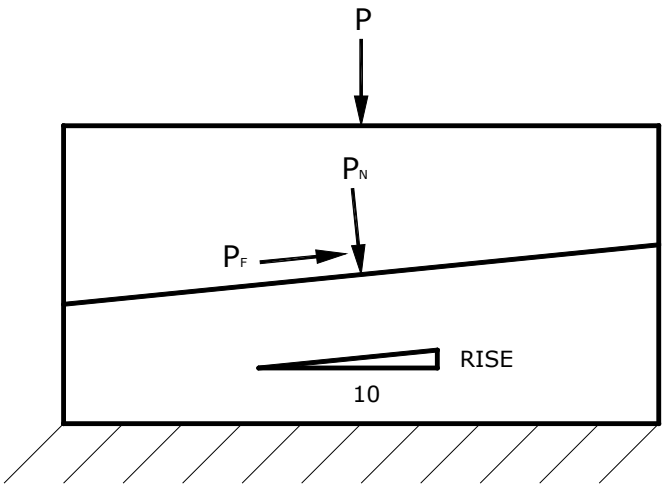

Figure 3-4 Forces acting on a pair of wedges

3.3 Clamping Connectors

3.3.1 Connector Type

As force is applied to the shear keys, whether they are inclined keys or square keys, the keys will have a tendency to rotate (Figure 2-9). Mechanical connectors are used to resist this rotation. Several various options were investigated for potential use as clamps. These include:

- Through bolts. Through bolts consist of machine bolts installed orthogonally to the slip interface, through the entire depth of the timbers and secured with a nut and washer. Through bolts require drilling holes through the beams, reducing their net cross section. For framing to sit directly on the top face of the keyed beam, through bolts would need to be countersunk into washer pockets, further reducing the net section. The bolt head and washer would also be left visible on the bottom face of the

beam. As most timber beams have their bottom face exposed as a finished surface, visible bolts could deter from the aesthetic appeal.

- Lag bolts. Lag bolts, like through bolts, would require drilling holes in the timbers and reducing their net cross section. Lag bolts could be installed entirely from the top (hidden face) and thus would be much less visible, but would still require countersinking. Installation of lags also requires the use of impact drivers.
- Continuously threaded screws. Screws that are threaded along the entire length are commonly used for radially reinforcement of curved glulam timbers. Unlike bolts or lags, they do not require pre-drilling, and they also interrupt considerably less grain. Screws can also self counter-sink.
- Dual threaded screws. Dual threaded screws are much like continuously threaded screws, however, they are threaded with slightly different pitches on an upper and lower portion of the shaft. As they are installed, the variance in pitch causes the middle of the screw to be axially pre-tensioned, drawing the two connecting timbers together.

In order to increase the rate and ease of fabrication, as well as limit the reductions made to the cross section of the timbers, screws were chosen to provide the clamping action required at the shear keys. OMG Fastenmaster Double Thread LogHog (Figure 3-5) screws were ultimately chosen from the various manufacturers due to their long-standing history in the timber framing market.

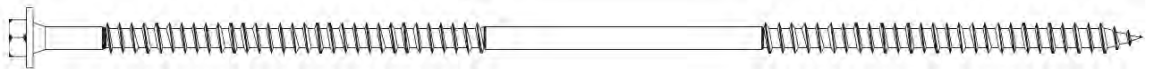

Figure 3-5 Double threaded log screw

3.3.2 Connector Placement

The placement of the connectors used to resist the rotation of the shear keys will directly determine the quantity of connectors required. As the distance from the shear key increases, the moment arm between the point of rotation and the connector increases, decreasing the capacity. However, excessive distance between the shear key and connector can result in bending of the individual timber layers, so a balance must be maintained. For ease of fabrication, the clamping fasteners were placed 2 inch from the center of the key's bearing area. See Figure 3-6.

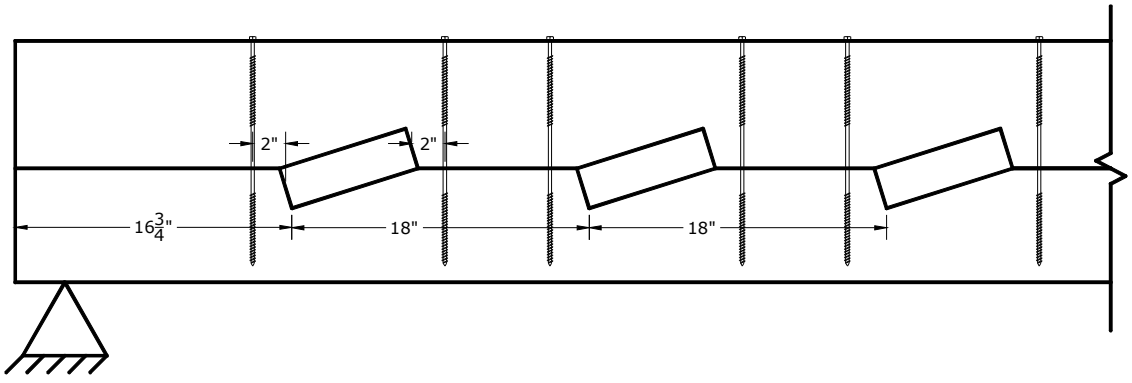

Figure 3-6 Key placement and screw location on keyed beams used in the full-scale testing

3.3.3 Connector Quantity

While previous authors provided recommendations for the clamping force required to secure joints, a mechanics-based approach was instead used for this research. The placement and number of screws required to adequately clamp each key was

determined after the key configurations were developed. The clamping required for the shear key configuration shown in Figure 3-3 (a), with white oak keys installed such that they are loaded perpendicular to grain, was calculated. Calculations can be found in Appendix D. A total of four LogHog screws (two pairs of two) were required to clamp each shear key. The governing compressive force in the key was determined from the cross-grain compressive capacity of the white oak shear key at the proportional limit. A similar clamping configuration was then used for all other shear key configurations.

3.4 Beam Size

The interlayer slip model and shear key stiffness model permit any sized beam to be used. Therefore, a timber size was chosen based on common practice and the availability of materials. Cross sectional dimensions are normally specified to the nearest two inch nominal increment (e.g., 6 inch by 6 inch nominal, 8 inch by 8 inch nominal) with lengths specified to the nearest two-foot increment (AF&PA,2005). The International Building Code (IBC) specifies timber cross sections must be at least 6 inches or 8 inches depending on their use in a structure to meet the classification of heavy timber (ICC, 2006). In order to incorporate all categories within the IBC heavy timber category, nominal 8 inch by 8 inch timbers were chosen. Based on the log inventory of the sawmill providing the timbers for the research, the maximum length of timbers was set at 14 feet.

3.5 Loading Configuration

A primary focus of the research was to predict actual keyed beam behavior using the theoretical interlayer slip model and shear key stiffness parameters developed in the previous section. For static load tests on simply supported full sized members, ASTM D198 provides guidance for the proper testing and loading procedure (ASTM, 2007). Per ASTM D198, two symmetric point loads should be placed at third-points on the beam, although other placements are permitted for special purposes. This loading configuration creates a constant shear, linear moment distribution in the ends of the beam, with a zero shear, constant moment distribution in the middle section.

ASTM D198 also provides guidance for determining the over-all length of the beam as

$$\frac{a}{h} = \phi \frac{S_R}{\tau_{MAX}} \tag{3-1}$$

where a is the distance from the end support to the nearest point load, h is the total depth of the beam, S_R is the published average modulus of rupture for the material, and τ_{MAX} is the average maximum shear stress. ϕ is an adjustment factor with a suggested range of 0.4 to 0.6 (ASTM, 2007). For a two layer beam fabricated from nominal 8 inch by 8 inch (7.5 inch by 7.5 inch approximate actual size) material, the beam depth will be 15 inches. Values published in the Wood Handbook for yellow poplar are 10,100 psi and 1,190 psi for modulus of rupture and shear stress, respectively (FPL, 1999). Using an adjustment factor ϕ of 0.5, the distance from the end support to the point load was calculated as 63.7 inches, and truncated to 63 inches for simplicity. With 14-foot timber

material, and accounting for three inches of bearing and overhang on each end, this results in a 36 inch spacing of the point loads at the center of the beam. ASTM D198 recommends equal spacing for the end and center sections, using a shorter center distance increases the length of the constant shear sections, which are the areas of particular concern in this research (ASTM, 2007). The loading configuration, along with the shear and moment diagrams, are shown in Figure 3-7.

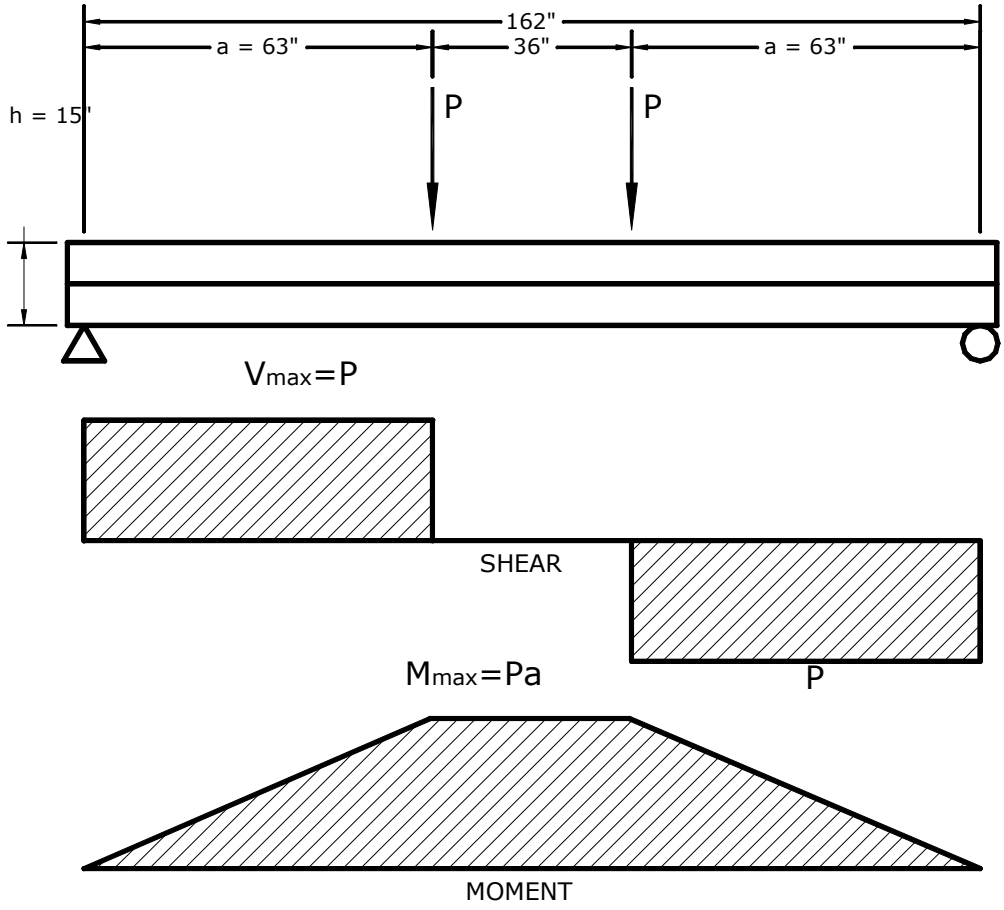

Figure 3-7 Loading configuration for full scale beam testing

3.6 Key Layout in Keyed Beam

In order to achieve full interaction (no slip allowed between the layers) in a two-ply keyed beam using the loading configuration shown in Figure 3-7, all of the horizontal shear developed in a full depth beam must be resisted by the shear keys. The minimum spacing between shear keys is limited by the shear strength parallel to grain of the timbers between each shear key. The maximum spacing between shear keys is limited by the shear flow that each key needs to resist. As slippage between layers will occur in the actual beams, using the interlayer slip model to develop the maximum shear key spacing would be most appropriate. The method used in this section was an approximation to ensure the testing configuration was reasonable.

The minimum spacing between shear keys, s_{MIN}, is limited by a block shear failure of the timber between keys, and was calculated by

$$s_{MIN} = \frac{2P}{b\, F_{v_{0.95}}} \tag{3-2}$$

where P is the cross-grain compressive strength of the shear key at the proportional limit (16,050-lb per Appendix D), b is the timber width (7.5 inch), and $F_{v_{0.95}}$ is the 95% inclusion value (5% exclusion) of the shear stress parallel to grain for unseasoned yellow poplar (Figure 3-8). A 95% inclusion limit was used for the shear stress, rather than the mean, to help ensure shearing of the timber between keys was not a limiting factor. $F_{v_{0.95}}$ was calculated by

$$F_{v_{0.95}} = F_{v_{AVG}} - \Phi^{-1}[0.95]\left(F_{v_{AVG}} COV\right) \tag{3-3}$$

where $F_{V_{AVG}}$ is 790 psi with a coefficient of variation (COV) of 0.14 (FPL, 1999) and $\Phi^{-1}[0.95]$ is the inverse standard normal value at a 95% confidence level (1.645). A linear distribution of the shear stress (Figure 3-8) was assumed, based on the connection detailing recommendations from Appendix E of the NDS (AF&PA, 2005), although a uniform stress distribution is more common in design practice. Use of the linear shear stress distribution appears to be a conservative approach, although it may be overly conservative due to the relatively low shear modulus of timber compared to other materials. Evaluating equations (3-3) and (3-2) resulted in $F_{V_{0.95}}$ = 608 psi and a minimum shear key spacing s_{MIN} of 7.04 inch.

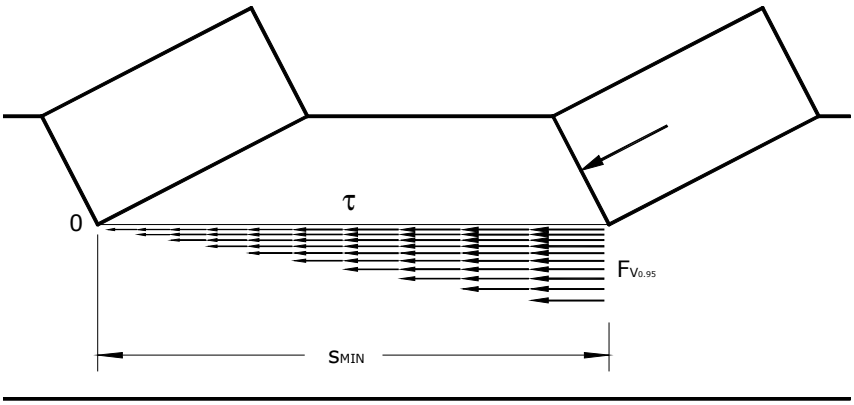

Figure 3-8 Assumed shear stress distribution at shear key notch

The maximum horizontal shear stress τ in a rectangular beam of breadth b and depth d subjected to bending is

$$\tau_{max} = \frac{3V}{2bd} \tag{3-4}$$

which occurs at midheight of the beam, where V is the vertical shear in the beam. We can write equation (3-4) in terms of shear flow q

$$q = \tau_{max} b = \frac{3V}{2d} \tag{3-5}$$

Due to a uniform shear distribution in the end sections of the keyed beam (Figure 3-7), the maximum spacing between shear keys s_{MAX} was determined by

$$s_{MAX} = \frac{P}{q} = \frac{2dP}{3V} \tag{3-6}$$

The vertical shear in the beam was determined based on the maximum point loads a simple stacked beam could carry based on the loading configuration shown in Figure 3-7. The maximum vertical shear V was determined to be 6,700 pounds using a modulus of rupture value of 6,000 psi for unseasoned yellow poplar (FPL, 1999). Using the point loads for a simple stacked beam acts as an upper bound on maximum shear key spacing; a full depth beam would require a smaller maximum shear key spacing. The maximum spacing between shear keys s_{MAX} was 23.96 inch.

With a minimum shear key spacing of 7.04 inches and an approximate maximum shear key spacing of 23.96 inches, a spacing of 18 inches was chosen for the test configuration (Figure 3-6). This larger shear key spacing (18 inches vs 7.04 inches min) was used to help ensure block shear of the timber between shear keys would not control when the Parallam material was used for shear keys.

4 Small Scale Testing

The small scale testing, which is discussed later in this section, is broken into the following categories:

- Yellow poplar (Lirodendron tulipifera) modulus of elasticity and modulus of rupture
- Screw axial stiffness and withdrawal capacity
- Screw shear stiffness
- White oak (Quercus alba) and Parallam PSL key stiffness
- Moisture content and specific gravity

These particular tests were conducted in order to verify that the parameters used in the interlayer slip model as well as the shear key stiffness models accurately represented the true behavior of the materials used in the full scale testing.

4.1 Testing Apparatus

All small scale load testing was conducted using a Tinius Olsen 120k Super L loading frame with 1.2-k, 6-k, 24-k, and 120-k load range settings. A 5-VDC rotational potentiometer was the sole apparatus used to determine applied load from the Tinius Olsen during testing. The limited number of windings in the rotational potentiometer resulted in load data being measured in set increments of

$$MEASURED\ LOAD\ INCREMENT = \frac{LOAD\ RANGE}{270} \tag{4-1}$$

Linear movement was determined using two Sensotec 30-VDC linearly variable displacement transducers (LVDTs). The LVDTs had a total 4 inch of measurable stroke, with a resolution of 0.001 inch.

An Optim MEGADAC 3415AV data acquisition system was used for recording the voltage readings from the rotational potentiometer and LVDTs. The MEGADAC also functioned as the power sources for the measuring equipment. Optim TCS 3.2 Windows based software was used to record the data as a tab delimited text format file at one second intervals during the testing.

4.2 Modulus of Elasticity and Modulus of Rupture

4.2.1 Static Bending Test Procedure

Static bending tests were conducted on small clear specimens of yellow poplar following ASTM D147 (ASTM, 2007). A total of eight clear 2 inch by 2 inch by 30 inch straight grained specimens were point loaded at the middle of a 28 inch span. Load was applied at a rate of 0.10 in/minute until failure. Load measurements were taken on the 6k load range and two displacement measurements of crosshead motion were recorded. The test set-up can be seen in Figure 4-1.

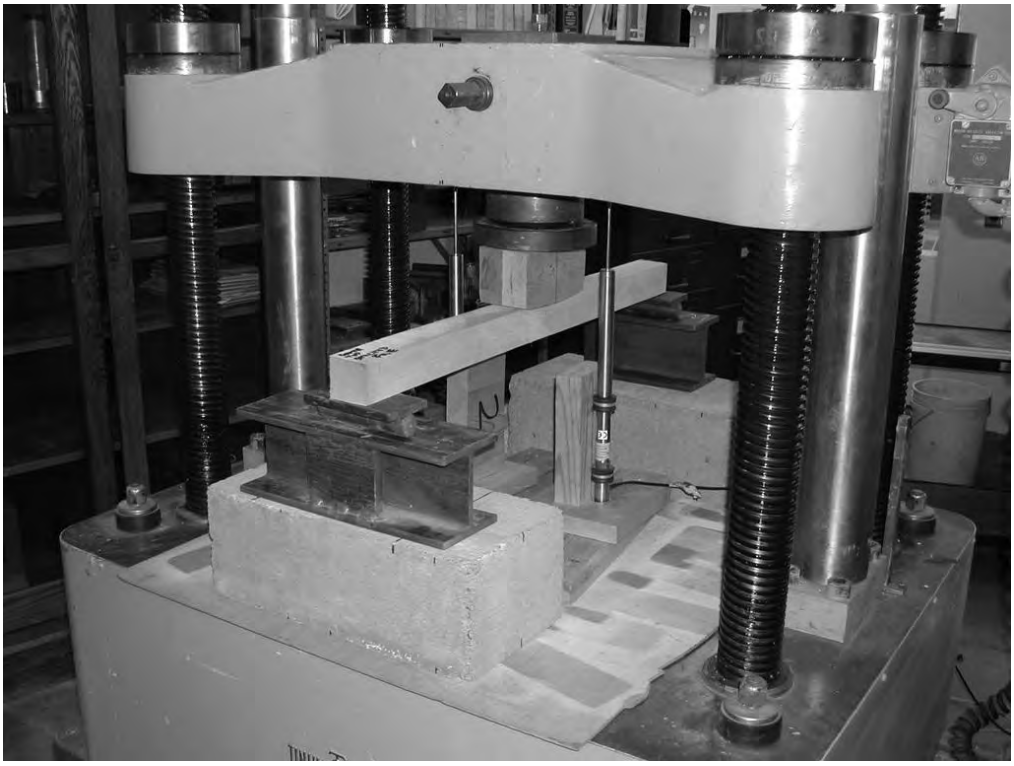

Figure 4-1 Setup for static bending tests

4.2.2 Static Bending Test Results

Eight static bending tests were conducted on yellow poplar samples. Failure often initiated as a compression side failure followed by a simple-tension or brash-tension failure at ultimate load (Figure 4-2). The definitions of simple-tension and brash-tension failures can be found in ASTM D143 (ASTM, 2007), with a brash-tension failure being a failure that has a small failure surface compared to a simple-tension failure. The average modulus of rupture was 10,444 psi when adjusted to 12% moisture content, according to the procedure outlined in section 4.6.1. The published value for modulus of rupture in the Wood Handbook is 10,100 psi (FPL, 1999). The average modulus of elasticity, again adjusted to 12% moisture content, was 1,459,000 psi, with the Wood Handbook value

being 1,580,000 psi. The results of the static bending tests are in Table 4-1 with load-displacement plots shown in Figure 4-3.

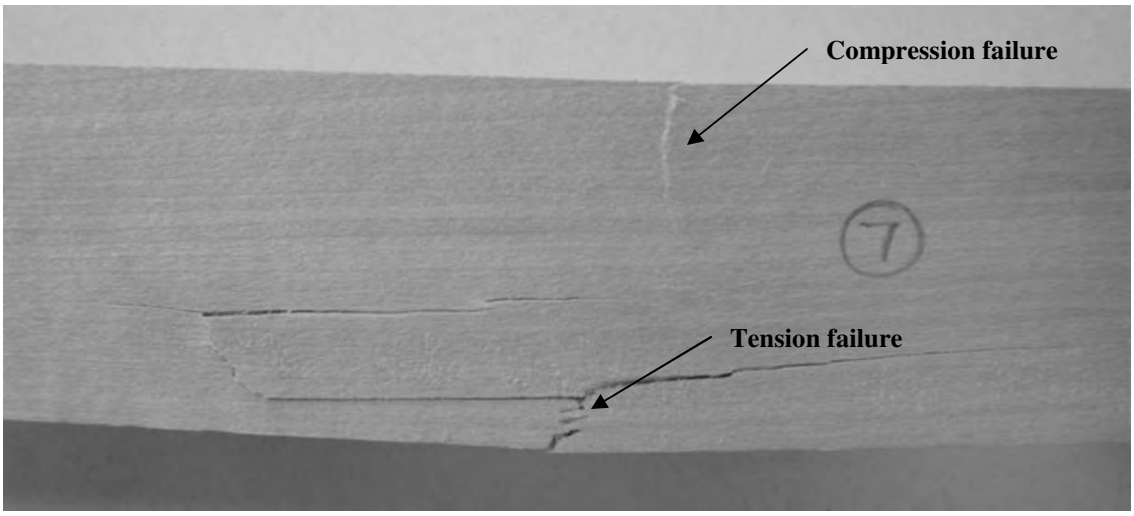

Figure 4-2 Static bending test compression failure followed by a simple-tension failure

Table 4-1 Static bending test results

Test	MC	SG	K	Failure Type	Failure Load	Test MOE	Adjusted MOE (12%)	Test MOR	Adjusted MOR (12%)
			lb / in		*lb*	*psi*	*psi*	*psi*	*psi*
1	8.0%	0.435	3715	Simple Tension	1748	1532000	1476000	10473	10685
2	8.0%	0.420	4180	Brash Tension	2084	1636000	1434000	12089	10320
3	8.2%	0.465	3874	Splintering Tension	1927	1501000	1562000	11106	11433
4	8.1%	0.468	4483	Simple Tension	2219	1652000	1571000	12360	11512
5	8.0%	0.420	3899	Simple Tension	1569	1534000	1434000	9162	10318
6	8.1%	0.425	3720	Compression	2039	1470000	1448000	11918	10434
7	15.6%	0.424	3628	Compression	1681	1381000	1443000	9551	10398
8	15.8%	0.374	3366	Simple Tension	1166	1363000	1300000	6894	9168
					Average	1509000	1459000	10444	10534
					St. Dev	104892	84809	1853	734
					COV	0.070	0.058	0.177	0.070

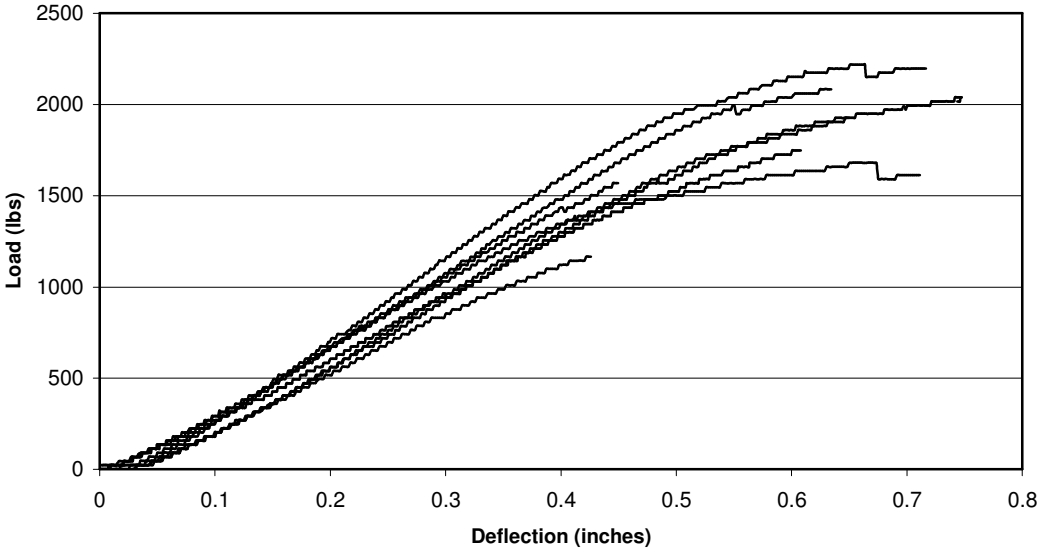

Figure 4-3 Load-displacement plots for static bending tests

4.2.3 Adjustment of Modulus of Elasticity for Shear Deformation

The modulus of elasticity determined from bending tests includes the effect of shear deformation. This modulus of elasticity is commonly referred to as the apparent modulus of elasticity, E_f. To calculate an actual longitudinal modulus of elasticity, E_L, the shear deformation component would need to be removed. The Wood Handbook suggests the longitudinal modulus of elasticity can be approximated by merely increasing the apparent modulus of elasticity by 10% (FPL, 1999).

Gromala proposed a more exact method using test data from a center-point loading (Gromala, 1985). His method was based on the assumption that there is even shear flow throughout a center-point loaded beam and that the material had uniform properties about its length. ASTM D198 includes Gromala's more rigorous method, which could be used as a guideline to adjust the apparent modulus of elasticity to the

actual longitudinal modulus of elasticity in this testing (ASTM, 2007). A modified procedure for this research is outlined in Appendix E, although with a limited number of small-scale and large-scale tests, accurately determining the shear modulus and longitudinal modulus of elasticity was not possible.

The current interlayer slip model solution does not explicitly differentiate between the compressive and tensile longitudinal modulus of elasticities or the bending modulus of elasticity. The interlayer slip model also does not take into account shear deformations, so an effective modulus of elasticity is used in this research. Also, the modulus of elasticity values published in most timber design references are the effective modulus of elasticity (AF&PA, 2005).

4.3 Screw Axial Stiffness and Withdrawal Capacity

Screws are used to provide the clamping force required to ensure layers of the built-up beam do not separate due to prying action of the shear keys. For this research, OMG Fastenmaster 13.5in Double Thread LogHog screws (shown in Figure 3-5) were used to provide the clamping force. See section 3.3.1 for a discussion of the different connector types and why LogHog screws were chosen. Due to slightly different pitches in the lower and upper portions of the threaded shaft, the LogHog screws are axially prestressed once installed. The prestressing helps ensure tight mating of the two layers of the beam. In order to accurately account for their behavior in the shear key stiffness model, their axial stiffness needed to be determined.

4.3.1 Screw Withdrawal Test Procedure

The test procedure for screw withdrawal tests is documented in ASTM D1761 (ASTM, 2007). In place of a withdrawal tests, push through tests were instead conducted, as the screws used in this testing (Double-Thread LogHogs, Figure 3-5) have a straight shaft. The push through testing allowed for tests to be run entirely in compression, without affecting the test mechanics.

Double Thread LogHog screws were installed into yellow poplar test specimens such that their second set of threads (those closer to the head) were set into the wood. Wood specimens varied in thickness from 2 inch to 3 inch, and the threaded portions of the screw shaft were visible on both faces of the screw. The wood sample was supported on a hollow test frame which is shown in Figure 4-4. Load was applied axially to the screw head through an aluminum bearing plate. Testing was conducted at a displacement-controlled rate of approximately 0.05 in/min until ultimate load was reached. Load and cross-head motion, averaged at two spots, were recorded at one second intervals. Load measurements were taken in the 6-k load range.

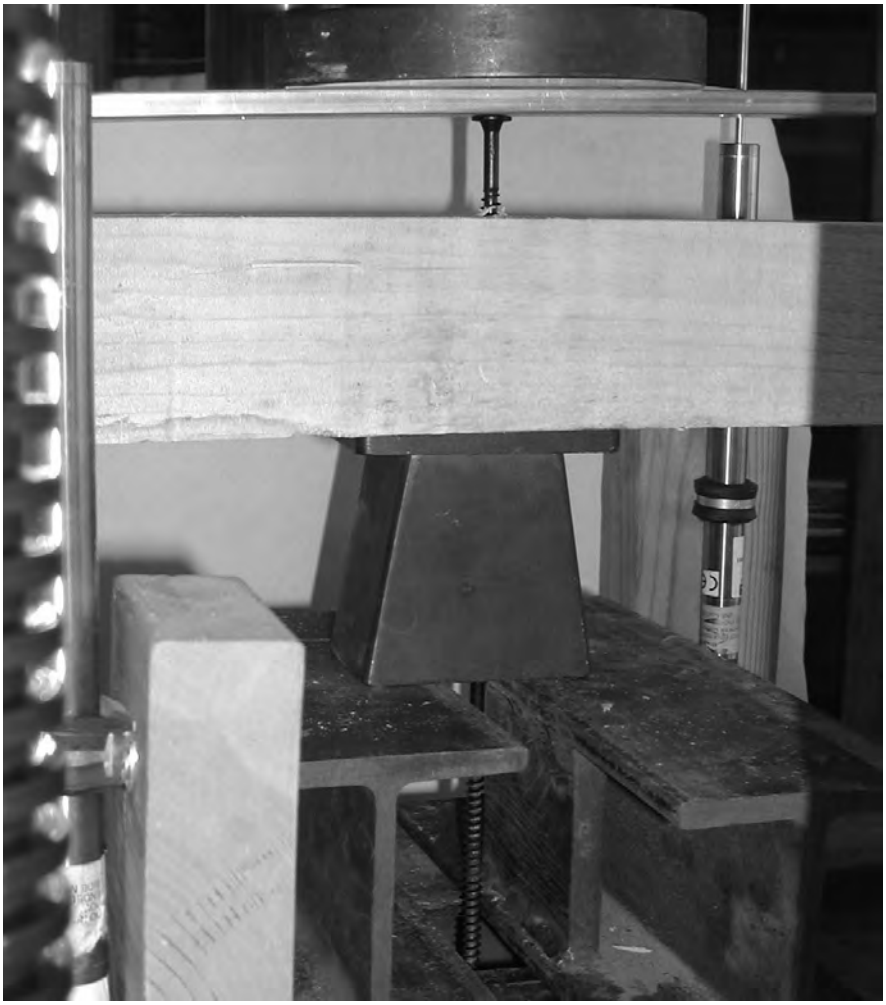

Figure 4-4 Screw push-through (e.g. withdrawal) testing

4.3.2 Screw Withdrawal Test Results

Twelve tests were conducted in 2 inch thick material, and six tests were conducted in 3 inch thick material for a total of eighteen tests. Each 2 inch piece of material was used for two tests, and each 3 inch piece of material was used for three tests, with a minimum of six inches of space between subsequent withdrawal (push-through) locations. The ultimate withdrawal capacity averaged 1,011-lbs per inch of penetration, with an axial stiffness of 16,435 lb/in/in. A summary of the results is shown in Table 4-2.

Results showed a direct linear relationship between the axial stiffness and the length of threads in the material. The ultimate withdrawal capacity of the screws occurred at approximately the same total deformation, regardless of the length of screw penetration. Load-displacement plots can be seen in Figure 4-5.

Table 4-2 Screw withdrawal test results

Test	MC	SG	K *lb / in*	K *lb / in / in*	Ultimate Load *lb*	Ultimate Load *lb / in*
1	12.1%	0.43	30835	16276	2034	1074
2			38181	20090	1972	1038
3	13.3%	0.426	33573	17858	1905	1013
4			22093	11674	1815	959
5	12.6%	0.428	25933	13211	1972	1005
6			37978	19622	1837	949
7	13.3%	0.424	32041	18377	1748	1002
8			31627	18006	1726	983
9	11.0%	0.42	32377	18704	1592	920
10			27038	15615	1615	933
11	12.5%	0.421	25009	14532	1682	977
12			25294	14757	1593	929
13	15.6%	0.469	43528	14585	3297	1105
14			50272	16904	3249	1093
15			54636	18343	3361	1128
16	15.2%	0.457	44707	14990	3114	1044
17			44932	14960	3047	1015
18			52168	17332	3091	1027
			Average	16435		1011
			St. Dev	2294		62
			COV	0.140		0.061

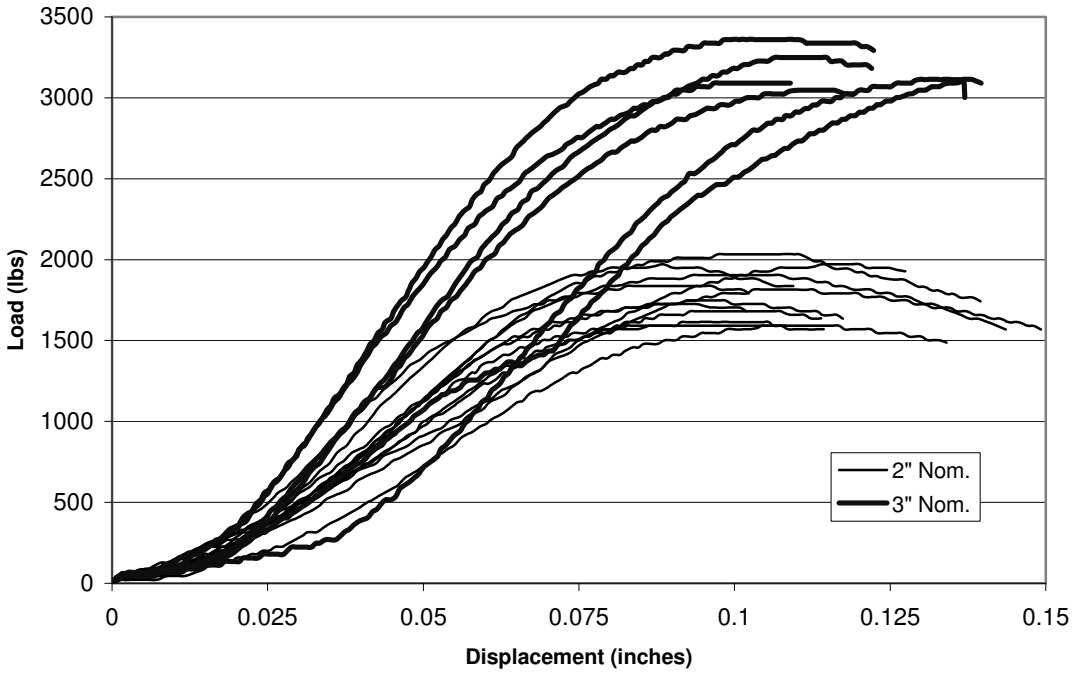

Figure 4-5 Load-displacement plots for screw withdrawal tests

After ultimate capacity was reached in the screw withdrawal tests, the screws continued to resist considerable axial force. Several tests were continued well past the ultimate load (to approximately 0.5 inch of displacement), with some load carrying ability still remaining. Figure 4-6 shows the deformation of these tests. Excessive displacement revealed a plug of wood that was being pulled through by the threads. While not within the scope of this research, quantifying the size and shape of this shear plug may be a method to predict the axial stiffness and capacity of threaded fasteners without resorting to physical testing.

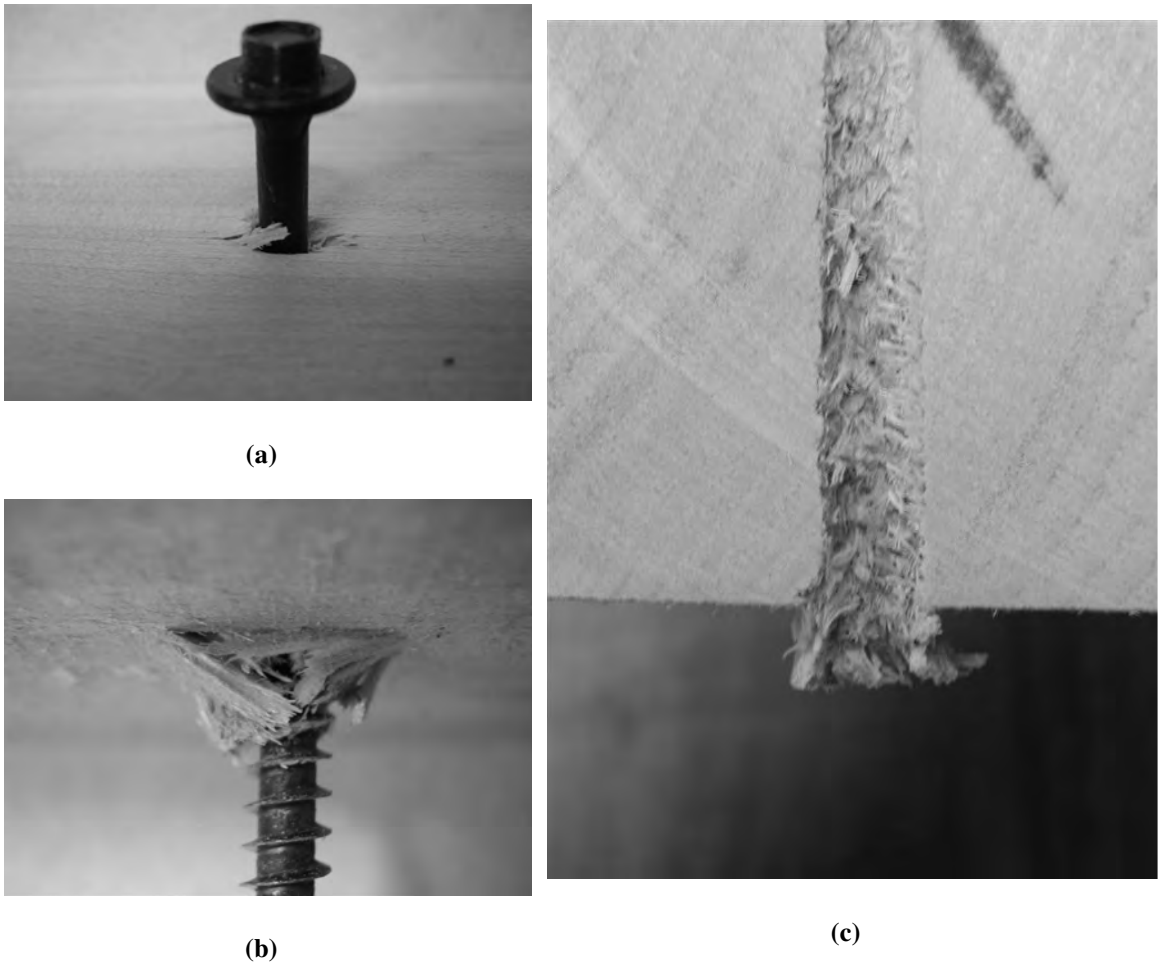

(a)

(b)

(c)

Figure 4-6 Screw withdrawal testing showing (a) entry of screw, (b) exit of screw, and (c) section through screw hole after screw had been removed.

4.4 Shear Key Stiffness

In order to verify the accuracy of the stiffness model developed in section 2.5, tests were conducted on various configurations and materials of shear keys. Based on material availability, two tests of each shear key configuration, shown in Figure 3-3, where conducted using 2.5 inch thick white oak keys as well as 2.5 inch thick Parallam PSL keys. The white oak keys were installed such that they were compressed

perpendicular-to-the-grain, while the Parallam PSL keys were compressed parallel-to-the-grain. The shear keys configurations are shown in Figure 3-1.

For each test, three yellow poplar timbers were fabricated with pairs of shear key notches to accept the shear keys. As the yellow poplar timbers were not completely seasoned, all end grain was sealed with end-grain sealer shortly after cutting. Each mating surface of the timbers was planed immediately before securing the test specimen together with LogHog screws.

Four LogHog screws were used for each connection, as determined in section 3.3.3. In order to eliminate interference between screws from opposing faces, the screw placements were staggered, although the distance from the bearing face of the notch to the centroid of the screws remained 2 inch. The LogHog screws available for testing were 13.5 inch long, which required the head to be left slightly proud of the timbers. The entire threaded portions of the screw shafts were installed into the timbers. The test set-up used for both white oak shear key and Parallam PSL shear key tests are shown in Figure 4-7 and Figure 4-8. White oak keys were installed using a pair of 3-lb drill hammers such that all shear key bearing faces were in full tight contact with the adjoining timber bearing faces. The Parallam PSL keys were driven in a similar fashion, although driving was halted early if the wedging action of the shear keys caused the layers to start to visibly slip.

Compressive testing was conducted at a displacement-controlled rate of 0.10 in/min until no additional load could be carried. The horizontal spreading of the test sample was measured across the shear keys during the testing with an LVDT. The vertical displacement (slip of the layers) for each test was measured along the length of

the timbers again using an LVDT. The points of measurement can be seen as black dots in Figure 4-7 and Figure 4-8. The measurements of vertical displacement as well as the horizontal spreading of the layers provide an average for the two shear key assemblies. Cross-head motion of the test frame was not recorded. Load measurements were taken on the 120k load range. The test specimen was visually aligned under the load head, with no additional effort made at ensuring the specimen remained aligned and centered during testing. Ends of the timbers were coated with Anchorseal end-grain wax sealer to retard drying of the timbers through the end-grain, and also helped reduce friction between the bearing plates and end of the timbers. After testing, moisture content and specific gravity tests were conducted on the three timbers, as well as each shear key.

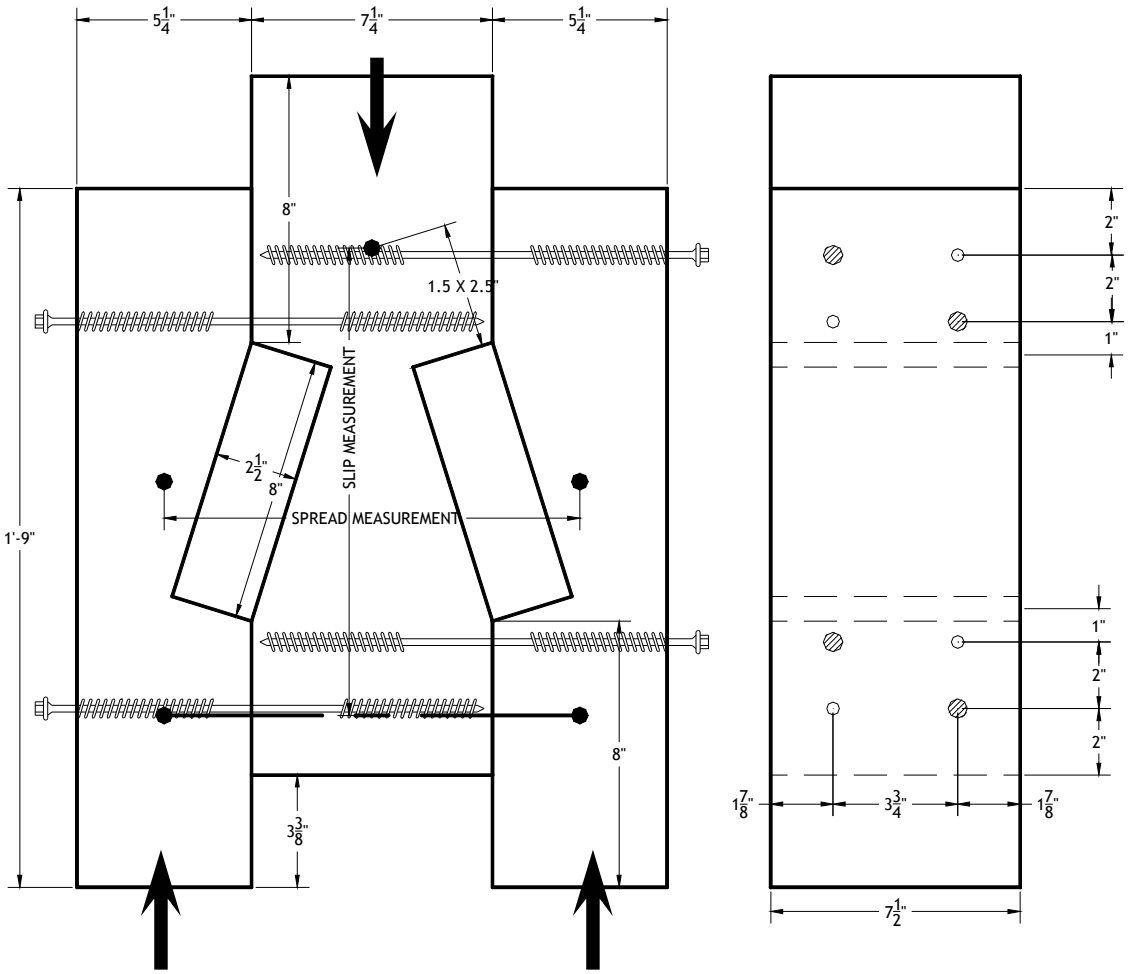

Figure 4-7 8in long shear key test configuration

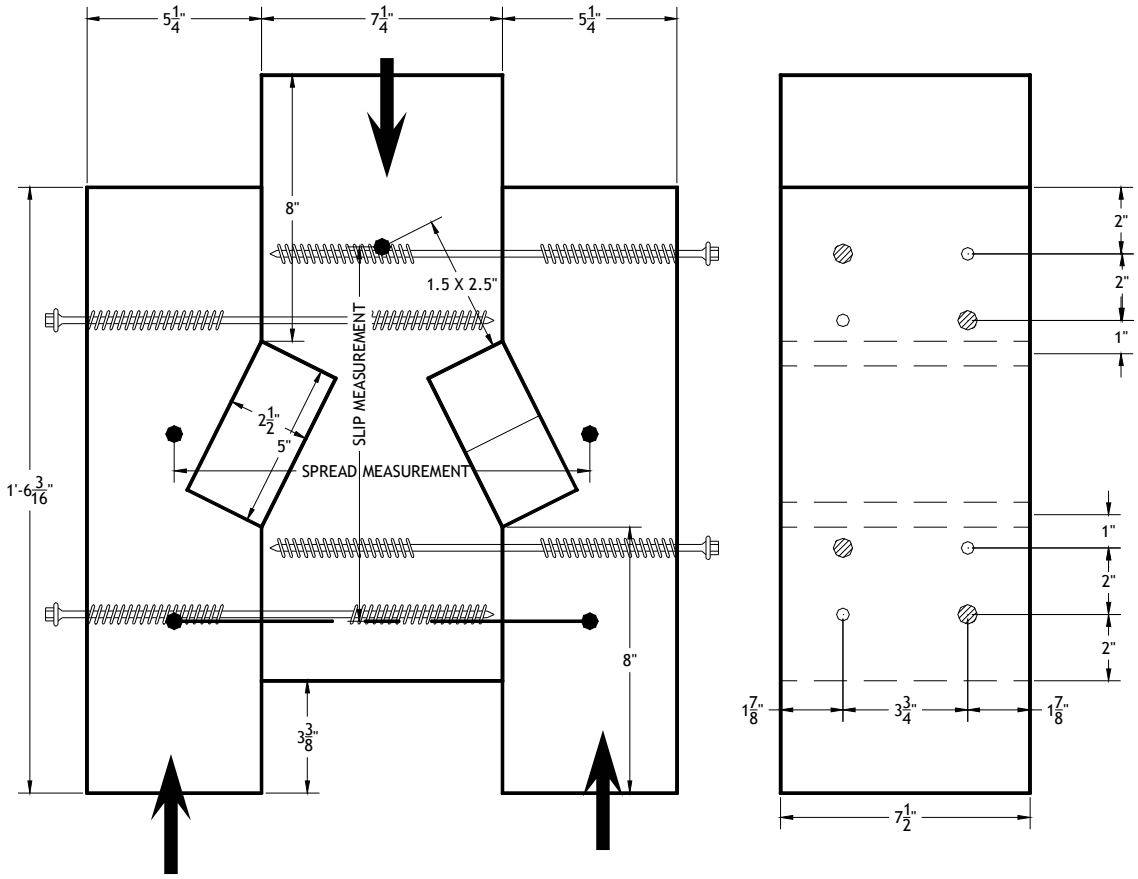

Figure 4-8 5in long shear key test configuration

4.4.1 White Oak Shear Key Test Results

Four white oak shear key tests were conducted (two tests with 8 inch keys, two tests with 5 inch keys). The average axial stiffness per key for the 8in key system was 210,250 lb/in while the average axial stiffness for the 5 inch key system was 160,000 lb/in. The results can be found in Table 4-3, while Figure 4-9 shows the load-vertical displacement plots (slip between the members) for these tests. The initial stiffness of the test configuration, up until 3-4 kips, was higher than the subsequent main stiffness of the joint. This higher initial stiffness was attributed to the small stiffness contribution from LogHog screws used for clamping. Further discussion of this is included in section 4.5.

Several pieces of oak shear key material appeared to have substantial iron staining. These pieces were used for the shear key material for test number three. After conducting moisture content and specific gravity testing, as well as a close visual examination of the material, the iron-stained material appeared to be northern red oak (*Quercus rubra).*

Table 4-3 Results from white oak shear key tests

Key Test	Key Size	Wedge Stock	Wedge MC	Timber MC	SG Wedge	SG Timber	Actual Stiffness *lb / in*	Failure
1	2.5 x 8	WO	28.8%	16.2%	0.643	0.453	369000	Screw Breakage
2	2.5 x 8	WO	31.3%	16.8%	0.669	0.468	472000	Excessive Deformation
3	2.5 x 5	NRO	17.8%	15.5%	0.603	0.446	348000	Screw Withdrawal
4	2.5 x 5	WO	30.3%	13.4%	0.665	0.435	292000	Screw Withdrawal
					2.5 x 8	Average	420500	
					2.5 x 5	Average	320000	

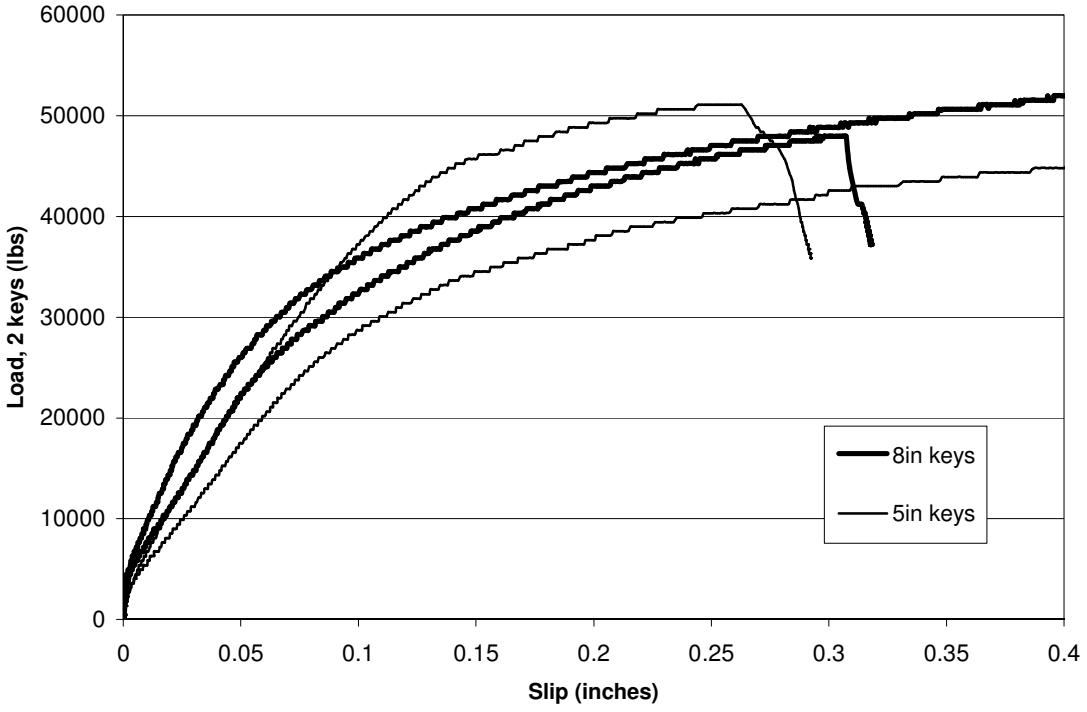

Figure 4-9 Load-slip plots for white oak shear key tests

The first two white oak key tests, which included the 8 inch shear keys, exhibited very little separation between the timbers as the shear keys were compressed. The second two key tests, which used the 5 inch shear keys, exhibited substantial separation between the layers, and the failure mechanism at maximum load was withdrawal of the clamping screws. This finding coincides with the anticipated behavior, as shorter keys require substantially more clamping force than the longer keys to resist the same force. Load-spreading displacement plots are included in Figure 4-10. A LVDT error was encountered during the third shear key test, so that plot is not included.

Audible "ticks" were noticed during the entire duration of the 8 inch shear keys tests. These ticks occurred at intervals of several seconds. With the 5 inch shear key tests, the noise was again heard near the beginning of the tests, but quickly diminished as the test specimen began to carry load. The noise was attributed to the build up and release of friction forces between the layers.

After the testing was complete and the test samples were disassembled, the 8 inch shear keys exhibited uniform indentation of 0.03-0.04 inches where they bore against the timber end grain. The 5in shear keys, which rolled slightly and forced the layers to separate, showed uneven bearing across the key face; one edge had no noticeable damage, while the other edge was compressed approximately 0.05 inches. The deformed keys can be seen in Figure 4-12(a) and Figure 4-12(b), respectively. No deformation of the timber end grain was noticeable in either case.

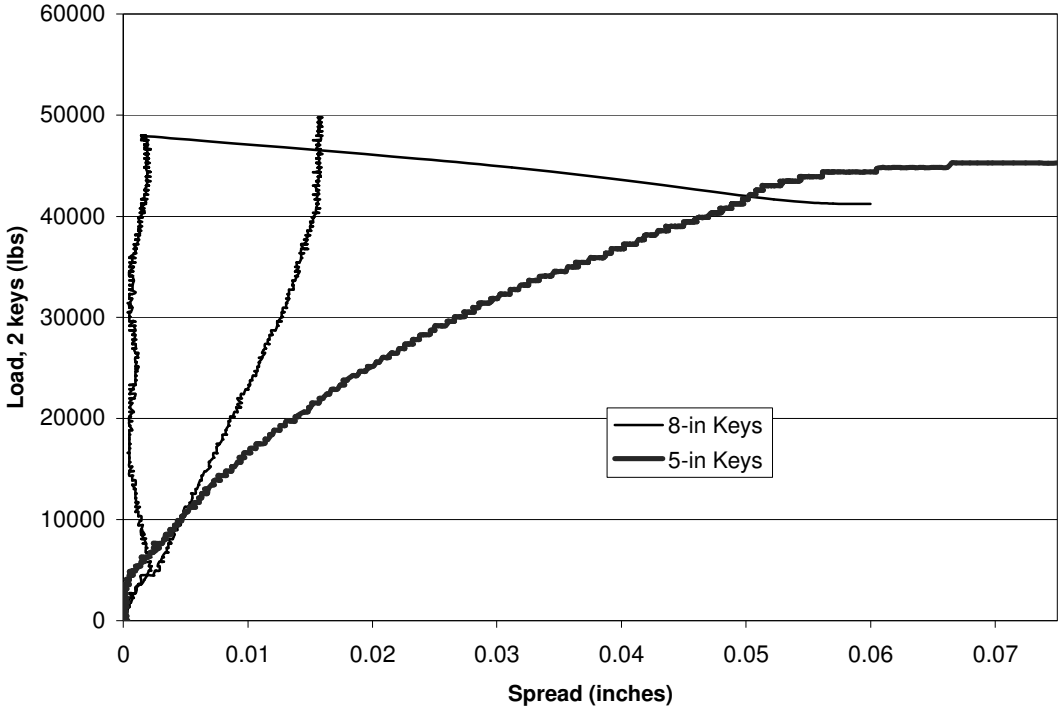

Figure 4-10 Load-spread plots of white oak shear key tests

4.4.2 Parallam PSL Shear Key Test Results

In a similar fashion to the white oak shear key tests, four Parallam PSL shear key tests were conducted (two tests with 8 inch keys, two tests with 5 inch keys). The average axial stiffness per key for the 8 inch keys was 590,750 lb/in while the average axial stiffness for the 5 inch keys was 449,000 lb/in. The results can be found in Table 4-4, while Figure 4-11 shows the load-slip plots for these tests.

The load-slip plots for the Parallam PSL tests did not exhibit the initial high stiffness behavior that was evident in the white oak shear key tests. During the installation and driving of the shear keys, considerable force was required to drive the keys in an attempt to achieve fully mated bearing faces. The wedging action of the shear

keys when driving caused the specimens to begin slipping, which negated the initial stiffness from the dowel bearing of the LogHog screws.

Table 4-4 Results from Parallam PSL shear key tests

Key Test	Key Size	Wedge Stock	Wedge MC	Timber MC	SG Wedge	SG Timber	Actual Stiffness *lb / in*	Ultimate Failure
5	2.5 x 5	PSL	0.078	11.1	0.605	0.435	1164000	Screw Withdrawal
6	2.5 x 5	PSL	0.078	11.6	0.602	0.414	632000	Screw Withdrawal
7	2.5 x 8	PSL	0.080	11.5	0.604	0.424	1146000	Screw Withdrawal
8	2.5 x 8	PSL	0.079	11.1	0.606	0.409	1217000	Screw Withdrawal
					2.5 x 5	Average	898000	
					2.5 x 8	Average	1181500	

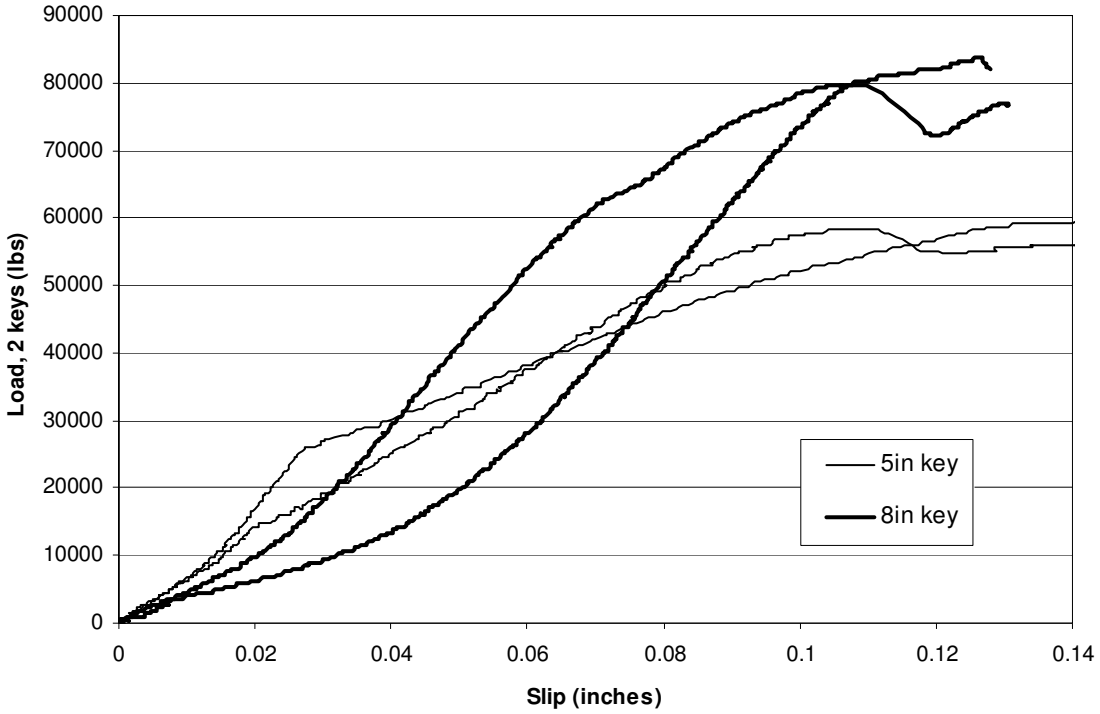

Figure 4-11 Load-slip plots for Parallam PSL shear key tests

Unlike the white oak tests, both the 5 inch and 8 inch key tests caused the layers to separate, with very little noticeable deformation of the shear keys. Separation of layers

occurred as a prying apart of the layers on one side of the shear key, except with test number six. The layers separated nearly uniformly on both sides of the key, with bending in the side member being evident. See Figure 4-12(d) and Figure 4-12(e). The specific gravity for the side piece exhibiting this behavior in test number six was 0.340; considerably lower than the center piece or the other side piece. Near the maximum load, crushing of the timber end-grain was evident in all of the tests, but with no noticeable deformation of the Parallam PSL keys.

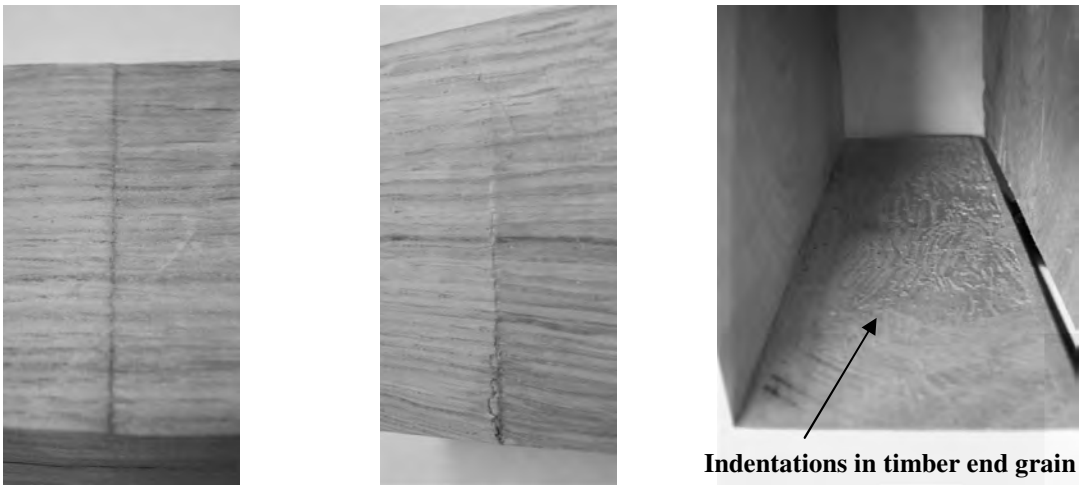

(a) (b) (c)

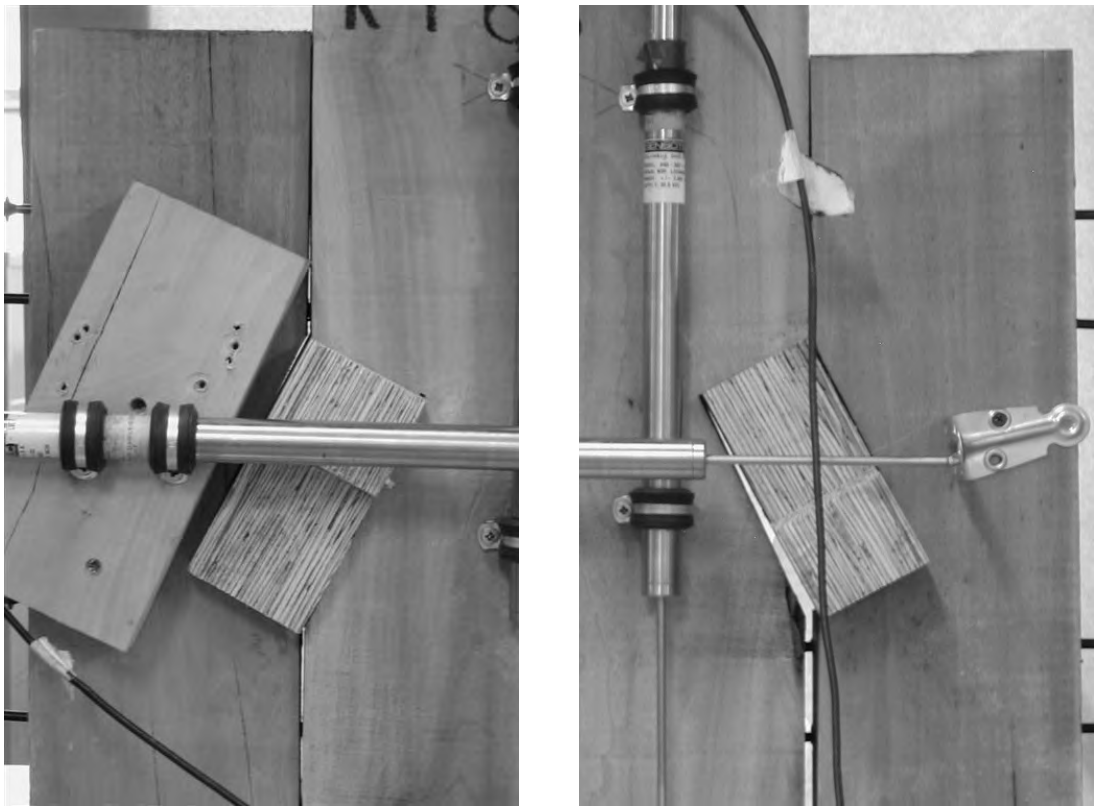

(d) (e)

Figure 4-12 (a) 8 inch white oak key compressed uniformly, (b) 5 inch white oak key with uneven compression due to rolling, (c) compression of the timber end-grain when using Parallam PSL keys, (d) uniform spreading of side member and (e) uneven spreading with rolling of side member for Parallam PSL key tests.

4.4.3 Shear Key Test Comparison to Stiffness Model

After the shear key tests were conducted, a comparison was made to the anticipated stiffness based on the shear key stiffness model that was developed in section 2.5.1. Tabulated modulus of elasticity values from the Wood Handbook (FPL, 1999) adjusted to the moisture content of the test specimens were used when calculating the anticipated stiffness. The calculation procedure is included in Appendix F.

The actual key stiffness from the physical testing and the calculated key stiffness values are included in Table 4-5. There appears to be reasonable agreement, given the high variation in moisture content in the oak wedge stock, with the exception of test number 5. This load-slip plot for this test included an initial stiff component, followed by a longer, less stiff component (Figure 4-11). The tabulated stiffness in Table 4-5 is based off of this initial stiff component, which may be capturing some other unanticipated behavior. Disregarding this outlier, percentage differences between actual and calculated stiffnesses are within the expected variations in modulus of elasticity (FPL, 1999).

Table 4-5 Key stiffnesses from physical tests as well as the theoretical model

Key Test	Key Size	Wedge Stock	Wedge MC	Timber MC	Actual Stiffness *lb / in*	Calculated Stiffness *lb / in*	Difference *%*
1	2.5 x 8	WO	28.8%	16.2%	369000	359400	-2.6%
2	2.5 x 8	WO	31.3%	16.8%	472000	358800	-24.0%
3	2.5 x 5	NRO	17.8%	15.5%	348000	394600	13.4%
4	2.5 x 5	WO	30.3%	13.4%	292000	358900	22.9%
5	2.5 x 5	PSL	7.8%	11.8%	1164000	643000	-44.8%
6	2.5 x 5	PSL	7.8%	11.6%	632000	643800	1.9%
7	2.5 x 8	PSL	8.0%	11.5%	1146000	1236600	7.9%
8	2.5 x 8	PSL	7.9%	11.0%	1217000	1241600	2.0%

The analytical shear key stiffness model was based on a mechanics approach, with only two other assumptions in behavior. The first assumption was the ratio of the longitudinal modulus of elasticity to the perpendicular modulus of elasticity of the timbers (modular ratio) and shear keys ($E_{\parallel} = 12E_{\perp}$). The second assumption was the depth of influence for the compression zone in the timber (2x the key width). In order to verify these assumptions, a least-squares error minimization routine was conducted on the calculated stiffness by varying the modular ratio as well as the depth of influence. The minimum sum of the squares of the difference between the actual and calculated stiffnesses was at a modular ratio of 12.71 and a depth of influence of 2.24 times the key width. This compares quite closely with the initial estimate of 12 and 2, respectively.

4.5 Screw Shear (Lateral) Stiffness

The screws used in the keyed beam are used exclusively for their ability to clamp the layers together, and thus their axial stiffness was of great concern. These screws can also directly resist the slipping between the layers by carrying load perpendicular to their shaft. Nails, bolts, and lag screws are common connectors used in wood connections that are loaded in a lateral fashion. Rather than attempt to predict the lateral stiffness of the LogHog screws, physical testing of a group of connectors was performed.

4.5.1 Screw Shear Test Procedure

Two test specimens, similar to those shown in Figure 4-7, but without the shear keys, were fabricated using the same number and placement of the LogHog screws. The location of the screws exceeds the required end and edge distances outlined within the NDS (AF&PA, 2005). The compressive testing was conducted at a displacement-controlled rate of 0.10 in/min until 0.5 inch of displacement was reached. The horizontal spreading of the test sample was measured across the shear keys during the testing with an LVDT. The vertical displacement (slip of the layers) for each test was measured along the length of the timbers again using an LVDT. Load data was recorded from the 24k load range.

4.5.2 Screw Shear Specimen Test Results

Loading of the screw shear test specimens resulted in a bi-linear load-slip plot, as shown in Figure 4-13. The results, which can be found in Table 4-6, showed very high initial stiffness, followed by a much lower final stiffness (approximately $1/10^{th}$ the initial stiffness). While the initial stiffness of the screw shear test specimens are quite high, the transition between the initial and final stiffness begins at a displacement of approximately 0.004in, and the subsequent low final stiffness remains linear for the range of displacements anticipated in the keyed beam tests. When compared to the total stiffness of the white oak and Parallam PSL shear key test specimens, the contribution from the clamping screws appears quite small, validating the exclusion of their lateral stiffness from the keyed beam analysis. This assumption to ignore the screw's stiffness may be

overly conservative if a larger quantity of screws, or screws with a higher lateral stiffness, were used. No spreading of the layers was observed or recorded.

Table 4-6 Results from screw shear tests

Test	Timber MC	SG Timber	Initial Stiffness *lb / in*	Final Stiffness *lb / in*
9	9.8%	0.442	2235000	23200
10	10.2%	0.453	2404000	20900
		Average	2319500	22050

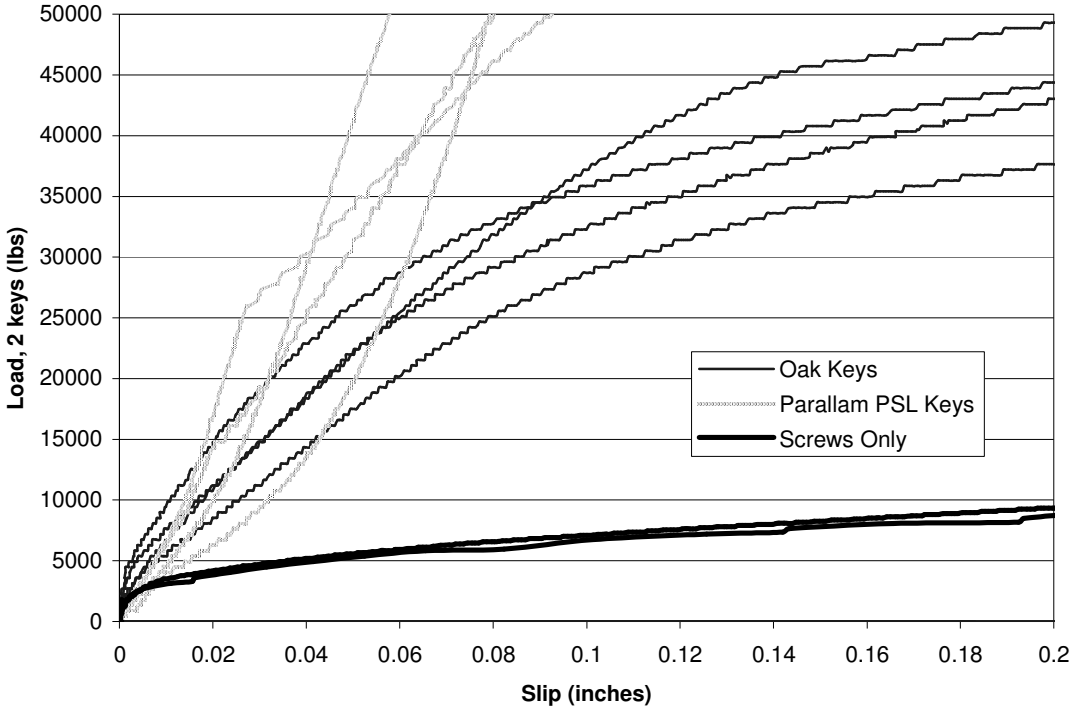

Figure 4-13 Load-slip plots for screw shear specimen tests

Each of the screws in the screw shear test specimens yielded in bending at two plastic hinge points, one on each side of the shear plane (See Figure 4-14). This yield mode is commonly referred to as the "Mode IV" yield mode, based on yield limit modes

described in the NDS (AF&PA, 2005). Localized crushing of the wood fibers near the shear planes was also observed, which is shown in Figure 4-15.

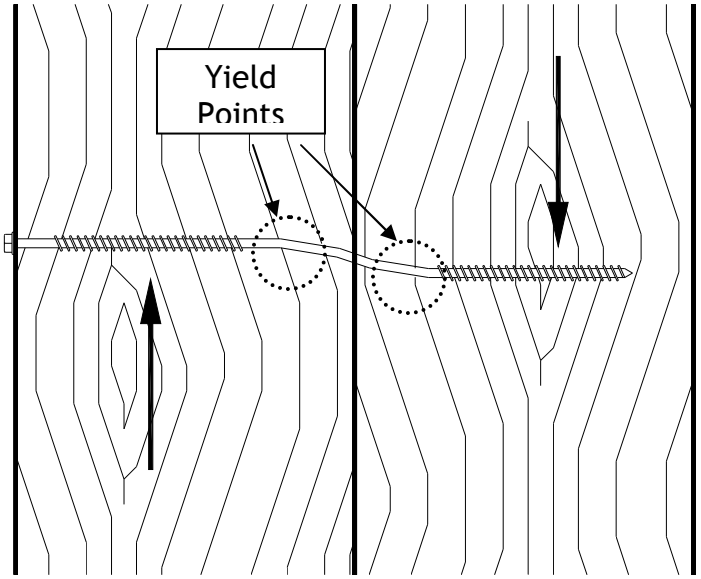

Figure 4-14 Yielding of screw subjected to shear (lateral) loading

Figure 4-15 Localized crushing of wood fibers from screw subjected to shear (lateral) loading

4.6 Moisture Content and Specific Gravity

Moisture content and oven dried specific gravity tests were conducted on each piece of timber used in the physical testing. Moisture content and specific gravity tests were also conducted for each pair of oak wedges. Moisture content tests were conducted according to the secondary oven drying method included in ASTM D4442, and specific gravity tests were conducted according to ASTM D2395 (ASTM, 2007).

Samples were cut from the test specimens within several hours after testing. The samples were taken from a representative section of the material away from any exposed end-grain. The dimensions of each sample were measured to the nearest 0.001" using calipers in two locations in each direction. The initial weight was recorded to the nearest 0.01g using a digital scale. Samples were then placed in a vented lab oven set to 217ºF. Samples were removed from the oven after their weight had stabilized or after 48 hours, whichever was longer. Results for the moisture content and specific gravity tests are included with the individual test data.

4.6.1 Adjustments in Modulus of Elasticity Based on Moisture Content

The moisture content of solid sawn material can vary greatly between the time the wood is harvested and when it is finally put into service. Changes in relative humidity can also affect the moisture content of wood in service. Wood's mechanical properties are sensitive to the moisture content of the material. Common wood science procedure is to use mechanical properties at 12% moisture content. Therefore during the small and

full scale testing, test results were adjusted to 12% moisture content when the material tested was wetter or drier than 12%.

The relationship between moisture content and material properties is described according to the Wood Handbook (FPL, 1999) as

$$E = E_{12\%}\left(\frac{E_{12\%}}{E_{green}}\right)^{\left(\frac{12-MC}{MP-12}\right)} \tag{4-2}$$

where MC is the moisture content in percent and MP is a species-specific constant that is slightly less than the fiber saturation point. Unless otherwise known, $MP = 25$ for most hardwood species. The $E_{12\%}$ and E_{green} values are taken from Table 4-3b of the Wood Handbook. When the moisture content exceeded 25%, which is the fiber saturation point of most hardwoods, the values for green material were used.

4.6.2 Adjustments in Modulus of Elasticity Based on Specific Gravity

The mechanical properties of wood are directly and positively correlated to its density. Thus, woods with higher specific gravities tend to have higher strengths and stiffnesses than those with lower specific gravities. To account for this, the Wood Handbook (FPL, 1999) lists a the relationship for all hardwood species at 12% moisture content as

$$E = 2{,}390{,}000G^{0.7} psi \tag{4-3}$$

which pertains to usage with the white oak material. The Wood Handbook also lists the relationship for all softwood species at 12% MC as

$$E = 2{,}970{,}000G^{0.84} psi \tag{4-4}$$

While yellow poplar is technically a hardwood, it behaves in certain fashions more like a softwood. A graphical comparison of equations (4-3) and (4-4) with the modulus of elasticities determined from the small scale bending tests suggest equation (4-4) is most appropriate for yellow poplar (Figure 4-16).

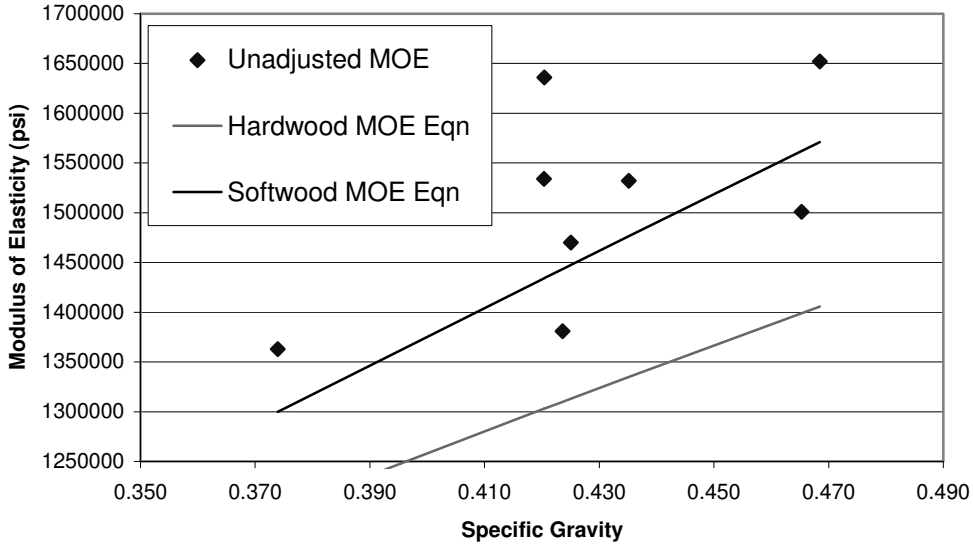

Figure 4-16 Comparison of Wood Handbook MOE equations to test data (typical)

To adjust the tabulated modulus of elasticity from the Wood Handbook for a particular test, the relationships shown in equations (4-3) and (4-4) were used to calculate an appropriate scaling factor and thus an adjusted modulus of elasticity. For white oak, the adjusted modulus of elasticity is calculated as

$$E_{ADJUSTED} = 1{,}780{,}000\left(\frac{239G^{0.70}}{178}\right)psi \qquad (4\text{-}5)$$

where 1,780,000 psi is the Wood Handbook published modulus of elasticity for white oak at 12% moisture content. For yellow poplar, the adjusted modulus of elasticity is calculated as

$$E_{ADJUSTED} = 1{,}580{,}000\left(\frac{297G^{0.84}}{158}\right)psi \tag{4-6}$$

where 1,580,000 is the Wood Handbook published modulus of elasticity for yellow poplar at 12% moisture content.

5 Full Scale Beam Testing

In order to verify the adequacy of the interlayer slip model for modeling the actual behavior of keyed beams, full scale keyed beam testing was conducted. This full scale testing consisted of loading four keyed beams; two with white oak keys, two with Parallam PSL keys. Two additional tests were conducted on a full-sawn beam and a simple stacked beam (no interaction between layers) to verify the upper and lower bounds on stiffness. The loading configuration for all of the beam tests is shown in Figure 3-7, with the keyed beam layout is shown in Figure 3-6.

5.1 Beam Fabrication

All beams were delivered to the testing lab in the unplaned, green (unseasoned) moisture condition sawn to the full dimension. Due to an extended period of time between the delivery of the material and the testing, significant drying, shrinkage, and checking occurred in the timbers. However, any preparation and fabrication of the stacked beams and keyed beams used in the full-scale testing was completed no more than 24 hours before the time of testing.

No preparation was required for the full-sized 8 inch by 16 inch beam, other than ensuring the bearing points were flat and orthogonal to the applied load and support reactions. Flat bearing points were also created on the two 8 inch by 8 inch stacked beams. The contact faces between the two stacked beams were planed with an electric hand planer to ensure uniform contact between layers.

Keyed beams were fabricated by first mating pairs of 8 inch by 8 inch timbers that had similar amounts of crown. Timbers were also oriented such that any seasoning check (or most substantial seasoning check if checked on multiple faces) was on a horizontal face (top or bottom). Although most timbers were relatively free of knots, timbers that exhibited the most knots were used as the top (compression) layer. The mating faces between the two timbers were then planed to ensure uniform contact between layers. The two layers where temporarily secured together when marking key notch locations on the timbers. This temporary clamping ensured all notches were aligned properly along the entire length of the timbers. Notches were cut using a circular saw and cleaned up using a framing chisel. All exposed end-grain was sealed with end-grain sealer after cutting.

Keyed beam layers, once notched (Figure 5-1(a)), were secured together with the LogHog screws about the entire length before any shear keys were installed. Before the screws were installed, the timbers were clamped together, which can be seen in Figure 5-1(b), to ensure uniform contact between layers. The clamping of the timbers together before insertion of the screws follows common timber construction practices. The locations for the LogHog screws can be found in Figure 3-6. Once the layers were fully secured together, the shear key wedges were installed. The shear key wedges were tightened by pounding on opposing wedges immediately before the testing commenced.

(a) **(b)**

Figure 5-1 (a) Paired and notched timbers with checks on the horizontal faces and (b) clamping apparatus used when installing the screws

5.2 Testing Apparatus

Full-scale testing was conducted using a structural steel self-reacting load frame. Load was applied using a MTS 55 kip hydraulic actuator controlled using a MTS 407 Controller. The hydraulic actuator had an available displacement of 10 inches. Load data was recorded from a MTS 661 55 kip force transducer using an IOtech Personal DAQ/55 data acquisition system. Hydraulic actuator movement (stroke) was measured using an in-line LVDT. Slip between the layers, as well as midspan deflection, was measured using two Sensotec 30-VDC LVDTs. All data were recorded to tab delimited text files. The test configuration can be seen in Figure 5-2.

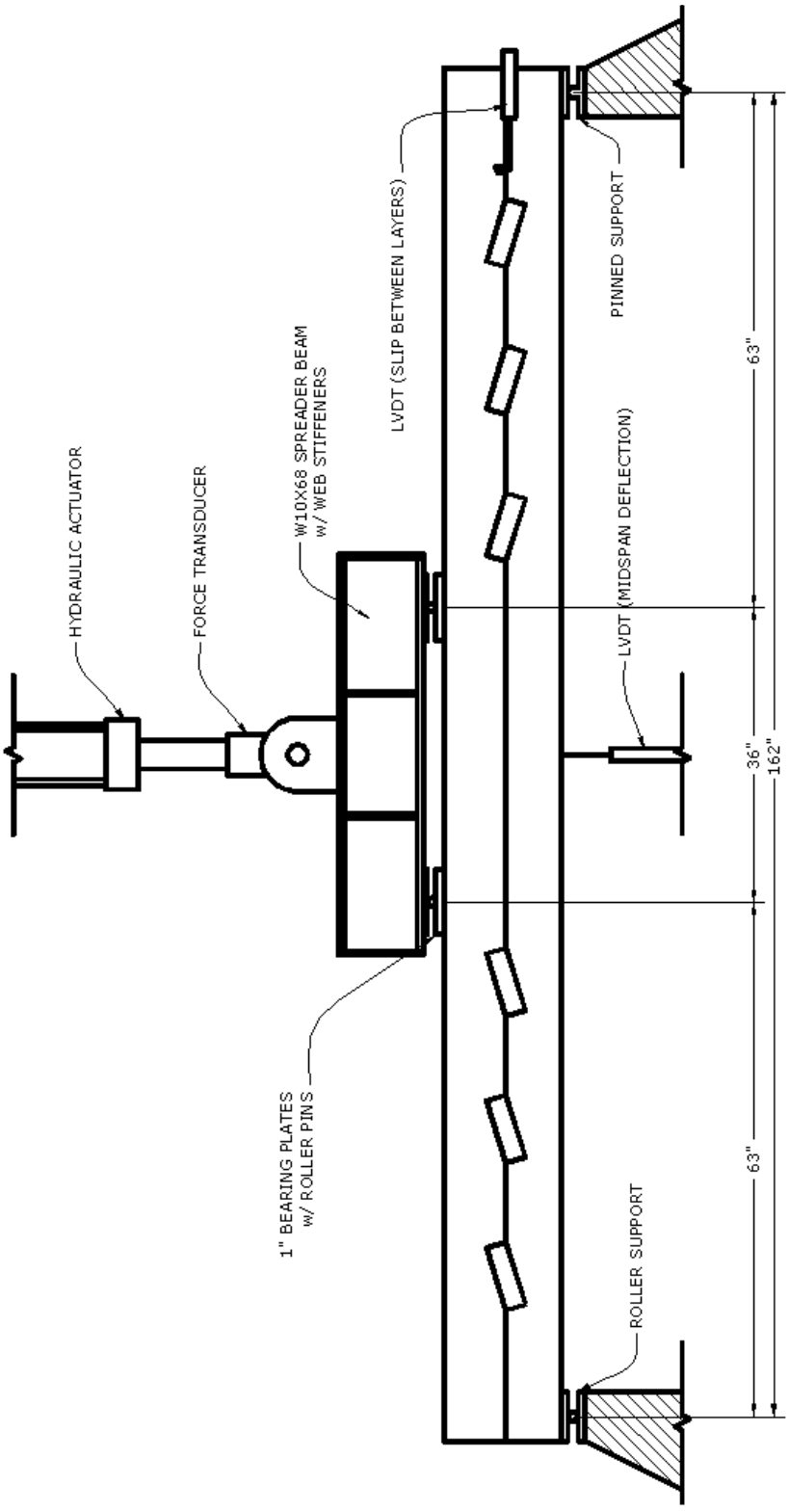

Figure 5-2 Full scale beam test configuration

5.3 Test Results

5.3.1 Full and Stacked Beams

The full depth and simple stacked beams were loaded until approximately 25% of the anticipated modulus of rupture was reached. The beams were then unloaded and cut into smaller pieces for use with the small scale testing discussed in section 4. The full depth beam displayed ring-shake at one end coupled with a substantial seasoning check (Figure 5-3). The simple stacked beams were relatively clear and defect free. During testing of the simple stacked beam, audible "clicking" was heard, which was attributed to the slipping between the layers. This phenomenon was also audible during the white oak key testing (section 4.4.1).

The load-deflection plots indicated slight initial softness, followed by very linear behavior until the test was stopped. The load-deflection plots, along with those for the keyed beam tests, can be found in Figure 5-4. As anticipated, the full depth beam provides an upper bound on stiffness for all of the beam tests, whereas the simple stacked beam acts as a lower bound. The stiffness of each keyed beam tests falls between the full depth and simple stacked beam stiffnesses. Moisture content, specific gravity, and stiffness data is included in Table 5-1.

Figure 5-3 Ring-shake and checking in the full depth beam

Longitudinal displacement between the layers (slippage) was recorded at both ends of the simple stacked span using LVDTs. The slippage at the ends was 0.139 inch and 0.073 inch (0.106 inch average) at 10 kips of applied load, compared to an anticipated 0.118 inch. Appendix G includes the procedure for determining the anticipated slip. A similar measurement was taken during the full depth test at the beam's neutral axis, although no movement was observed, as expected.

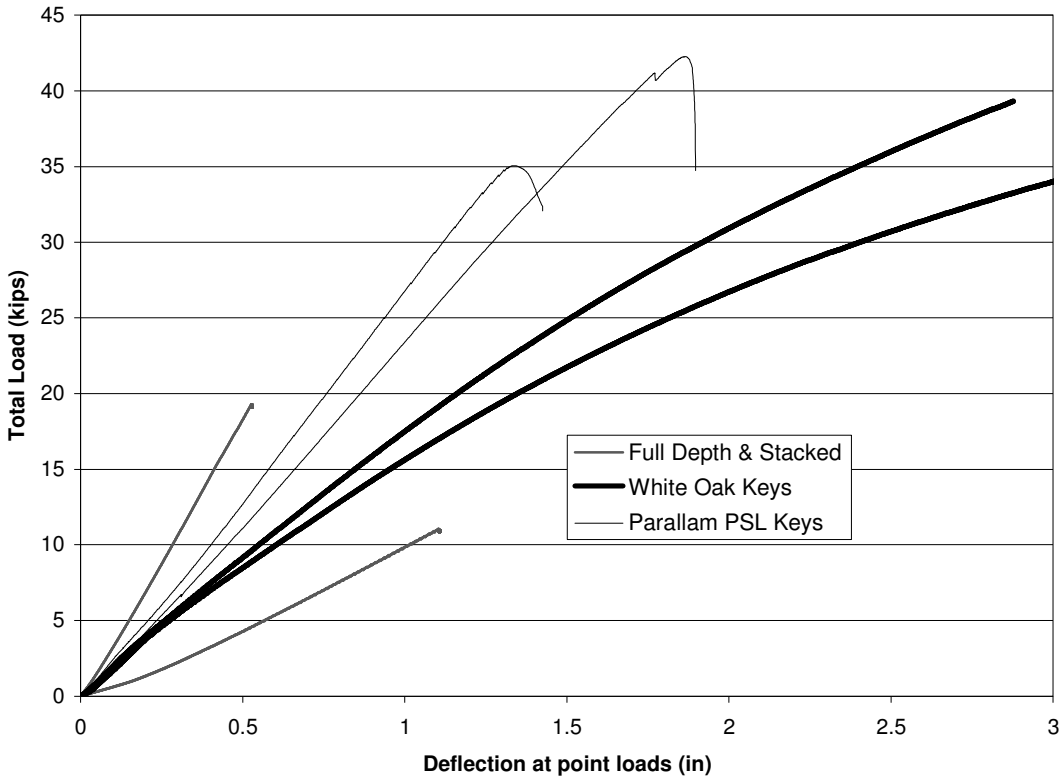

Figure 5-4 Load-deflection plots of full-scale beam tests

Table 5-1 Full-scale beam test results

Test	b (avg) *in*	d (avg) *in*	Timber Moisture Content (avg)	Specific Gravity (avg)	Material	Key Moisture Content (avg)	Specific Gravity (avg)	Actual I (Full Depth) *in^4*	Stiffness *lb / in*	Apparent E *psi*
Full	7.59	15.53	21.2%	0.443				2371	38400	1254000
Stacked	7.69	7.63	15.6%	0.429				2277	11200	381000
1	7.61	7.06	16.0%	0.453	WO	33.4%	0.638	1785	15100	655000
2	7.72	7.44	11.4%	0.407	WO	26.5%	0.632	2120	17300	632000
3	7.58	7.50	10.3%	0.367	PSL	7.8%	0.605	2132	24500	889000
4	7.59	7.45	11.8%	0.424	PSL	7.9%	0.607	2092	28000	1036000

In Table 5-1 above, the "Actual I" represents the moment of inertia for the full beam cross-section. "Apparent E" is the apparent modulus of elasticity (modulus of elasticity including shear deformations) of a partially-composite beam based on a full depth beam cross sectional properties.

5.3.2 Keyed Beams with White Oak Shear Keys

Two keyed beams with white oak shear keys and identical configurations were tested on the same load frame and in the same manner as the full depth and simple stacked beams. Load-deflection plots are shown in Figure 5-4 and pertinent test data is tabulated in Table 5-1. The deflection shown in Figure 5-4 is recorded as the movement of the hydraulic actuator. Load was applied until failure occurred.

For the first beam, failure occurred at 34.1 kips of applied load, and occurred when cracking in the bottom face of the bottom layer appeared, which coincided with a slight drop in load. While the beam appeared to be able to still resist some loading, the test was inadvertently interrupted, so no additional load was applied. The keyed beam is shown in Figure 5-5. Audible "ticking" was again apparent during the testing. Horizontal slip was measured using LVDTs mounted at each end of the beam, and a load-slip plot is shown in Figure 5-6. The shape of the load-slip plots suggests similar behavior, as anticipated, at each end of the beam. The non-linear shape of the plots, when compared to the linear behavior of the full depth and simple stacked beams, suggests slippage did not occur at a uniform rate, which is related to the non-linear behavior of the beam load-deflection plots shown in Figure 5-4. After testing, the shear keys were removed from the keyed beam, and the shear keys near the ends of the beam exhibited substantial deformation, similar to those from the small-scale key tests (Figure 4-12). The shear keys near the center of the span exhibited substantially less deformation. This uneven load distribution between keys is most likely the culprit for the non-linear behavior seen in the load-deflection and load-slip plots (Figure 5-4,Figure

5-6), as keys nearer the beam end reached their crushing point sooner than those near the middle.

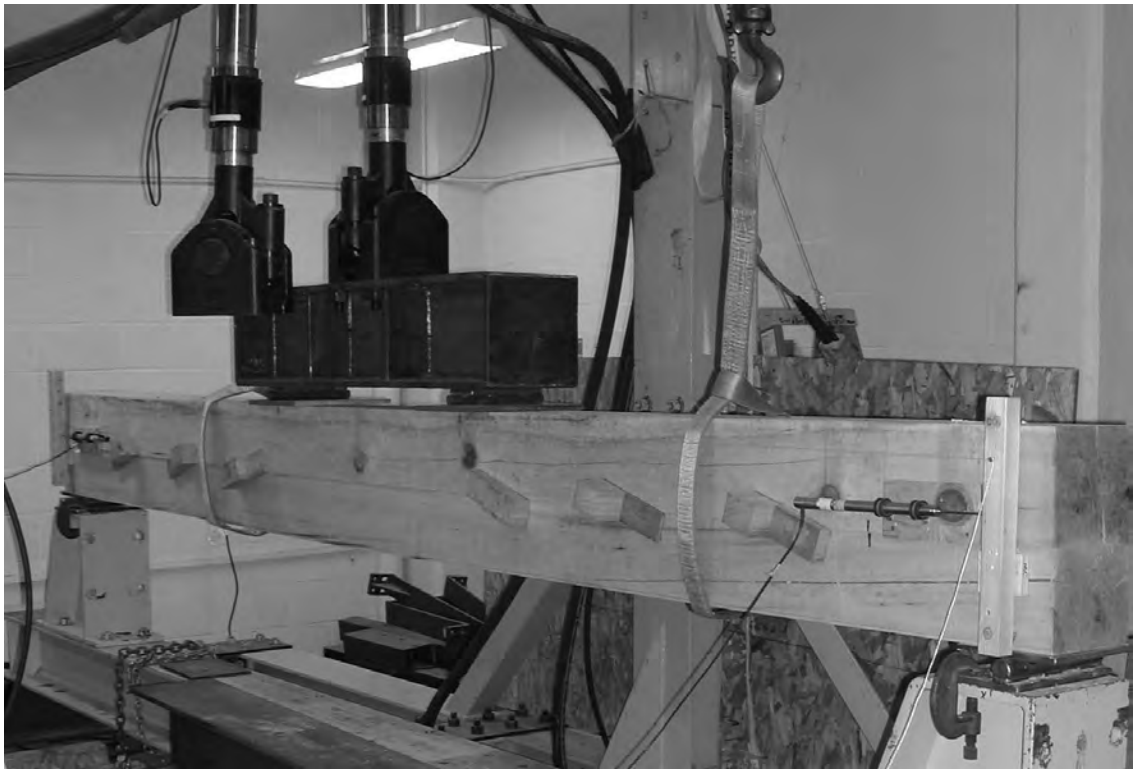

Figure 5-5 Keyed beam using white oak shear keys under load

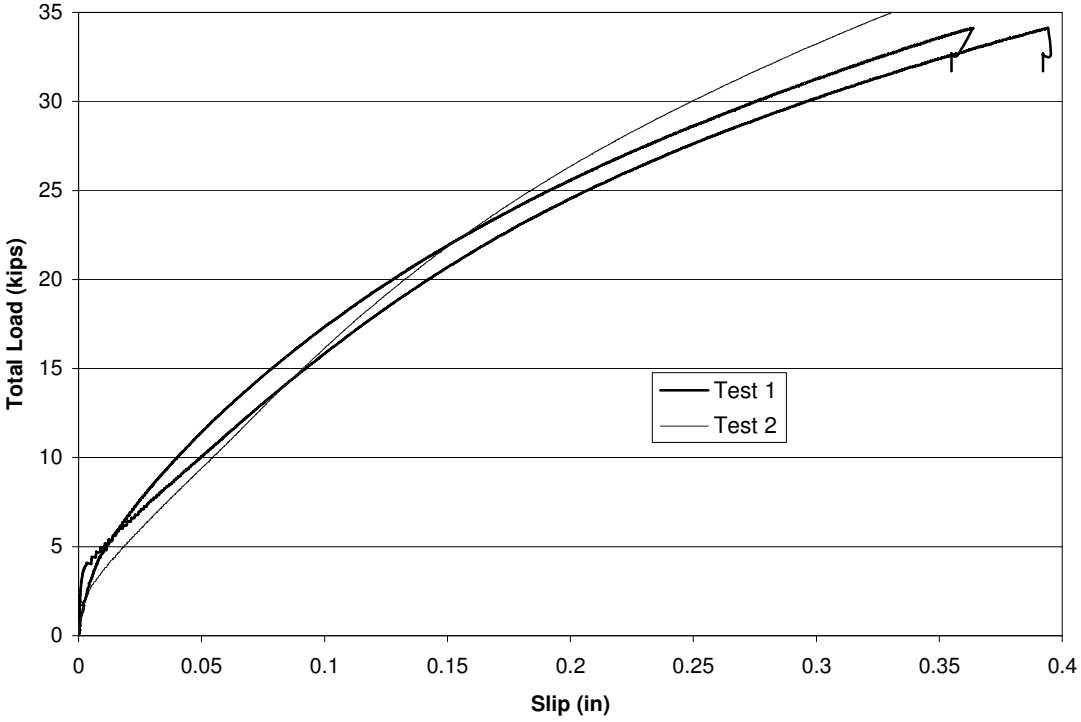

Figure 5-6 Load-slip plots for white oak shear key tests

For the second beam, failure consisted of a sudden tensile failure of the bottom layer which propagated nearly instantly upwards to the center of the top layer. This sudden breakage occurred at an applied load of 39.6 kips, and the beam failed to carry any additional load after breaking. The broken keyed beam, which is shown in Figure 5-7, exhibits similar cracking behavior to that seen in the small scale flexure tests (Figure 4-2). Once the beam failed, additional cracks propagated from the re-entrant corners of the inner shear keys (Figure 5-8). These cracks were not apparent before sudden failure of the beam. Slip between the layers was only measured at one end of the beam for this test, as the results from test 1 showed very similar movements at each end. The other LVDT was placed under the midspan of the beam to confirm vertical displacement under loading, and quantify the compliance in the test frame and supports (see section 5.4.3).

The LVDT was removed from under the beam after approximately 20 kips of load was applied to eliminate any possible damage. As in test 1, the shear keys at the ends of the beam exhibited substantial permanent deformation, while those nearer the center of the span showed only minimal crushing.

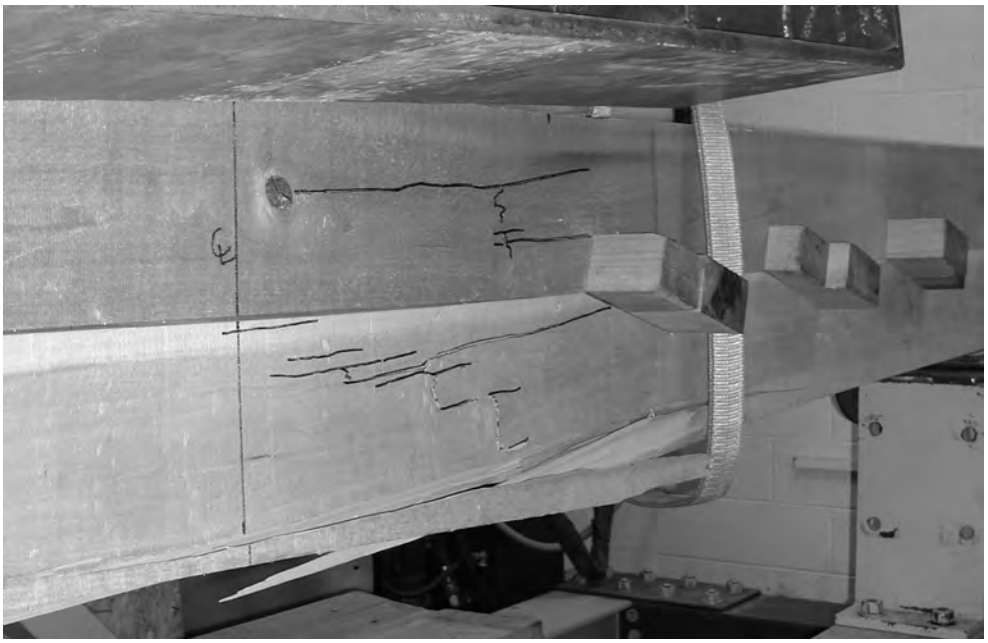

Figure 5-7 Cracked keyed beam using white oak shear keys

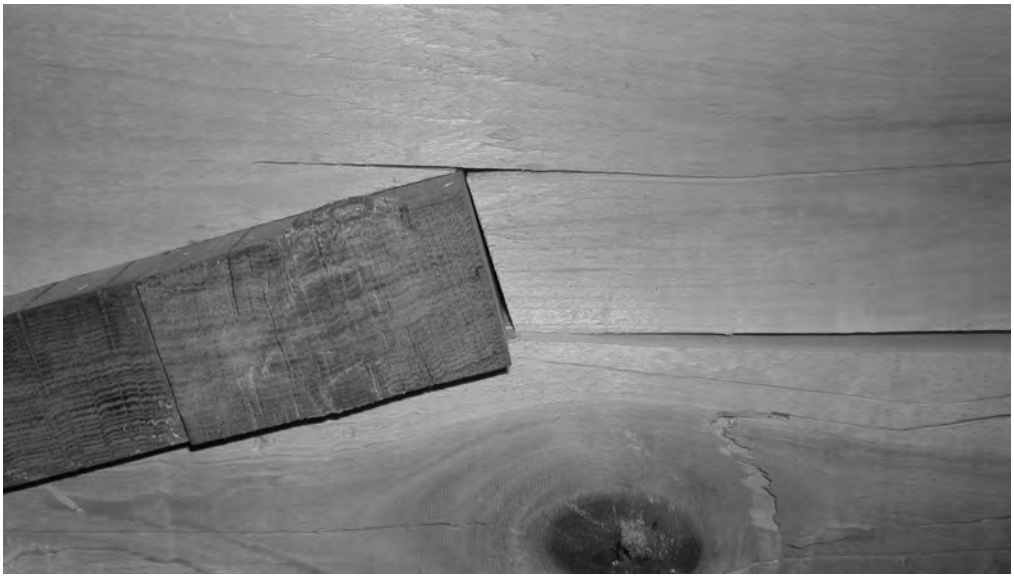

Figure 5-8 Crack propagating from re-entrant notch corner

5.3.3 Keyed Beams with Parallam PSL Shear Keys

Two keyed beams of identical configuration were tested using Parallam PSL shear keys. These beams had the same layout as the keyed beams with white oak shear keys discussed in the previous section. Mid-span deflection was measured along with interlayer slip at one end of the beams. Load-deflection plots for these tests can be found in Figure 5-4, which show very linear behavior up until the point of buckling. Despite efforts to brace the hydraulic loading ram, the beam buckled laterally due to three-hinged column action, with two hinges (points of rotation) occurring at the top and bottom pins on the hydraulic ram, and the third hinge (point of rotation) occurring where the beam sat atop the test-frame supports. Other pertinent test data is included in Table 5-1. Figure 5-9 shows a loaded beam shortly before buckling occurred.

The first Parallam PSL-keyed beam buckled suddenly at a load of 42.4 kips. For the next test, additional bracing was added to the hydraulic ram and considerable effort was taken to ensure the ram and beam were plumb and square. Despite these efforts, the second beam still buckled at a lower load level than the first (35.1 kips). The ultimate loads for both keyed beams using Parallam PSL keys was controlled by the loading instability, not material failure.

Timber beams with a depth-to-breadth ratio of 2:1 or less do not normally fail in lateral torsional buckling, and bracing is not required for their in-service use (AF&PA, 2005). The keyed beams tested in this research have a depth-to-breadth ratio of 2:1, so lateral bracing of the beam was not initially included. To limit the possibility of damaging equipment or risking injury, no additional testing was conducted on the

Parallam PSL-keyed beams after they buckled. Therefore, ultimate load of the Parallam PSL-keyed beams was never reached.

Unlike the white oak-keyed beams, the Parallam PSL-keyed beams had the prevalent audible "ticking" noise from interlayer slipping only until around 10 kips of load. After 10 kips of load, the frequency of ticks diminished, and the ones that occurred were considerably less audible. Slight cracking noises were heard in the beams shortly before buckling occurred as well. The cracking may have been from fibers nearing their rupture point, but was more likely an indication of the impending buckling. Very little slip was noticed between the layers during testing, and the keys did not appear to rotate or compress. After the testing, the keys were removed from the beam, and no end-grain crushing of the keys or the timbers was apparent. However, crushing of the keys or end-grain may have occurred if the beams had reached the material failure capacity before reaching the buckling/stability capacity of the load frame.

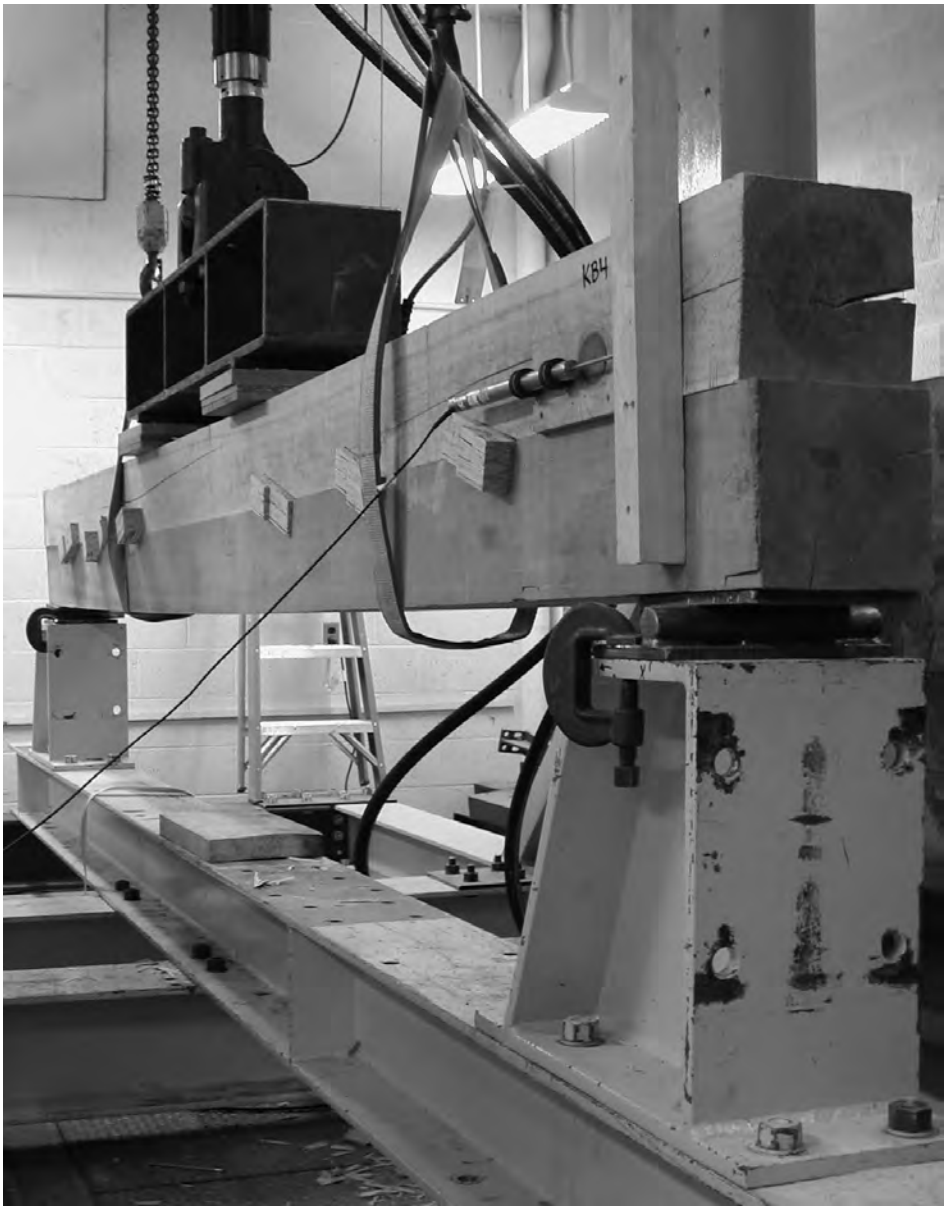

Figure 5-9 Parallam PSL-keyed beam under load

5.4 Adjustments to Test Results

As with the small scale testing, the moisture content, specific gravity, and cross sectional dimensions varied between each timber used in the full-scale beam testing. The moisture content and specific gravity also varied in the white oak shear keys. In order to compare the results between the different tests, adjustments to the keyed beam test

stiffnesses were made to account for these variations. These adjustments are based on published relationships between modulus of elasticity and specific gravity and moisture content (FPL, 1999).

5.4.1 Moisture Content and Specific Gravity

The stiffnesses of the keyed beam tests were adjusted for variations in moisture content and specific gravity of the timbers. The process used is similar to that set forth in section 4.6 for the small scale testing. With the assumption that modulus of elasticity of the timbers a controlling factor in beam and following section 4.6.1, the adjustment for moisture content (FPL, 1999) is

$$K_{ADJ} = K_{UNADJ} \frac{\left(\frac{E_{12\%}}{E_{green}}\right)}{\left(\frac{E_{12\%}}{E_{green}}\right)\left(\frac{E_{12\%}}{E_{green}}\right)^{\left(\frac{12-MC}{13}\right)}} \tag{5-1}$$

where K_{UNADJ} is the unadjusted stiffness of a particular test, $E_{12\%}$ is the published modulus of elasticity for yellow poplar at 12% moisture content (1,580,000psi), E_{green} is the published green moisture content (1,220,000psi), and MC is the averaged moisture content of the timbers at the time of testing. Equation 5-1 simplifies to

$$K_{ADJ} = \left(\frac{158}{122}\right)^{\left(\frac{MC-12}{13}\right)} \tag{5-2}$$

In a similar fashion to the procedure outlined in 4.6.2, it is possible to adjust the keyed beam test stiffness for variations in specific gravity (FPL, 1999) by

$$K_{ADJ} = K_{UNADJ} \frac{2.97 G_{12\%}^{0.84}}{2.97 G_{ACT}^{0.84}} = K_{UNADJ} \frac{G_{12\%}^{0.84}}{G_{ACT}^{0.84}} \quad (5\text{-}3)$$

where $G_{12\%}$ is the published specific gravity for yellow poplar (0.42) and G_{ACT} is the actual specific gravity of the beam at the time of testing determined using ASTM D2395 (ASTM, 2007). The adjusted stiffness values for the full-scale beam tests, which include all of the applicable adjustments, are shown in Table 5-2. Although only two tests of each type were conducted, a comparison of the values for the white oak keyed beams and for the Parallam PSL keyed beam shows these adjustments reduced a substantial amount of variation in the actual beam stiffnesses. In Table 5-2, "Apparent E" is the modulus of elasticity of a partially-composite beam based on a full depth beam cross sectional properties.

Table 5-2 Adjusted stiffness values for full-scale beam tests

Test	Actual I *in^4*	Stiffness *lb / in*	Stiffness (adjusted) *lb / in*	Apparent E *psi*	Apparent E (adjusted) *psi*	Efficiency
Full	2371	38400	39200	1254000	1281000	100.0%
Stacked	2277	11200	10900	381000	372000	29.0%
1	1785	15100	18100	655000	787000	61.4%
2	2120	17300	17500	632000	639000	49.9%
3	2132	24500	26300	889000	954000	74.5%
4	2092	28000	27900	1036000	1032000	80.6%

The moisture content and specific gravity data of the white oak shear keys used in the first two keyed beam tests was not used to adjust the stiffness of the keyed beam tests in this section (i.e., the "Apparent E" has not been adjusted to account for variations in key specific gravity and moisture content). This white oak key specific gravity and moisture content data is included in section 6 when comparing the keyed beam tests to the anticipated results from the interlayer slip model outlined in section 2.

5.4.2 Variations in Cross Section

Slight variations in cross-section can greatly impact the stiffness of both simple beams as well as keyed beams, with the moment of inertial being the cross-sectional property controlling flexural stiffness behavior. To account for these variations so all of the tests can be compared on consistent basis, the stiffness of each test was adjusted to a 7.5 inch wide by 15 inch deep timber by

$$K_{ADJ} = K_{UNADJ} \frac{\left(\frac{(7.5)(15)^3}{12}\right)}{\left(\frac{(b_{act})(d_{act})^3}{12}\right)} = K_{UNADJ} \frac{2109.375}{I_{ACTUAL}} \tag{5-4}$$

where b_{act} and d_{act} are the actual beam breadth and depth in inches. These adjustments to account for variations in cross section have been applied to the adjusted stiffness values in Table 5-2.

5.4.3 Test Frame Compliance

During all of the tests, beam deflection was measured using the stroke movement of the hydraulic ram. This measurement of deflection may include flexural deflection, crushing of bearing plates, and other test frame compliance issues. In order to isolate the effects of frame compliance, additional deflection measurements were taken during the testing of the second white oak keyed beam, along with both of the Parallam PSL keyed beams, using an LVDT. The LVDT was placed under the beam near midspan, and recorded movement of the bottom edge of the beam compared to the base of the test

frame. When approximately 20 kips of load had been applied, the LVDT was removed from under the beam, to limit the possibility of damage.

A comparison of the beam stiffness determined from the hydraulic ram stroke and the separate LVDT suggest that compliance of the test frame does not have a significant effect on the beam stiffness (Table 5-3). For two tests, the LVDT measured slightly less movement than the hydraulic ram stroke, while the opposite was encountered for the other test.

Table 5-3 Differences in stiffness from test frame compliance

Test	Stiffness *lb / in*
2 (stroke)	17,300
2 (LVDT)	17,600
3 (stroke)	24,500
3 (LVDT)	25,200
4 (stroke)	28,000
4 (LVDT)	26,100

6 Analysis of the Interlayer Slip Model using Full Scale Test Data

An accurate analytical interlayer slip model is desirable, as it would permit a reasonable design procedure. Therefore, comparing the anticipated behavior of a keyed beam from the interlayer slip model with full-scale physical test data becomes a primary focus in this research.

6.1 Comparison of Test Data

In order to compare physical test data from previous sections, data was adjusted to a normalized value to account for variations in moisture content, specific gravity, and cross sectional dimensions of the timbers. These adjustments were required to permit a direct comparison of the results from different test configurations. In this section, the focus is on comparing results from full-scale beam tests to predicted results from the interlayer slip model. The interlayer slip model can directly account for variations in section properties and elastic moduli. Therefore, material and section properties from the in situ test conditions will be used, rather than normalized values.

6.1.1 Interlayer Slip Model Input Parameters

In order to use the interlayer slip model developed in section 2, several material and section properties are required. Before the cross sectional areas and moment of inertias can be calculated, the breadth b and depth d of the individual timbers are required. To determine the timber's modulus of elasticity, the moisture content MC and specific gravity G are also required. For the shear keys, the key thickness t is required to determine the key stiffness. Also, for the white oak keys, the shear key moisture

content and specific gravity is also required to determine the modulus of elasticity. For the Parallam PSL keys, the manufacturer's published values for modulus of elasticity were used. The various section properties can be found in Table 6-1.

Table 6-1 Physical data on keyed beam tests for use with the interlayer slip model

Test	Layer	b	d	A	MC	G	E_{tim} (calc)
		in	*in*	in^2	*%*		*psi*
1	*top*	7.63	7.49	57.1	17.4%	0.465	1547000
	btm	7.59	6.63	50.3	14.7%	0.441	1561000
2	*top*	7.69	7.38	56.8	10.4%	0.361	1391000
	btm	7.75	7.50	58.1	12.4%	0.452	1666000
3	*top*	7.56	7.44	56.2	9.3%	0.327	1280000
	btm	7.60	7.56	57.5	11.4%	0.406	1536000
4	*top*	7.57	7.39	55.9	12.9%	0.442	1620000
	btm	7.61	7.50	57.1	10.7%	0.405	1532000
				Avg	12.4%	0.412	1517000

Test	Key	t	MC	G	E_{key} (calc)
		in	*%*		*psi*
1	A	2.51	37.2%	0.678	1247000
	B	2.47	32.9%	0.628	1180000
	C	2.44	30.1%	0.608	1153000
2	A	2.48	22.0%	0.652	1213000
	B	2.38	29.0%	0.630	1184000
	C	2.50	28.4%	0.614	1161000
3	A	2.41	7.8%	0.605	2100000
	B	2.44	7.8%	0.605	2100000
	C	2.42	7.9%	0.606	2100000
4	A	2.44	7.9%	0.606	2100000
	B	2.41	8.0%	0.608	2100000
	C	2.43	7.9%	0.607	2100000

Actual modulus of elasticity values for individual timbers and shear keys were not able to be directly measured. In order to calculate these values, the published relationships between modulus of elasticity and moisture content and specific gravity were used (FPL, 1999).

For the timbers, the relationship between specific gravity and modulus elasticity for softwoods was used for material at 12% moisture content (see section 4.6.2). The actual timber modulus of elasticity E_{tim} in psi was calculated as

$$E_{tim} = 1{,}580{,}000\left(\frac{0.42^{0.84}}{G_{tim}^{\ 0.84}}\right) \tag{6-1}$$

where 1,580,000 is the modulus of elasticity for yellow poplar at 12% moisture content, 0.42 is the published specific gravity of yellow poplar at 12% moisture content, and G_{tim} is the oven dry specific gravity of the timber based on volume at approximately 12% moisture content (FPL, 1999). Note this modulus of elasticity is predicting the actual modulus of elasticity of the timber at the time of testing; it is not a modulus of elasticity normalized to a particular moisture content or specific gravity, as discussed in previous sections. These calculated modulus of elasticies are found in Table 6-1.

The modulus of elasticity for the white oak shear keys was calculated using the published relationship between it and specific gravity for green hardwood material (FPL, 1999). The shear key modulus of elasticity E_{key} in psi was determined by the relationship

$$E_{key} = 1{,}250{,}000\left(\frac{0.68^{0.72}}{G_{key}^{\ 0.72}}\right) \tag{6-2}$$

where 1,250,000-psi is the modulus of elasticity for green white oak, 0.68 is the specific gravity of white oak at 12% moisture content, and G_{key} is the oven dry specific gravity of the shear key based on green volume (FPL, 1999). These calculated elastic moduli are included in Table 6-1. Keys designated by "A" are the keys that were closest to the ends, where as the "C" keys were those closest to the center of the beam and applied point load. To provide symmetry during physical testing, the shear keys closest to the ends of the beams were cut from the same piece of material. Likewise the shear keys closest to the point loads were cut from the same piece of material, and the middle set of shear keys were also fabricated in a similar fashion.

Adjustments to timber and key modulus of elasticity due to variations in moisture content were made in a fashion similar to that shown in equation 5-2 (see section 5.4.1), such that

$$E_{calc} = E_{12\%}\left(\frac{E_{12\%}}{E_{green}}\right)^{\left(\frac{12-MC}{13}\right)} \tag{6-3}$$

where $E_{12\%}$ and E_{green} are the published modulus of elasticity values for a given species, taken from the Wood Handbook (FPL, 1999), and MC is the moisture content, in percentage, of the material. Most of the white oak shear keys exceeded the average fiber saturation point for most hardwoods of 25% (FPL, 1999). Mechanical properties, in particular modulus of elasticity, do not vary significantly with changes in moisture content above the fiber saturation point. When a material's moisture content was above the fiber saturation point, 25% was used instead.

6.1.2 Analysis Results

The solution of the interlayer slip model equations for a two-layer beam with symmetrically placed point loads was used for this comparison. The development of the solution is included in Appendix C. The analysis and specific solutions of the interlayer slip model based on the full-scale test data parameters are included in Appendix H. The results of the analyses can be seen in Table 6-2. A graphical comparison of the load-deflection plots from testing and the analytical solution using the interlayer slip model are shown in Figure 6-1.

Table 6-2 Comparison of analytical and full-scale testing stiffnesses

Test	Key	Model *lb/in*	Test *lb/in*	Difference %
1	OAK	16806	15100	10.2%
2	OAK	19228	17300	10.0%
3	PSL	26558	24500	7.7%
4	PSL	28708	28000	2.5%
			Avg.	7.6%

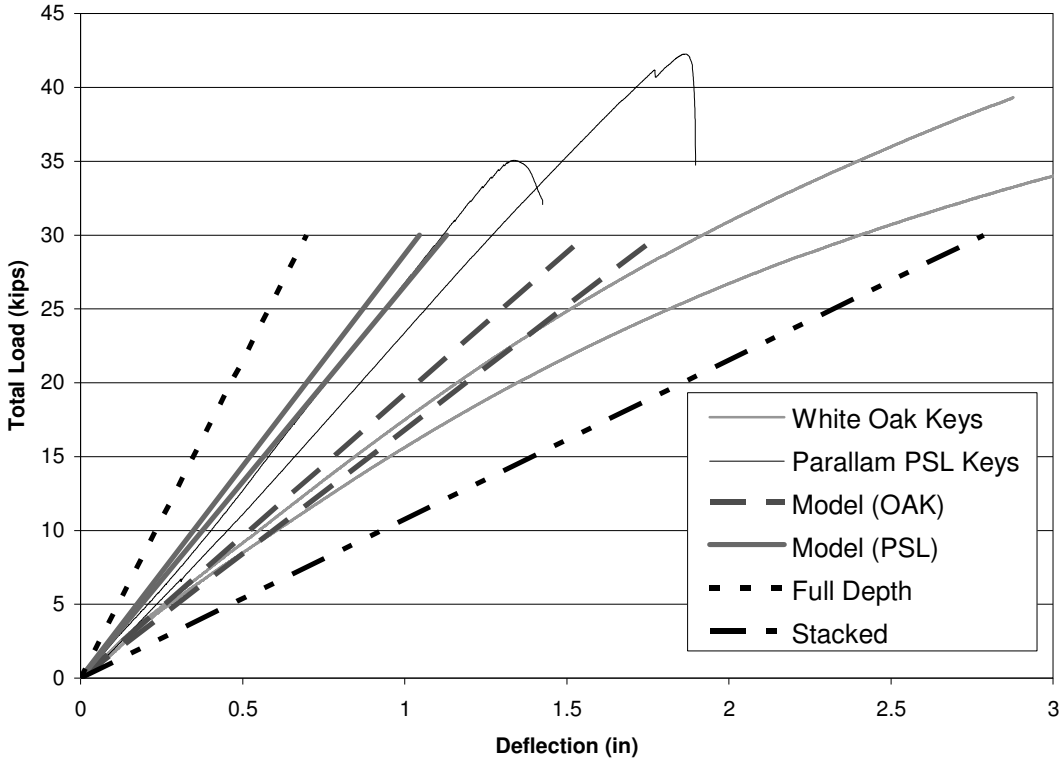

Figure 6-1 Comparison of load-deflection plots and interlayer slip model solutions

The stiffnesses from the interlayer slip model were slightly higher than the actual test results in all four comparisons, although by an average value of only 7.6%. For flexural members, whether simple stacked, full depth, or composite beams, the modulus of elasticity of the material has a dominant effect on the stiffness of the member. The published average coefficient of variation for timber modulus of elasticity is 0.22 (FPL, 1999), suggesting that variations between the calculated and actual keyed beam stiffnesses may be attributed to natural variations in modulus of elasticity of the material.

The slightly larger difference between the calculated and actual stiffnesses for the keyed beams using white oak keys may be attributed to the non-linear behavior of these

tests. As was discussed in 5.3.2, the physical testing showed a disparate amount of shear key crushing between the shear keys nearest the beam ends and those closest to midspan, which is likely due to non-linear behavior and beam softening. Also, the non-linear shape of the load-deflection plots means some subjectivity is required when determining the initial stiffness from the straight-line portion.

The small-scale white oak shear key tests discussed in section 4.4 exhibited a bi-linear behavior (Figure 4-9); an initial stiff region followed by secondary region of substantially less stiffness. This bi-linear behavior is quite common in wood when it is subjected to cross-grain compressive forces (ASTM D143, 2007). The development of a bi-linear model for the cross-grain stiffness of the white oak shear keys would better capture the actual behavior of the shear keys. Using this bi-linear stiffness in the interlayer slip model would more accurately capture the non-linear behavior exhibited in testing. However, the small difference (7.6%) between the stiffnesses from the physical testing and the interlayer slip model do not appear to justify the additional computational effort required to perform a non-linear analysis.

6.2 Shear Key Spacing Methodology

The interlayer slip model requires calculating two constants, C_F and C_M, which can be found in equations (2-18) and (2-19). Both of these constants include a component for determining the stiffness per unit length of the shear keys, $\sum \frac{K_i}{s_i}$. The individual key stiffness K is calculated by the process developed in section 2.5, but determining the appropriate key spacing distance s each shear key acts over is less

certain. This section investigates several possible approaches to calculating an appropriate key spacing, and compares the various outcomes when each approach is used in conjunction with the interlayer slip model.

6.2.1 Simplified Approach

Perhaps the simplest approach for determining the effective stiffness per unit length is to sum all of the shear key stiffnesses and distribute this evenly over the entire length of the beam, such that

$$\frac{\sum K_i}{L} \tag{6-4}$$

This approach, which was used to calculate the beam stiffnesses in section 6.1, is based on the assumption that there is even load distribution between each shear key. The full-scale beam tests conducted with white oak shear keys showed substantially different amounts of crushing in the shear keys, suggesting that even load distribution is perhaps not appropriate. The PSL-keyed beams did not display disparate deformation between individual shear keys, suggesting they may have carried load evenly. However, the material failure load of these beams was never reached. This simplified approach for determining effective stiffness more accurately predicts the stiffness of the beams with the Parallam PSL keys than the beams with white oak keys.

6.2.2 Shear Stud / Composite Beam Approach

Steel-concrete composite beams are commonly found in commercial construction. A wide-flange steel section is on the bottom (tension portion) of the composite beam, and a cast-in-place concrete deck is used on the top (compression portion). The initial

interlayer slip model, developed by Newmark, was intended to model this specific type of beam (Newmark, 1951). The approach used when determining the number of shear studs for these types of composite beams includes making a section cut at any point along the beam, and the shear studs in that section must be able to resist the difference in the tension and compression force components generated by composite action. Common design procedure for steel-concrete composite beams used as bridge girders is to have varying shear stud spacing, to account for the varying shear about the length from a uniformly distributed load, whereas a uniform shear key spacing is more common for steel-composite beams used in occupied structures. For the keyed beam configuration used in this testing, the moment in the beam (Figure 3-7) varies linearly between the reaction and applied point loads resulting in a constant shear and key spacing.

In order to use this composite beam approach with this keyed beam testing, it was assumed each shear key resisted the forces starting at the shear key heel except for the end key. The resultant spacing and points of assumed action are shown in Figure 6-2.

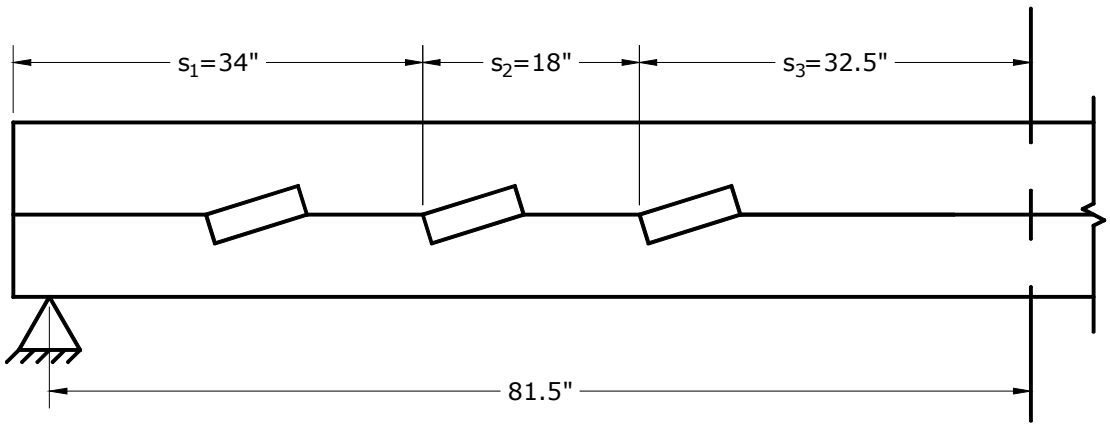

Figure 6-2 Assumed shear key spacing using a composite beam approach

The lowest stiffness term ($\frac{K_i}{s_i}$) is associated with the shear key nearest the end of the beam, while the highest stiffness term is associated with the middle key. Using a springs in parallel analogy, the majority of the force being resisted should be carried by the stiffest "spring", which corresponds with the middle key. However, the assumed spacing shown in Figure 6-2 does not appear consistent with the observed key crushing from the white oak tests. Results from the interlayer slip model (included in Table 6-3) using these shear key spacings predict substantially stiffer keyed beams than were observed.

Table 6-3 Comparison of various methods for determining shear key spacing

Test	Method	Beam Stiffness (lb/in)		Difference
		Calculated	Actual	%
1	Simple	16806	15100	10.2%
	Composite	23994		37.1%
	Trib. Width	24060		37.2%
2	Simple	19228	17300	10.0%
	Composite	27514		37.1%
	Trib. Width	27582		37.3%
3	Simple	26558	24500	7.7%
	Composite	33138		26.1%
	Trib. Width	33172		26.1%
4	Simple	28708	28000	2.5%
	Composite	36198		22.6%
	Trib. Width	36234		22.7%
				7.6%
			Avg.	30.7%
				30.8%

6.2.3 Tributary Length Approach

In structural analysis, a common design approach for determining load paths is using a tributary area approach, where forces or loads are distributed based on half the

distance between points of interest. Using this approach, the corresponding spacings between keys were determined (Figure 6-3).

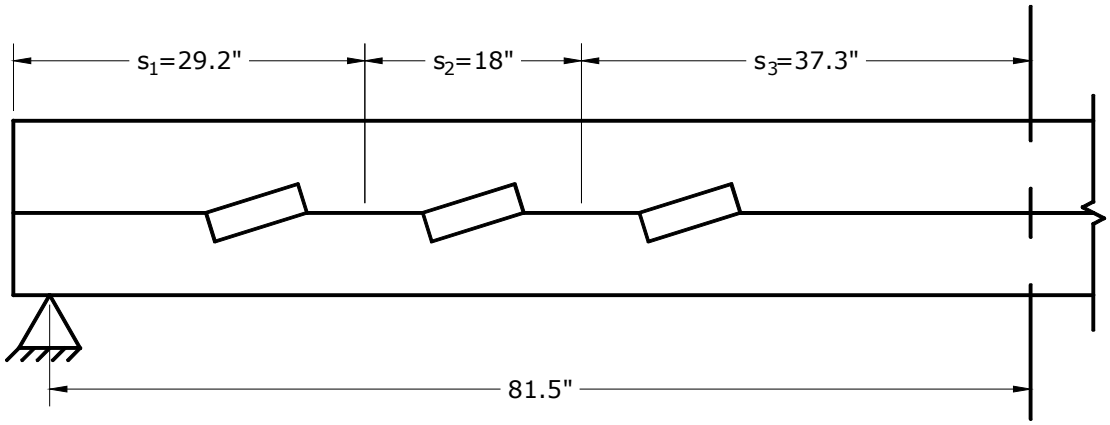

Figure 6-3 Assumed shear key spacing using tributary length approach

Like the composite beam approach, the highest stiffness term ($\frac{K_i}{s_i}$) is associated with the middle shear key. However, the lowest stiffness term using the tributary length approach is in the shear key nearest the center of the span. This appears to match the observed crushing behavior of the white oak shear keys better than the composite beam approach. However, this method results in the same predicted stiffness of the keyed beams as the composite beam approach, which is considerably stiffer than the observed beam behavior (Table 6-3).

6.2.4 Recommended Spacing Calculation

The composite beam and tributary length approaches are quite common in design, although appear to capture beam behavior worse than a simplified approach. Based on the shear flow diagrams (see Figure 2-12a and Figure 2-12b), the variations in the full

depth analysis and built up beam analysis suggest these method may not accurately capture beam behavior. As the shear keys increase in stiffness (tests 3 and 4 in Table 6-3), the differences between the various methods decrease, indicating that built up beams with nearly complete interaction between layers (no slip), the composite beam and tributary length methods may be appropriate. Closer shear connector spacing, as is common with shear studs in composite steel-concrete beams, may play a contributing role.

The computational effort for determining the shear key spacing for any of the three methods above is relatively minor. Compelling arguments can be made for the validity or appropriateness of the composite beam and tributary length approaches, the limited amount of test data for comparison precludes any conclusive findings. Therefore, continued use of the simplified approach for calculating the shear key spacing for use with the interlayer slip model is suggested, as it appears the most consistent with the observed physical-testing results.

6.3 Material Parameter Sensitivity

As shown in the previous section, the interlayer slip model is quite sensitive to the method used for determining shear key spacing. Additional investigations were conducted to determine the interlayer slip model's sensitivity to changes in various material properties and key configurations. The material properties and key configuration used in section 6.1 were used as the baseline for comparison.

6.3.1 Modulus of Elasticity of Timbers

For both full depth beams and simple stacked beams, the timber modulus of elasticity is the only material property that affects the flexural stiffnesses. Thus, using the interlayer slip model to determine the stiffness of keyed beams should also be sensitive to changes in the timber modulus.

The published average modulus of elasticity from the Wood Handbook (FPL, 1999), adjusted for specific gravity, was used in this research. In order to examine the interlayer slip model's sensitivity to variations in timber modulus, the four analyses conducted in section 6.1 were reexamined using timber modulus one standard deviation higher and lower than the published average. The coefficient of variation for modulus of elasticity of small, clear wood specimens is 0.22 (FPL, 1999). For a yellow poplar timber at 12% moisture content, the average published specific gravity is 1,580,000 psi (FPL, 1999) which results in a lower bound for the sensitivity analysis of 1,232,000 psi and an upper bound of 1,928,000 psi. No adjustments were made to these values for variations in specific gravity.

As anticipated, the interlayer slip model stiffness was very sensitive to changes in timber modulus of elasticity (Table 6-4). Changes in timber modulus result in a nearly linear response in beam stiffness across the evaluated range. Based on these observations, knowing the timber modulus of elasticity is unsurprisingly crucial in predicting the beam stiffness. This observation holds true whether the beam is a solid beam or one with partial interaction between layers.

Table 6-4 Variations in stiffness with changes in timber modulus of elasticity

	Beam Stiffness		
	-1 Std Dev	Avg	+1 Std Dev
Test	*lb/in*	*lb/in*	*lb/in*
1	14246	17012	19600
2	16488	19682	22674
3	23760	29332	34556
4	23312	28782	33910

6.3.2 Cross-grain Modulus of Elasticity

The shear keys are the link between the individual layers of a built-up beam, so variations in their modulus (and thus stiffness) are anticipated to have a direct correlation to the amount of interaction that occurs between the beam layers. Therefore, the sensitivity of the interlayer slip model to changes in the shear key modulus of elasticity was also investigated.

Published data for most wood species includes the longitudinal modulus of elasticity. If the shear keys are installed such that they are being loaded parallel to the grain, this published value can be used directly. However, with solid wood keys, installing wedge shear keys in such a fashion proved problematic (see section 3.2.2), so solid wood keys were installed such that they were being compressed across the grain. Compressing the keys across the grain requires the use of elastic ratios, as species specific published cross-grain modulus values are not readily available.

The elastic ratio assumed earlier for analysis purposes was $E_{\parallel} = 12E_{\perp}$ for both the timber and key material. For this sensitivity study, several other ratios were examined (1:1, 1:2, 1:4, 1:8, 1:16, 1:20, 1:24), with the timber and key material always maintaining the same ratio. The analysis process was similar to that conducted in section 6.1, with no

changes to the other material properties. The results of these analyses are plotted in Figure 6-4.

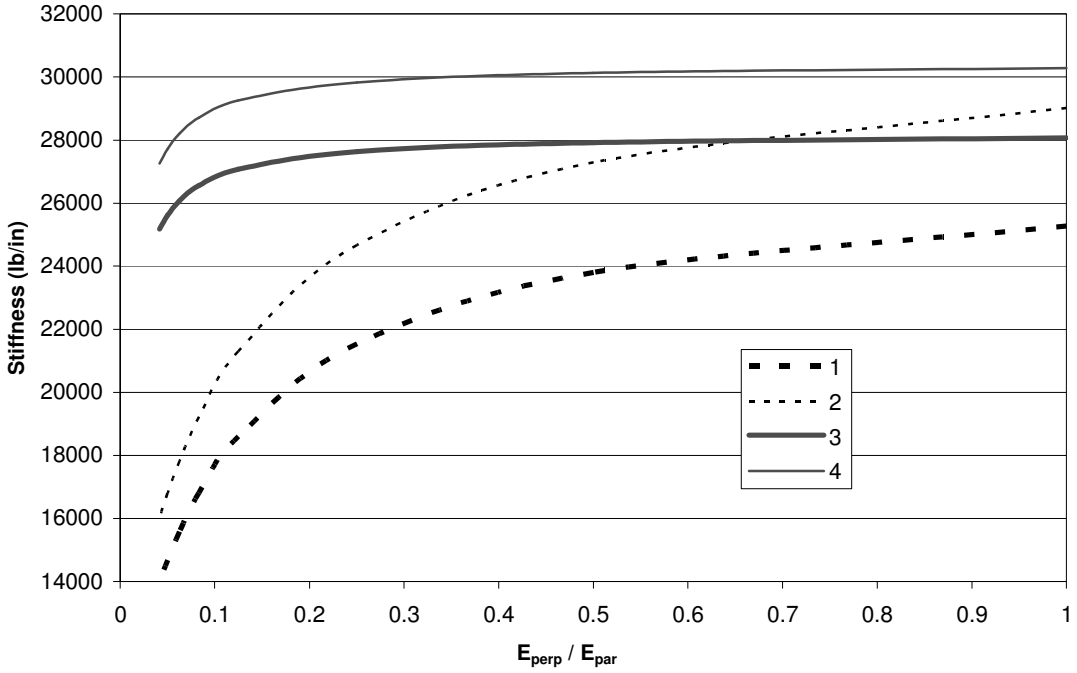

Figure 6-4 Relationship between elastic ratio and calculated beam stiffness for each beam test

For beam tests 1 and 2, the white oak keys were installed such that they were being compressed perpendicular to their grain, and thus the interlayer slip model was quite sensitive to changes in the assumed elastic ratio. With beam tests 3 and 4, Parallam PSL was used for the shear keys, which were being compressed parallel to the grain. Thusly, the variation of the elastic ratios did not affect the stiffness of the key, only the angle to the grain bearing stiffness of the timber at the face of the key. As the elastic ratio approached 1:1, the key stiffness had less effect on the overall stiffness of the beam.

The stiffness data from the interlayer slip model analyses using various elastic ratios was compared to the observed stiffness from the full-scale beam testing. The average difference between the observed and modeled stiffness are shown in Figure 6-5. An elastic ratio of $E_{\parallel} = 19.2E_{\perp}$ ($0.052E_{\parallel} = E_{\perp}$) results in no average difference between the observed and modeled keyed beam stiffnesses. This ratio compares closely to an elastic ratio of 1:20 suggested by Bodig and Jayne (1982). Although using an elastic ratio of 1:20 appears to be more appropriate than the originally assumed ratio of 1:12, the small-scale key testing showed an optimal elastic ratio of 1:12.7 (section 4.4.3). The limited number of small-scale and full-scale tests does not allow for any meaningful statistical conclusion that a particular elastic ratio is more appropriate than another.

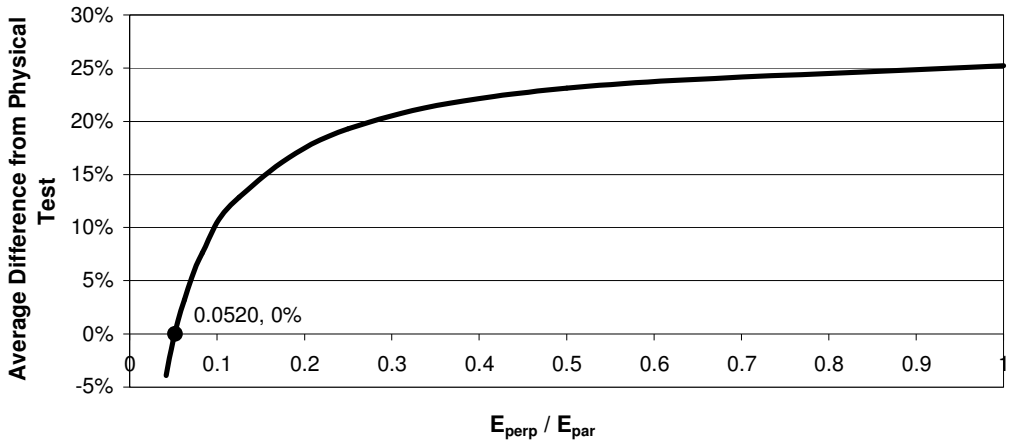

Figure 6-5 Difference between test and model stiffness with varying elastic ratios

6.3.3 Clamping Connectors

Four double-threaded LogHog screws per key were used to provide the clamping force between the layers of all the built-up keyed beams (see section 3.3.3 and Appendix D). In order to investigate the effect of the clamping connector stiffness on the keyed

beam stiffness, the number of screws included in the interlayer slip model was varied from 1 to 10 screws. The same material and section properties used in section 6.1 were used for this comparison, the results of which are shown in Figure 6-6.

Increasing the number of clamping screws appears to have a point of diminishing returns on increasing the overall stiffness of the keyed beams. Keyed beams using Parallam PSL material appear significantly more susceptible to changes in clamping quantity, as these keys are substantially stiffer than white oak keys, and thus more prone to rolling.

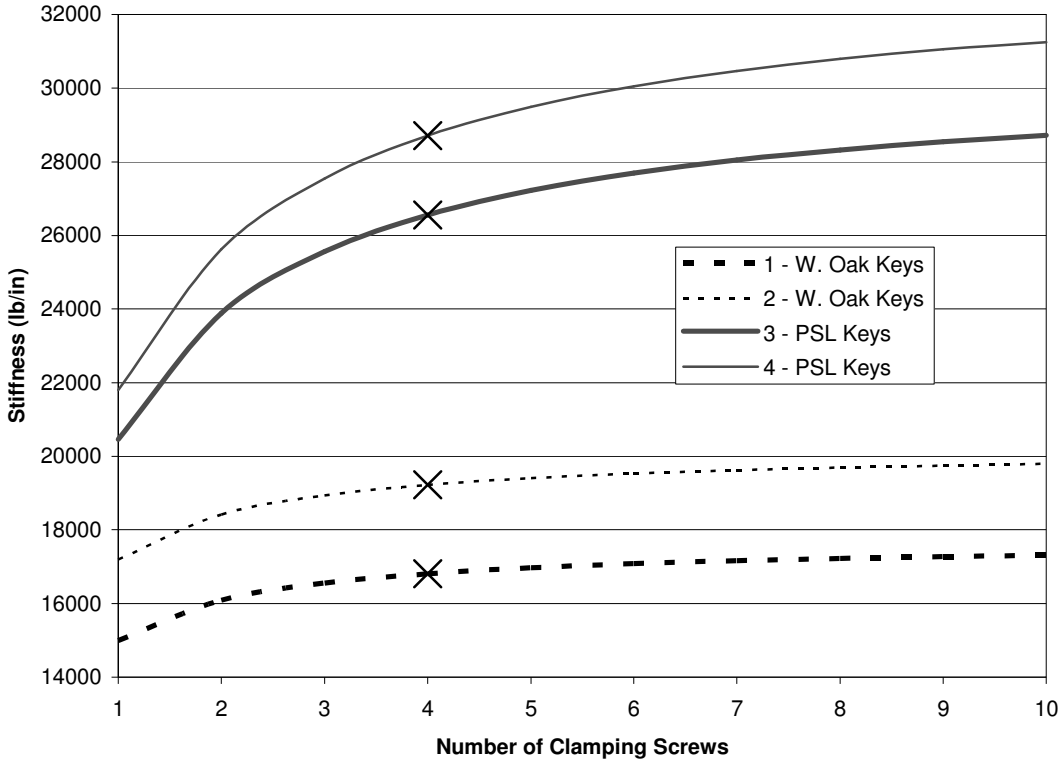

Figure 6-6 Relationship between the number of clamping screws and modeled beam stiffness

6.3.4 Key Size

All full-sized beam tests conducted with this research used 2.5 inch thick by 8 inch long shear keys (Figure 3-3). In order to determine the effect of the key size on the keyed beam stiffness, various sizes of keys were analyzed using the interlayer slip model. For this comparison, 2.5 inch thick keys that varied in length (2.5, 5, 6.5, 8, 11, 14 inch) were analyzed, using the material properties, section data, and key spacing from section 6.1. The results are shown in Figure 6-7.

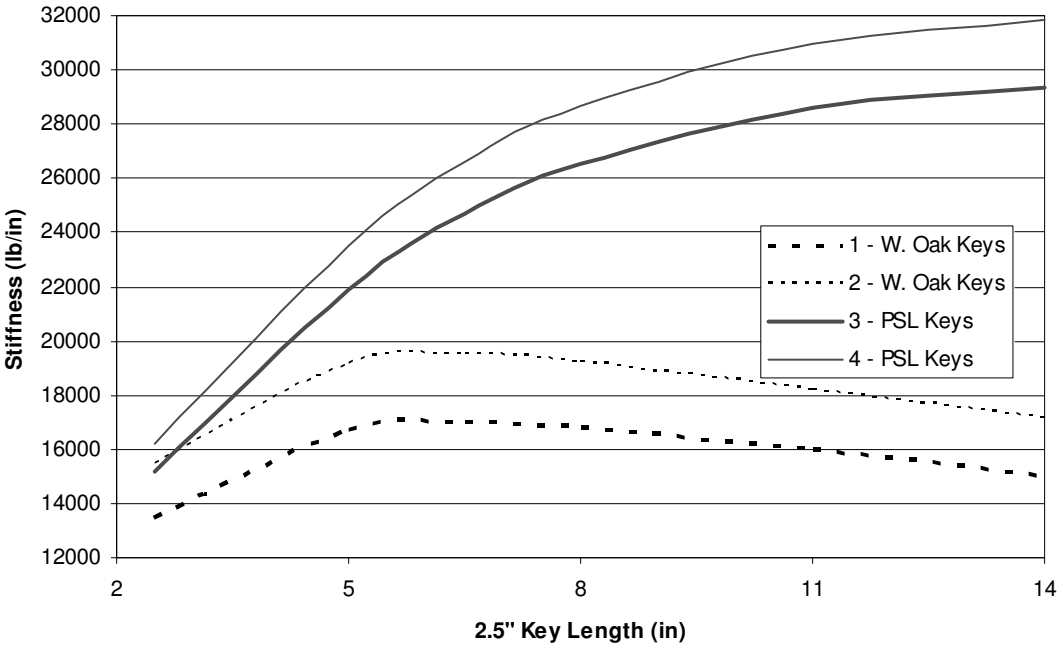

Figure 6-7 Relationship between key length and model stiffness

The use of short shear keys, which have a higher axial stiffness than very long shear keys, tends to result in keyed beams with a relatively low overall stiffness. This phenomenon is attributed to a short key being more likely to roll, as well as bearing

against the timber at a steeper angle to the grain. For the inclined key configurations using white oak keys, the highest beam stiffness occurred using the 2.5 inch by 6.5 inch key. Longer and shorter keys result in lower beam stiffnesses. This comparison was made assuming a constant number of clamping screws (four). Changing the number of clamping screws will likely shift the optimal key length slightly. Unlike with the white oak keys, the beam stiffness of the tests using Parallam PSL keys continually increased as the key length increased. The Parallam PSL keys had a higher compressive stiffness than the keyed beam timbers, which accounts for this behavior.

These findings appear consistent with Kidwell's recommendation to use shear keys with a 1:2 (2.5 inch by 5 inch) aspect ratio when being compressed across the grain (Kidwell, 1898). Karlsen's suggested aspect ratio of 1:5 (2.5 inch by 12.5 inch) appears reasonable from a stiffness standpoint when the keys are being loaded parallel to the grain, for which he advocated (Karlsen, 1967). However, fabricating a keyed beam using keys with a 1:5 aspect ratio may be problematic, due to the excessive length required for spacing between keys. Based on these results, the optimal key size appears to be a function of how the key modulus relates to that of the timber modulus. A thickness-to-length ratio of 1:2 to 1:3 (2.5 inch by 5 inch to 2.5 inch by 7.5in) appears reasonable for use with white oak keys, and this corresponds with a point of diminishing returns using the stiffer Parallam PSL keys.

6.4 Comparison to Kidwell's Test Data

In conjunction with this research, four keyed beams were constructed and tested, all with the same shear key spacing and loading configuration. While these physical tests

compared to the interlayer slip model quite well, further comparison with other keyed beam tests conducted by Kidwell was also conducted (Kidwell, 1898). Although Kidwell's research was conducted in the 19th century, enough detail was included in the research report to analyze his test configurations. According to Kidwell:

> "…it has been considered advisable to give a full report of each test, so that the reader will be put in full possession of all the facts necessary to enable him to draw his own conclusions, which may not always coincide with those of the writer."

6.4.1 Determining Material Properties

Kidwell provided numerous observations on the test frame, loading, and key configurations he used when testing the built-up beams (Kidwell, 1898). He also provided the species and weight of the tested beams, although he did not include moisture content or oven dry specific gravity. Based on Kidwell's discussion about the amount of time the test materials had to season before being used, along with the unit weight of the material at the time of testing, the material appeared to vary in moisture content in the range of 15-20%. Kidwell used #1 eastern white pine (*Pinus strobus*) for the timbers, which has a corresponding modulus of elasticity of 1,100,000 psi in the approximate moisture content range (AF&PA, 2005; FPL, 1999). The white oak shear keys were purportedly well seasoned, so a modulus of elasticity of 1,780,000 psi was used, which corresponds to the published stiffness at 12% moisture content (FPL, 1999).

Published values for certain material's elastic modulus have changed over time depending on specific growth characteristics of individual species. The original testing

for the eastern white pine and white oak test data included in the Wood Handbook was conducted by the Forestry Division of the USDA in the 1890s as part of nearly 40,000 physical tests (Fernow, 1892). Published values in the Wood Handbook for eastern white pine and white oak have remained constant (FPL, 1935; FPL, 1999). Other contemporary sources for Kidwell's day list modulus of elasticity values similar to the Wood Handbook (Snow, 1903). No adjustments have been made in this section for Kidwell's testing of old-growth material.

Kidwell used ½" diameter through bolts with oversized bearing washers to provide the clamping force between the layers of the keyed beam (Kidwell, 1898). The axial stiffness of the bolt was calculated as

$$k_{clamp} = \frac{AE}{L} = \frac{\left(\frac{0.5^2\pi}{4}\right)(24{,}000{,}000)}{5.5} = 857{,}000 lb/in \qquad (6\text{-}5)$$

where A is the cross sectional area of the bolt, E is the modulus of elasticity of ductile iron (Beer and Johnston, 1992), and L is the length of the bolt (total height of the built-up beam). The above calculation provides an upper bound for the clamping stiffness, as there will be some deformation underneath the bearing washers at each end of the bolt. However, the results of the interlayer slip model analysis in the subsequent sections did not appear overly sensitive to changes in this clamping stiffness.

Based on observations made when comparing the interlayer slip model to the full-scale test results conducted for this research, Kidwell's data was compared to two solutions to the interlayer slip model. One solution was based on 1:12 ratio of parallel to perpendicular elastic modulii ($E_{\parallel} = 12E_{\perp}$), the other with an ratio of 1:20 ($E_{\parallel} = 20E_{\perp}$).

6.4.2 Brunel's Beam

Kidwell fabricated and conducted two tests on what he described as "Brunel's beam," which is based on a design proposed by I.K. Brunel. Brunel's design included a built-up beam using inclined white oak shear keys to provide interaction between the layers. The white oak shear keys were installed as a pair of wedges such that they would be compressed across the grain. The layers were clamped together using 0.5 inch diameter bolts. The basic style of this beam is very similar to the full-scale beams tested in this research using inclined keys. Figure 6-8 shows the layout of the beams tested by Kidwell. The beams were tested by applying a point load at mid span until ultimate load was reached. Deflection measurements were taken at midspan in 0.0625 inch increments. The load-deflection plots of Kidwell's two tests are included in Figure 6-9. The test numbering (0F and 0G) used in the figures and tables correspond to his test numbering procedure.

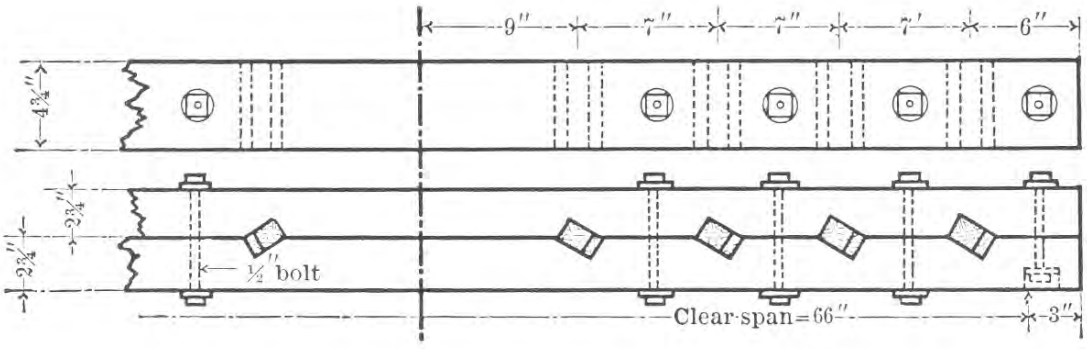

Figure 6-8 Key configuration in Brunel's beams (Kidwell, 1898)

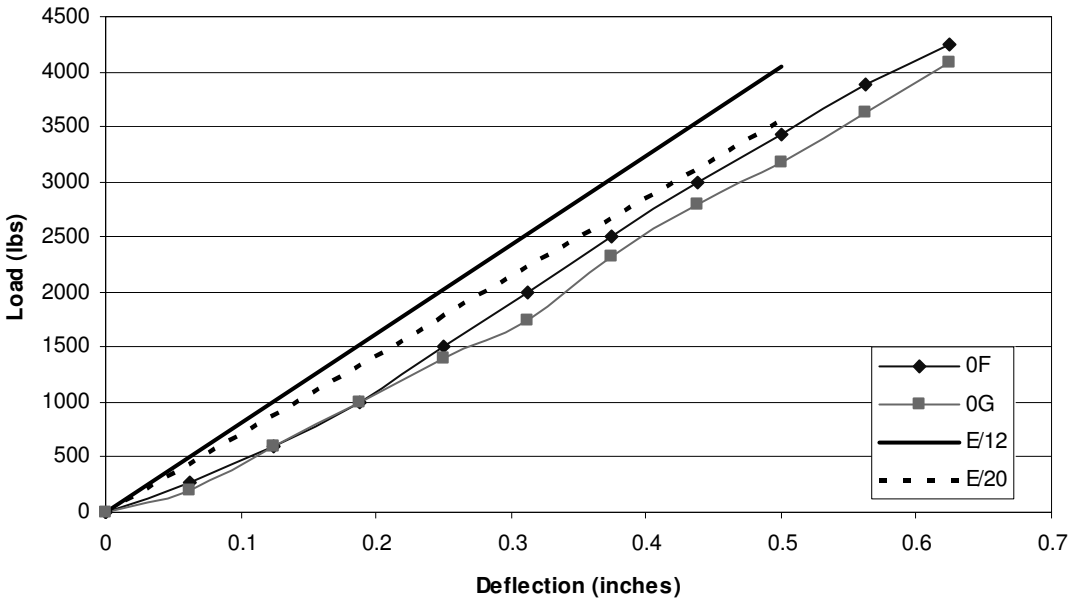

Figure 6-9 Load-deflection plots for Brunel's beams (Kidwell, 1898)

The interlayer slip model solution for a single point load (included in Appendix B) was used to analyze Brunel's beams. The simplified approach for determining shear key spacing was used (the summation of all the shear key stiffness over the length of the beam) for the analysis. The test stiffnesses and calculated stiffness are included in Table 6-5. The interlayer slip calculations can be found in Appendix H.

Table 6-5 Comparison of Brunel's beam stiffnesses to the interlayer slip model

Test	Ult. Load	Calc. Stiffness $E_{\|\|}=E_{\perp}/12$	Calculated Stiffness $E_{\|\|}=E_{\perp}/20$	Test	Difference $E_{\|\|}=E_{\perp}/12$	Difference $E_{\|\|}=E_{\perp}/20$
	lb	*lb/in*	*lb/in*	*lb/in*	*%*	*%*
0F	9780	8089	7112	8000	1.1%	-12.5%
0G	8660	8089	7112	7500	7.3%	-5.5%
				Avg.	4.2%	-9.0%

As with the full-scale testing conducted specifically for this research, the interlayer slip model resulted in a slightly stiffer beam than was observed during the

physical testing. However, the average difference between the calculated stiffness and the actual stiffness for these beams was 4.2% using an elastic ratio of $E_{\parallel} = \frac{E_{\perp}}{12}$ and 9.0% using a ratio of $E_{\parallel} = \frac{E_{\perp}}{20}$. Looking at the two tests individually, it appears the 1:12 elastic ratio fits the first test better, whereas 1:20 fits the second test data better, suggesting the interlayer slip model accurately represents the historical beam tests fairly well, but that optimal elastic ratio falls somewhere between 1:12 and 1:20.

6.4.3 Joggled Beam

Kidwell conducted additional tests on what he described as a joggled beam (that is, a beam where the keys are not inclined) (Kidwell, 1898). The key stiffness terms that were developed in section 2.5 can account for both the inclined keys and the square (non inchclined) keys. Kidwell conducted five tests on the joggled beams using white oak shear keys, and an additional two tests on joggled beams using cast iron shear keys. The configuration of the joggled beams can be seen in Figure 6-10 and Figure 6-11.

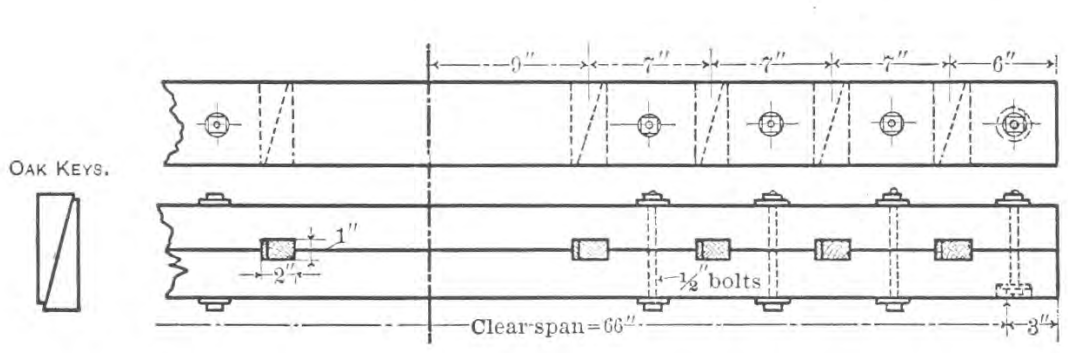

Figure 6-10 Key configuration for joggled beam using white oak keys (Kidwell, 1898)

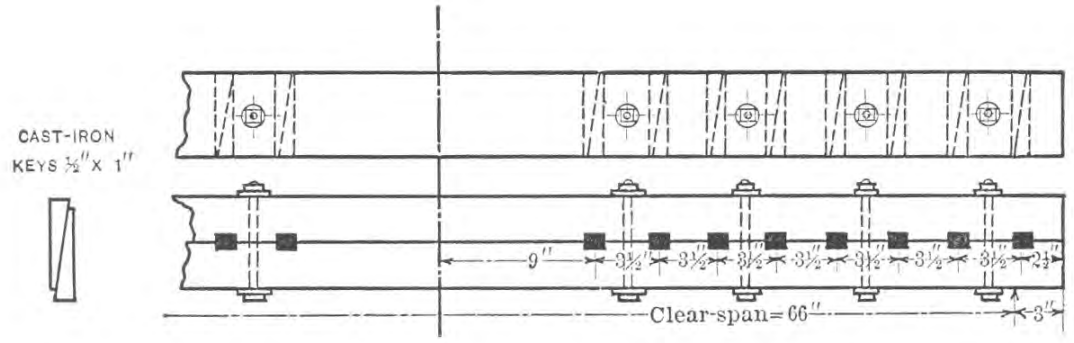

Figure 6-11 Key configuration for joggled beam using cast iron keys (Kidwell, 1898)

The interlayer slip model was again employed to compare the theoretical stiffness of the joggled beams to the observed stiffness. The load-deflection plots of the joggled beams with white oak keys using Kidwell's data can be found in Figure 6-12. The tabulated stiffnesses are in Table 6-6. As before, the stiffness predicted from the interlayer slip model is slightly higher than observed beam stiffness. Kidwell observed a substantial defect in the bottom face of beam 23, which he believed caused the reduced stiffness and premature failure. Excluding this defective beam, the average difference between the predicted stiffness and the observed stiffness is 7.5%, which again shows the interlayer slip model appears to be correctly predicting the behavior of built-up wooden beams. On average, an elastic ratio of $E_{\parallel} = \frac{E_{\perp}}{20}$ appears to best capture the beams' behavior.

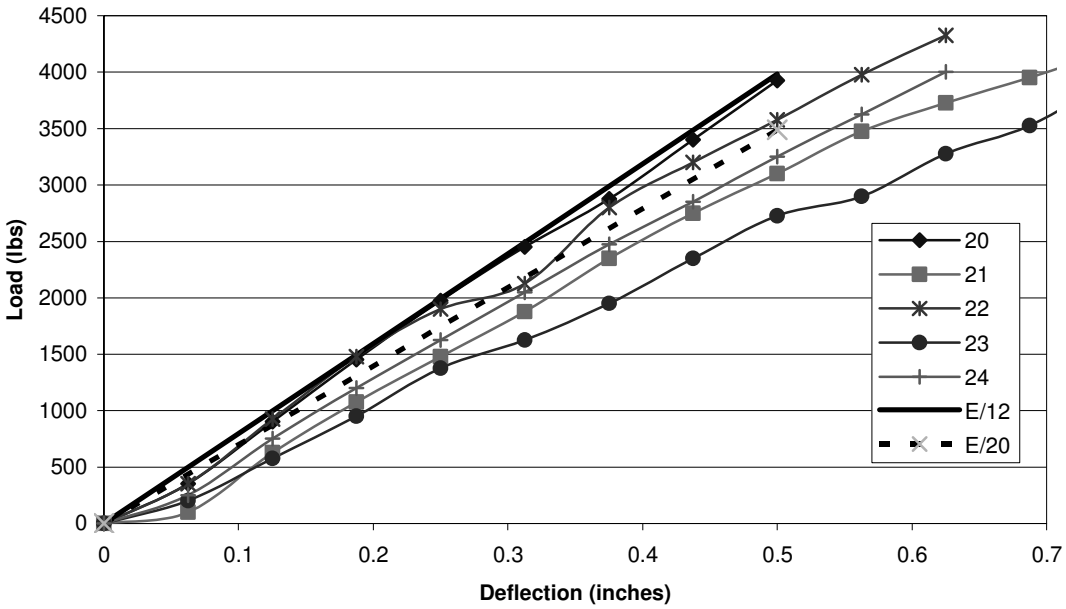

Figure 6-12 Load-deflection plots for joggled beams using white oak keys

Table 6-6 Comparison of joggled beam stiffnesses to interlayer slip model

Test	Ult. Load	Calc. $E_{\|\|}=E_{\perp}/12$	Stiffness Calculated $E_{\|\|}=E_{\perp}/20$	Test	Difference $E_{\|\|}=E_{\perp}/12$	Difference $E_{\|\|}=E_{\perp}/20$
	lb	*lb/in*	*lb/in*	*lb/in*	*%*	*%*
20	10600	7961	6974	7800	2.0%	-11.8%
21	6800	7961	6974	6900	13.3%	1.1%
22	8400	7961	6974	7800	2.0%	-11.8%
23	5260	7961	6974	6400	19.6%	8.2%
24	8660	7961	6974	6950	12.7%	0.3%
				Avg.	9.9%	-2.8%

Kidwell also conducted testing on two joggled beams using pairs of cast iron wedges as shear keys. Assuming a modulus of elasticity of the cast-iron keys as 24 Mpsi (Beer and Johnston, 1992), it is possible to use the interlayer slip model to predict the stiffness of the beams. Due to the cast iron keys being smaller, twice as many were used than the white oak keys, although with the same number of clamping connectors. These

variations were taken into account when using the interlayer slip model. Kidwell's load-deflection plots are shown in Figure 6-13, with the corresponding stiffness data shown in Table 6-7.

The interlayer slip model appears to accurately predict the stiffness of the built-up beams using cast-iron keys, again with elastic ratio of $E_{\parallel} = \frac{E_{\perp}}{20}$ best capturing actual beam behavior. The interlayer slip model over predicted the stiffness in one case, and under predicted the stiffness in the other case, although by minimal amounts. The theoretical upper-bound to this particular test configuration (assuming a full depth solid beam), is a stiffness of 10,663 lb/in. Therefore, using cast-iron keys, it appears it is possible to achieve beams nearly as stiff as their full depth counterpart.

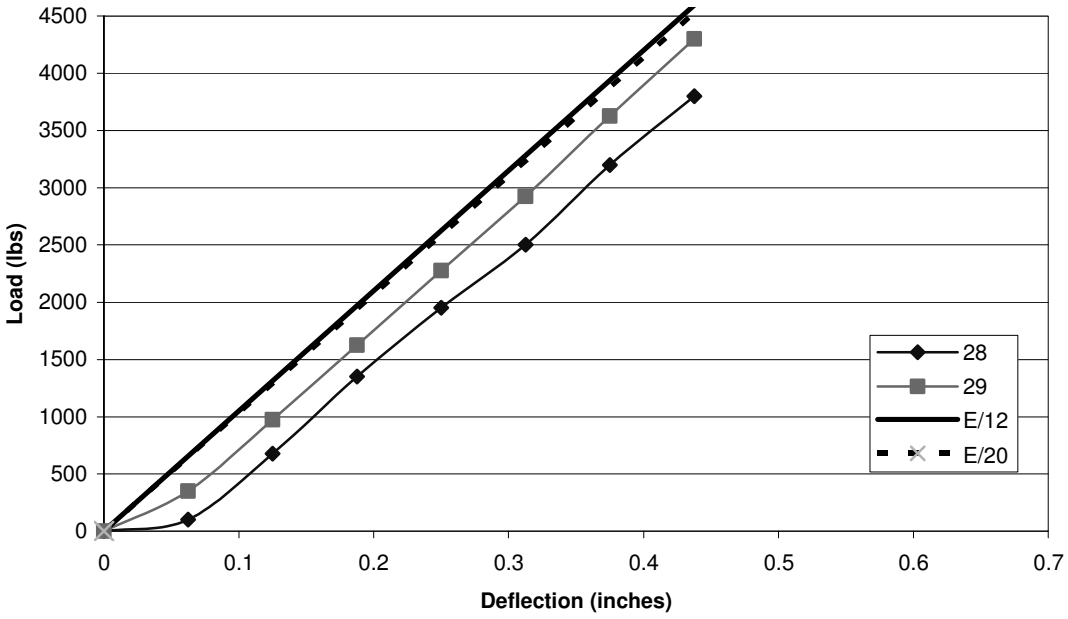

Figure 6-13 Load-deflection plots for joggled beams using cast iron keys

Table 6-7 Comparison of joggled beam stiffnesses to interlayer slip model

Test	Ult. Load	Calc. $E_{\|\|}=E_{\perp}/12$	Stiffness Calculated $E_{\|\|}=E_{\perp}/20$	Test	Difference $E_{\|\|}=E_{\perp}/12$	Difference $E_{\|\|}=E_{\perp}/20$
	lb	*lb/in*	*lb/in*	*lb/in*	*%*	*%*
28	10190	10500	10346	10100	3.8%	2.4%
29	11190	10500	10346	10600	-1.0%	-2.5%
					1.4%	0.0%

6.4.4 Three Layer Beam

The interlayer slip model developed in section 2 was based on a built-up beam made with n-plies, with specific solutions for a two layer beam in section 2.1.2 and a three layer beam in section 2.1.3. However, all work using the interlayer slip model after that point has focused on beams built from two plies. While no physical testing was conducted on three-layer keyed beams for this research, Kidwell conducted a full scale test on one, which is the basis for this comparison (Kidwell, 1898).

Kidwell's test on a three-layer beam (his test number 27), the configuration of which is shown in Figure 6-14, employed the use of 1 inch by 2 inch white oak shear keys installed square to the timber being compressed perpendicular to the grain. As with the joggled beams described above, the shear key stiffness terms already developed are capable of handling this key configuration.

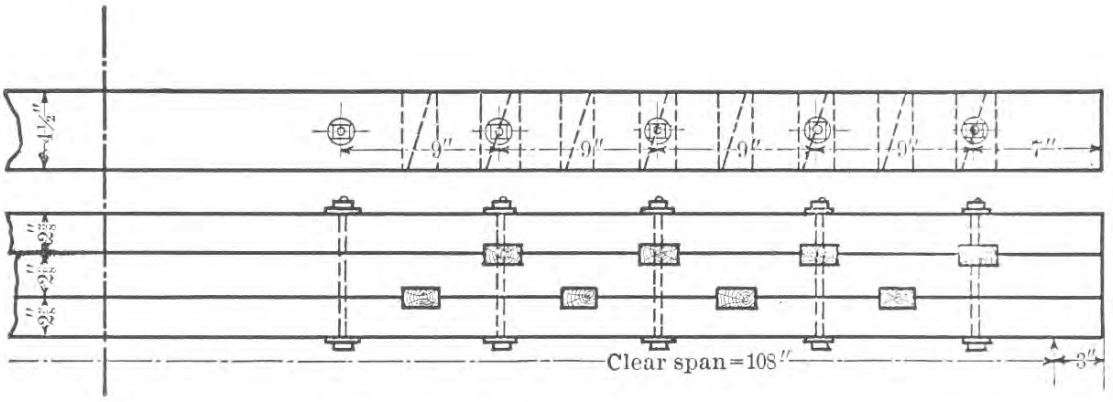

Figure 6-14 Key configuration for three-layer beam using white oak keys (Kidwell, 1898)

The load-deflection plot for Kidwell's test, along with the data from the interlayer slip model analysis, is shown in Figure 6-15. The three-layer beam exhibited considerable non-linear behavior, with very limited initial linear behavior. As anticipated, a three-layer beam is considerably less stiff than the equivalent full depth beam or two-layer beam due to the two interlayer slip planes (compared to one interlayer slip plane with a two-layer beam). Calculations for using the interlayer slip model for this particular test are included in Appendix H. Stiffness data is included in Table 6-8. Two ratios of the parallel to grain modulus of elasticity to the perpendicular grain modulus were analyzed (1:12 and 1:20), both of which were stiffer than the initial stiffness observed in the physical test. As observed in the previous comparisons, the modular ratio of 1:20 appears as consistent, if not more so, with observed data than a ratio of 1:12. However, determining an initial stiffness from the physical test's non-linear load-deflection may be a controlling factor in this comparison.

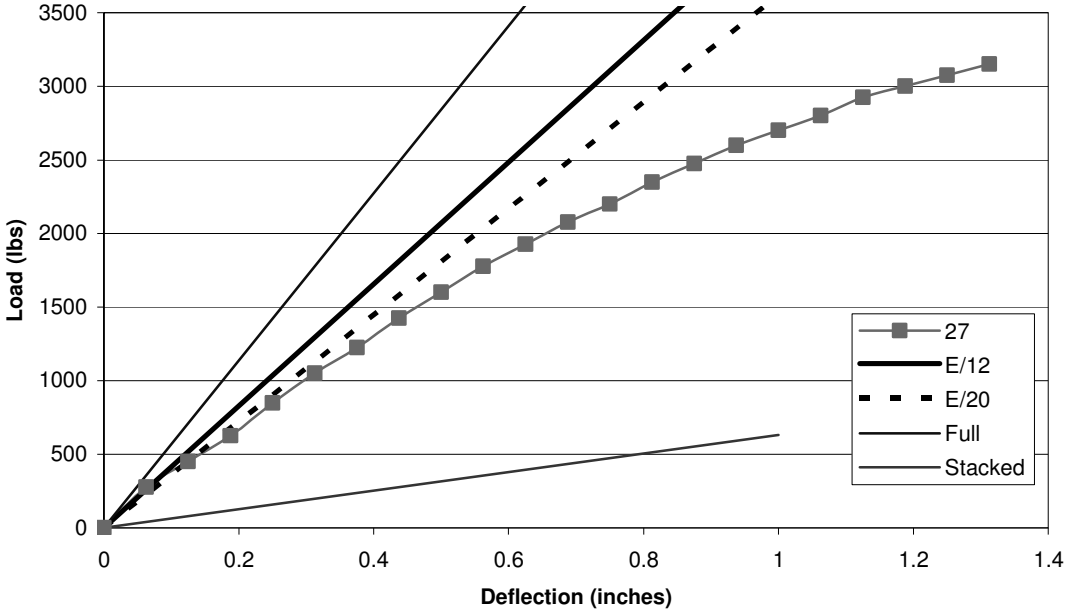

Figure 6-15 Load-deflection plots for three-layer beam using white oak keys

Table 6-8 Comparison of three-layer beam stiffness to interlayer slip model

Test	Ult. Load	Initial Stiffness Calc. $E_{\|\|}=E_{\perp}/12$	Initial Stiffness Calculated $E_{\|\|}=E_{\perp}/20$	Initial Stiffness Test	Difference $E_{\|\|}=E_{\perp}/12$	Difference $E_{\|\|}=E_{\perp}/20$
	lb	*lb/in*	*lb/in*	*lb/in*	*%*	*%*
27	5400	4140	3620	3600	13.0%	0.6%

Beams consisting of more than three layers are not discussed in this research for several reasons. The cumulative effect of in-service moisture related cross-sectional changes in built-up heavy timber beams made from more than three layers would be very difficult to address, in particular when ensuring that adequate key-clamping forces could be maintained. Another limiting factor for excessively deep built-up beams is their relatively inefficiency for long spans, as a truss system can carry loads considerably more efficiently than an equivalent depth beam.

6.4.5 Discussion of Results

The interlayer slip model appears to predict the behavior of Kidwell's historical data quite well. With the equations developed in section 2, it was possible to model both inclined shear keys ("Brunel's beam") and square shear keys ("joggled beams") made from various materials. A three-layer beam using white oak shear keys was also modeled. As was noticed in the full-scale testing of beams for this research, the white oak keyed beams have more variation in stiffness from one test to another compared to those with manufactured key material (Parallam PSL or cast-iron wedges). Assuming a ratio of 1:12 for the parallel-to-grain to perpendicular-to-grain elastic modulii appears to over predict the stiffness (6.8% stiffer for all of Kidwell's tests). An assumed elastic ratio of 1:20, as has been suggested by previous authors (Bodig and Jayne, 1982) slightly under predicts the beam stiffness (3.6% softer).

7 Ultimate Stress

The focus of the physical testing along with the comparisons to the interlayer slip model up until this point have focused on deflection and stiffness. In order to evaluate the failure and safe working loads, determining the stress in the layers is required.

7.1 Predication of Failure Load

The flexural stress in a wooden member at the time of a bending failure is commonly referred to as the modulus of rupture (MOR). The average modulus of rupture for most species of wood is published in the Wood Handbook (FPL, 1999), or can be found from small scale testing. For a built-up beam, failure can be described as occurring when the stress at either the top or bottom face exceeds the material's modulus of rupture. That is,

$$\begin{aligned} \sigma_T\left(\frac{h_T}{2}\right) &> MOR_T \\ \sigma_B\left(\frac{h_B}{2}\right) &> MOR_B \end{aligned} \tag{7-1}$$

where h_T and h_B are the depths of the top and bottom layers, respectively. Similarly, σ_T and σ_B are the stresses in the top and bottom layers at these points, as calculated from equations (2-43) and (2-44). For a specific loading configuration, both the moment M and the axial force in the layers F from composite action can be written as functions of the applied load. Setting the applied stress equal to the average published modulus of rupture (rather than the inequality described in equation (7-1)) allows for direct solution for the anticipated failure load.

7.2 Comparison to Full Scale Testing

The extreme fiber stress at the maximum load for each of the four keyed beams was calculated using the procedure outlined in section 2.4. The stress at maximum load was calculated using test data from the physical tests (see Table 6-1). Calculations for determining the stress are included in Appendix I, and the relevant information is summarized in Table 7-1. The extreme fiber stress for a simple stacked beam as well as a full depth beam subjected to the applied load are also included as upper and lower limits. Statistical data is not included, as only tests 1 and 2 showed signs of rupture at the maximum load (tests 3 and 4 buckled due to inadequate bracing of the hydraulic actuator).

Table 7-1 Stress at maximum load for full-scale beam tests

		Stress @ Max. Load							
Test	Max. Load	Calculated $E_{\|\|}=E_{\perp}/12$	Calculated $E_{\|\|}=E_{\perp}/20$	Full Beam	Simple Beam	Published MOR	Adjusted MOR	Calc. vs MOR $E_{\|\|}=E_{\perp}/12$	Calc. vs MOR $E_{\|\|}=E_{\perp}/20$
	lb	*psi*	*psi*	*psi*	*psi*	*psi*	*psi*	*%*	*%*
1	34130	6213	6669	4252	8503	10100	6898	-9.9%	-3.3%
2	39620	6759	7254	4994	9987	10100	7427	-9.0%	-2.3%
3*	42370	6012	6109	4685	9370	10100	6974	-13.8%	-12.4%
4*	35060	4691	4925	3879	7759	10100	7618	-38.4%	-35.3%

* Ultimate load was never reached

The calculated stress is based on the material properties of the timber at the time of testing, rather than the published values based on a normalized 12% moisture content. In order to compare the calculated stresses to the published modulus of rupture, the published modulus of rupture (MOR) values were adjusted following the procedure set forth in the Wood Handbook (FPL, 1999), which has been used in the previous sections.

The anticipated modulus of rupture, MOR_{ACT}, based on the material's moisture content and specific gravity is calculated as

$$MOR_{ACT} = MOR_{12\%}\left(\frac{MOR_{12\%}}{MOR_{GREEN}}\right)^{\left(\frac{12-MC}{13}\right)}\left(\frac{G_{ACT}^{1.01}}{G_{12\%}^{1.01}}\right) \tag{7-2}$$

where $MOR_{12\%,GREEN}$ are the published MORs for wood at 12% moisture content as well as in the green state, MC is the moisture content of the material, and $G_{ACT,12\%}$ is the actual and published oven dry specific gravity of the material. The average moisture content and specific gravity (shown in Table 6-1) of the top and bottom layers in each test were used when calculating the anticipated modulus of rupture.

Published modulus of rupture values are based on testing conducted on small, clear, straight grained samples. However, it has been shown that the strength of beams decreases as the size increases (FPL, 1999). Therefore, published allowable bending stress values take into account the cross-sectional size of the timber (AF&PA, 2007). To account for the larger cross sections used in this research's testing component, adjustments were made to the modulus of rupture following the procedure outlined in the Wood Handbook (FPL, 1999). The adjusted modulus of rupture, MOR_{ADJ}, was calculated as

$$MOR_{ADJ} = MOR_{ACT}\left[\frac{h_2L_2\left(1+\frac{ma_2}{L_2}\right)}{h_1L_1\left(1+\frac{ma_1}{L_1}\right)}\right]^{\frac{1}{m}} \tag{7-3}$$

where MOR_{ACT} is the modulus of rupture from equation (7-2), h and L are the depth of the test specimens, a is the distance between the symmetrically placed point loads, and m is a constant, normally taken as 18. The published modulus of rupture values in the Wood Handbook and other sources are determined according to ASTM D143 (ASTM, 2007), which consists of 2 inch by 2 inch material spanning 28 inch and loaded by a point load at midspan. Taking this information into account, along with the loading configuration for the full scale testing, equation (7-3) can be rewritten as

$$MOR_{ADJ} = MOR_{ACT}\left[\frac{56}{810\left(h_T + h_B\right)}\right]^{\frac{1}{18}} \tag{7-4}$$

where h_T and h_B are the depths of the top and bottom layers of the built up beam. The adjusted moduli of rupture values are included in Table 7-1.

The extreme fiber stress in the keyed beam was calculated using elastic ratios of $E_{\parallel} = 12E_{\perp}$ and $E_{\parallel} = 20E_{\perp}$, with the 1:20 ratio providing slightly better results than the 1:12 ratio. Statistical data is not included in Table 7-1, as only tests 1 and 2 showed signs of rupture at the maximum load (tests 3 and 4 buckled due to inadequate bracing of the hydraulic actuator). However, based on this limited amount of data, it appears the interlayer slip model appears to be accurately predicting the extreme fiber stress.

7.3 Comparison to Kidwell's Historical Testing

In order to further investigate the accuracy of the interlayer slip model at predicting the extreme fiber stress at rupture, Kidwell's test data was also analyzed in a fashion similar to section 7.2. The results of the analysis are included in Table 7-2.

Moisture content and specific gravity information was not available for Kidwell's test data, and his physical tests were conducted on small beams, so no adjustments to the published modulus of rupture were made. Kidwell noted a substantial defect in test 23, which he believed caused its premature failure.

Table 7-2 Stress at maximum load for Kidwell's beam tests

Test	Max. Load	Stress @ Ultimate				Published MOR	Calc. vs MOR	
		Calc. $E_{\|\|}=E_{\perp}/12$	Calculated $E_{\|\|}=E_{\perp}/20$	Full Beam	Simple Beam		$E_{\|\|}=E_{\perp}/12$	$E_{\|\|}=E_{\perp}/20$
	lb	*psi*	*psi*	*psi*	*psi*	*psi*	*%*	*%*
0F	9780	8592	9333	6738	13477	8600	-0.1%	8.5%
0G	8660	7608	8264	5967	11933	8600	-11.5%	-3.9%
20	10600	9552	10115	7303	14607	8600	11.1%	17.6%
21	6800	6128	6489	4685	9370	8600	-28.7%	-24.5%
22	8400	7570	8016	5788	11575	8600	-12.0%	-6.8%
~~23~~	~~5260~~	~~4740~~	~~5020~~	~~3624~~	~~7248~~	~~8600~~	~~-44.9%~~	~~-41.6%~~
24	8660	7804	8264	5967	11933	8600	-9.3%	-3.9%
28	10190	8428	8721	7021	14042	8600	-2.0%	1.4%
29	11190	9254	9578	7710	15420	8600	7.6%	11.4%
						Avg*	-5.6%	0.0%

* Test 23 Data Removed

The extreme fiber stress in Kidwell's beams were calculated using elastic ratios of $E_{\|} = 12E_{\perp}$ and $E_{\|} = 20E_{\perp}$, again with the 1:20 ratio providing slightly better results than the 1:12 ratio. Based on these findings, the interlayer slip model appears to accurately predict the failure stress of a keyed beam.

7.4 Discussion of Results

As can be seen in Table 7-1 and Table 7-2, using the interlayer slip model appears to be a viable method to calculate the failure stress in a beam with partial interaction between layers. As has been observed in the previous sections, an elastic ratio where

$E_{\parallel} = 20E_{\perp}$ appears to best represent the beam behavior, based both on stiffness and on strength criterion.

For the test configurations used, the maximum stress occurs at the applied point loads (recall Figure 2-6). Any defect near these points can increase the likelihood of stress concentrations, which are not captured by the interlayer slip model. Although the second full scale test showed cracks propagating from the reentrant corner of the shear key notches nearest the applied point load (Figure 5-8), these stress concentrations did not appear to have any impact on the beam capacity.

8 Design Procedure

The interlayer slip model developed in section 2 appears to predict the behavior of actual keyed beams quite well (section 6). For common design situations, the exact material properties of each individual piece of material used in a built up beam will not be known, and the size and configuration of shear keys will need to be developed. Therefore, a method for determining a design capacity of a particular configuration from readily available published design information is required.

The design of a built-up keyed beam is an iterative process. The size and number of layers in the built up beam needs determined. Likewise, the number and type of shear keys, their spacing, and the number of clamping connectors needs to be chosen before the beam can be analyzed. After the initial analysis, the timber sizes and shear key components can be adjusted accordingly, followed by a re-analysis of the beam.

8.1 Shear Key and Clamping Connector Design

Design of a shear key and clamping connector is based on the force being transferred between the layers of the built-up beam. Exact and simplified methods for analyzing the stress and stiffness of a built up beams are detailed in subsequent sections. However, determination of the capacity of the shear keys and clamping connectors should follow the same proceedure, regardless of whether an exact or simplified procedure is used for the design of the beam.

8.1.1 Shear Key and Timber Compressive Strength

The capacity of a shear key can be limited by either the compressive capacity of the shear key or the compressive capacity of the timber at the shear key notch. Using the notation shown in Figure 2-8, the horizontal shear capacity N of a key is

$$N = \min \begin{vmatrix} btF'_{c,key} \\ btF'_{c,tim} \end{vmatrix} \tag{8-1}$$

where b is the lesser breadth of the two layers being connected by the shear key and t is the depth of the notch perpendicular to the interface. $F'_{c,key}$ and $F'_{c,tim}$ are the adjusted allowable compressive stresses in the key and timber, respectively, determined in accordance with section 4 of the National Design Specification for Wood Construction, henceforth referred to as the NDS (AF&PA, 2005). The NDS includes published allowable compressive, shear, tensile, and bending stress values, determined following the appropriate ASTM standards depending on size and material, along with adjustment factors for variations in anticipated in-service moisture content, size, and temperature. These adjustments apply to a built-up beam in a similar fashion to a solid or simply stacked beam.

When calculating $F'_{c,key}$ for a key installed such that it is being compressed perpendicular to the grain, all of the adjustment factors included in the NDS should apply. For $F'_{c,key}$ when the key is being compressed parallel to the grain as well as all instances of $F'_{c,tim}$, all adjustment factors apply except for the column stability factor. Solid sawn shear keys should be made from clear, straight grained material (see 3.1.2),

and thus tabulated allowable stresses for select structural material should be used for the keys.

8.1.2 Shear Key Spacing

The minimum spacing between shear keys is determined by the material properties and key configuration, and is independent of the external load that is applied to the beam. The spacing is determined by ensuring there is adequate shear resistance between the shear key notches to develop the full design capacity of the shear key. The NDS includes a non-mandatory suggestion to use a more conservative linear shear stress distribution (AF&PA, 2005) (see section 3.6), although common design practice in timber construction is to use a less conservative uniform stress distribution (Goldstein, 1999). For a shear key designed to resist a horizontal shear force N (Figure 2-8), the minimum shear key spacing is

$$s_{\min} = \frac{N}{bF'_v} \tag{8-2}$$

where F'_v is the adjusted allowable horizontal shear strength of the timber, calculated in accordance with section 4 of the NDS (AF&PA, 2005).

The maximum spacing between shear keys can be determined by using the shear flow q for a beam. The maximum spacing, $s_{\max}$, can be found by setting the shear key capacity equal to the area under the shear flow diagram and solving for the horizontal spacing. The maximum spacing is therefore dependent on the applied load, as different moment distributions result in different shear distributions. A solid beam of uniform

cross section along the length has a constant first moment and moment of inertia, so the shape of the shear diagram accurately depicts the shape of the shear flow diagram.

For a beam with a pair of equal, symmetrically placed concentrated loads, the moment distribution is linear and the shear diagram is constant at the ends, with constant moment and no shear in the middle (see Figure 3-7). Using the shear flow diagram for a solid beam to approximate for the shear flow diagram for a built up beam, the maximum shear key spacing is therefore constant along the end sections based on the area under the shear flow diagram (Figure 8-1a). A beam subjected to a uniformly distributed load has a parabolic moment distribution and linear shear distribution about the entire length. The linear distribution of shear (and thus shear flow) results in a larger maximum shear key spacing near the middle of the span than near the ends (Figure 8-1b).

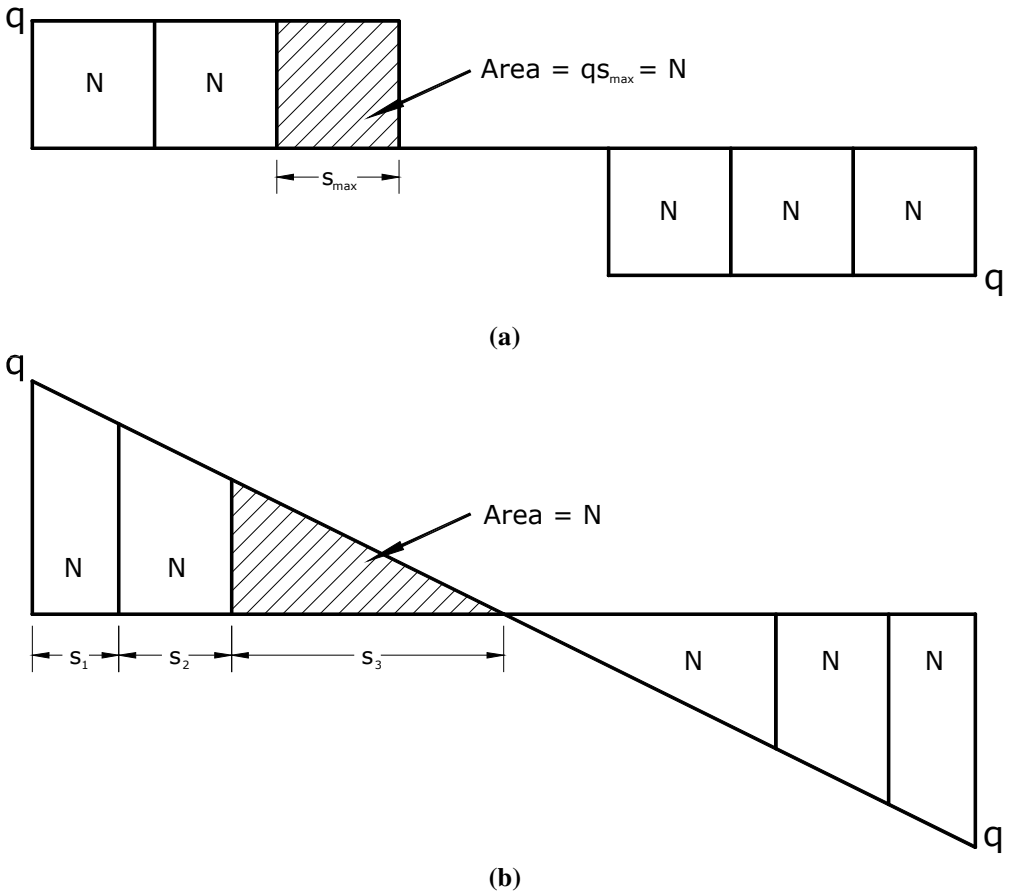

Figure 8-1 Shear key spacing for a beam with (a) two concentrated point loads, and (b) a uniformly distributed load.

For a built-up beam that has full composite action between the layers, equation (2-58) can be used to determine the shear key spacing. However, a built-up beam has only partial composite action between the layers, the shear force is determined by the differential equation described in equation (2-14), where the shear force is determined by the change in axial force about the length. Therefore, the maximum shear key spacings determined from the shear flow curve of the full-depth beam will vary slightly from the spacings determined from the built-up beam shear flow curve). As the area under the full-depth beam curve is always greater than the built-up beam curve (see Figure 2-12a

and Figure 2-12b, use of the shear flow diagram for from a full depth beam to determine shear key spacing for design purposes appears adequate and slightly conservative.

8.1.3 Clamping Strength Requirements

Sufficient clamping connector strength should be used to generate the full design compressive capacity of the shear keys. The sensitivity analysis conducted in section 6.3.3 suggests that excessive clamping connector stiffness has a diminishing benefit on the stiffness of a built-up beam, so specifying additional connectors beyond the design capacity of the shear keys appears to be an inefficient method of increasing built-up beam performance.

The minimum required clamping force, R, is found by summing moments about the point of rotation in a shear key (see Figure 8-2 and Appendix D), such that

$$R = \frac{Nt}{w + t} \tag{8-3}$$

where N is the horizontal capacity of the shear key, t is the depth of the shear key notch perpendicular to the interface, and w is the length of the shear key parallel to the interface. Equation (8-3) is based on the clamping connector being installed a distance t away from the shear key notch, which is shown Figure 8-2.

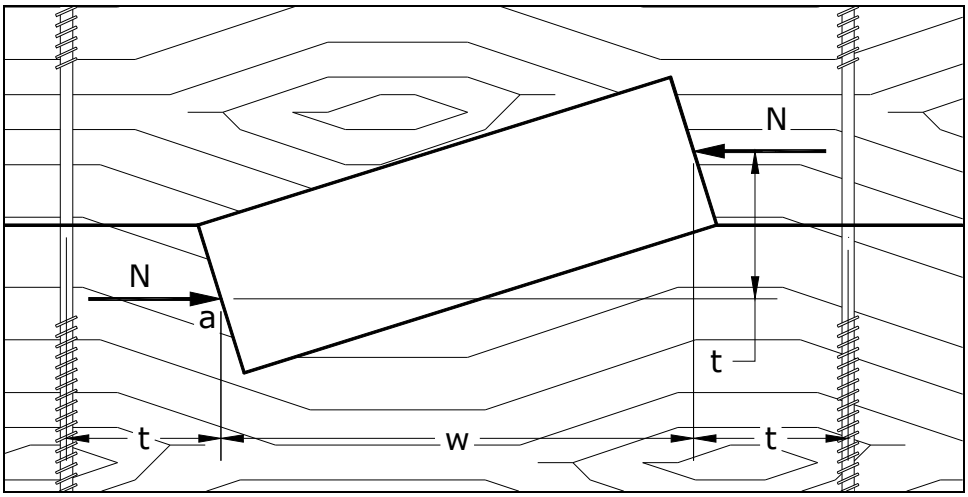

Figure 8-2 Clamping connector geometry

When clamping connectors are used on both ends of the shear key, the clamping force R should be divided evenly between each end. Design of the clamping connectors should follow the appropriate design standards or published manufacturer data for proprietary connectors.

8.2 Full Design Procedure

The interlayer slip model provides an exact method to analyze the actual bending stress, deflection, and horizontal shear in a built-up beam. Thus, the model can be employed for determining a built-up beam's adequacy to resist design loads.

8.2.1 Beam Bending Stress

The common design methodology for timber flexural members is to ensure the applied stress is less than some maximum allowed stress (commonly referred to allowable stress design, or ASD). With a solid, full depth rectangular beam, the maximum bending stress occurs at the extreme fibers (top and bottom) of the beam. If the built-up beam has nearly full interaction between the layers, it acts similarly to a solid

beam. Likewise, if the built-up beam has limited action between the layers, it acts similarly to two stacked beams, which have similar stresses on the top and bottom of each layer. Therefore, the maximum stress will always occur on the top and bottom faces of a two-layer beam, assuming no material defects or other discontinuities that can cause stress concentrations.

For a two layer built-up beam with partial interaction, equations (2-43) and (2-44) can be used to evaluate the stress at any point. The process outlined in section 2.4 can be used for beams with additional layers. Using these equations, the extreme fiber bending stress in the top and bottom layers, f_b, can be compared to the maximum adjusted allowable bending stress, F'_b, such that

$$f_b \leq F'_b \tag{8-4}$$

where F'_b is determined using section 4 of the NDS (AF&PA, 2005), and the tabulated bending stress is based on the lowest bending stress of an individual layer. For the size adjustment factor, using the cross sectional area of the full depth beam is slightly conservative compared to that of a simply stacked beam or some other equivalent depth beam. Using the lateral-torsional stability factor for the full depth beam is suggested, although it is slightly unconservative for a partially composite beam, as there is not full lateral interaction between layers. For common design configurations, the clamping connectors required to resist shear key rotation should provide sufficient lateral restraint to cause the beam to act rigidly in torsion.

8.2.2 Beam Stiffness

As discussed in detail in section 6, the interlayer slip model can accurately predict the stiffness of actual built-up beam using wood keys. For design purposes, using the published modulus of elasticity values from the NDS for determining the beam and key stiffness is consistent with the design procedures for solid sawn beams. As with the bending stress, the modulus of elasticity is adjusted for variations in moisture content and temperature, resulting an adjusted modulus of elasticity value, E', used in calculating beam deflections. These adjusted elastic moduli can be used with the interlayer slip model to predict the actual keyed-beam deflection, which can be compared to serviceability requirements outlined in the governing building code.

8.3 Simplified Design Procedure

While the interlayer slip model can be used for design purposes, solving the governing differential equations and analyzing each individual solution for new loading conditions is impractical if built up beams are to be used in regular design practice. An approach that provides a similar level of performance with reduced effort is therefore desired.

To predict the stiffness of a built-up beam, the Eurocode (2004) uses an approximation based on an effective "EI" (modulus of elasticity multiplied by the moment of inertia), which is described in further detail by Thelandersson and Larsen (2003). This method is based on a sinusoidal loading condition with a uniform connector spacing, where the connector shear stiffness is known. The approach of using an effective "EI" is analytically quite convenient as it allows for the use of existing

structural analysis methods for a solid timber cross section to be used. For keyed beams made from similar species of wood, the modulus of elasticity will be the same for all layers, so an effective moment of inertia is able to capture the interlayer slip's effect on beam stiffness. Expansion of the Eurocode method is investigated in this research a possibility for keyed beams.

For a stacked beam with no interaction between the layers, the moment of inertia of the combined beam of n layers is

$$I_{stacked} = \sum_{i=1}^{n} I_i \tag{8-5}$$

where I_i is the moment of inertia for the ith layer. Using the parallel-axis theorem, the moment of inertia for a built-up beam with full interaction between the layers (e.g. a full depth beam) is

$$I_{full} = \sum_{i=1}^{n} I_i + \sum_{i=1}^{n} A_i d_i^2 \tag{8-6}$$

where A_i is the cross-sectional area and d_i is the distance from the centroid of the built-up beam to the centroid of the ith layer. The moment of inertia of a built-up beam with partial interaction will have a moment of inertia that falls somewhere between that of a stacked and full depth beam, such that

$$I_{eff} = \sum_{i=1}^{n} I_i + \lambda \sum_{i=1}^{n} A_i d_i^2 \tag{8-7}$$

where λ is some number between 0 (simple stacked beam) and 1 (full-depth beam), and is the efficiency of the keys at providing interaction between the layers (see section 2.6). Individual solutions of the interlayer slip model for a given loading configuration can

yield closed form solutions for λ if the shear key stiffness and spacing is known. However, development of a method for calculating a simplified λ is not included in this research due to the limited number of physical tests from which to draw conclusions.

The lateral-torsional buckling adjustment to the tabulated allowable design bending stress included in the NDS does not include a moment of inertia term. To allow for use of this term, the effective EI discussed above should be adjusted to account for the reduced beam stiffness entirely in the modulus of elasticity term. This change can be accounted by the relationship

$$E_{full} I_{eff} = E_{eff} I_{full} \tag{8-8}$$

where E_{full} is the tabulated modulus of elasticity of the timber, E_{eff} is an effective modulus of elasticity of the beam for use in the beam lateral-torsional stability adjustment factor calculations, and I_{full} is the full depth moment of inertia of the beam.

9 Conclusions

9.1 Summary

The main focus of this research was to investigate whether the traditional interlayer slip model, in conjunction with a shear key stiffness model, would be able to accurately predict the strength and stiffness of a built up keyed beam that has partial interaction between layers. To verify this hypothesis, solutions of the governing interlayer slip differential equations were developed for several common loading configurations, small scale testing was conducted to determine key and connector stiffness parameters, and full scale beam testing was also conducted. Test data from historical sources was compared to solutions of the interlayer slip model.

Based on the findings from the investigations conducted as part of this research, several significant contributions were made to the field of interlayer slip analysis and timber engineering. Specifically,

- the interlayer slip model was expanded to include the ability to model any n-layer beam.
- the interlayer slip model's ability to accurately model keyed beam behavior was verified through comparison to full-scale tests.
- an analytical model was developed that captured the stiffness behavior of various shear key assemblies.
- a robust analytical design procedure was developed allowing for the design and analysis of keyed beams made with various key configurations and subjected to different loading conditions.

9.2 Qualified Recommendations

Based on observations made and data collected during this research, several recommendations can be made about the behavior or design of keyed beams. These recommendations are intended for engineers and fabricators that design and build keyed beams.

- When shear keys made from solid wood are used, they should be installed such that they are compressed perpendicular to the grain. While the perpendicular to the grain compressive stiffness of wood is considerably less than the parallel to the grain compressive stiffness, ease of installation of the shear key wedges makes up for this shortcoming. Installing the shear keys such that they are compressed parallel to the grain can easily result in damaged keys (see Figure 3-2). Keys made from manufactured material, such as Parallam PSL, can be easily installed such that they are compressed parallel to the grain, and thus are considerably more efficient than an equivalent sized solid sawn shear key.

- For yellow poplar and white oak, using an elastic ratio of 1:20 (i.e., $E_{\parallel} = 20E_{\perp}$) appears to best model actual timber behavior. As yellow poplar acts more like a softwood (despite being classified as a hardwood) and white oak is representative of most hardwoods used in heavy timber construction, an elastic ratio of 1:20 should be used for other species as well.

- Shear key stiffness has a strong impact on overall beam efficiency and stiffness. Therefore, using shear keys with higher compressive stiffnesses will result in higher beam stiffnesses. However, shear key compressive stiffnesses that greatly exceed the bearing stiffness of the timber (such as cast-iron keys) at the shear key notch provide diminishing returns on beam efficiency.

- All shear keys require a clamping mechanism in order to resist rotation when loaded. Several options exist for clamping connectors, as is discussed in detail in section 3.3. However, overly stiff or an excessive number of clamping connectors does not have a substantial effect on keyed beam efficiency or stiffness. Enough clamping capacity should be provided such that the shear key is more likely to compress than rotate; any additional clamping capacity beyond this point has limited benefit (see section 6.3.3).

- Inclined shear keys are preferable to square shear keys, in that they require substantially less key material, which in turn results in less material being removed for shear key notches in the main timbers. With modern cutting tools, making inclined shear key notches requires a similar level of effort as square shear key notches. Inclined shear keys also are in pure compression, whereas square shear keys are subjected to compression as

well as shear. However, inclined shear keys can only resist slipping in one direction.

- Concentrated loads can cause spikes in the extreme fiber bending stress of the timber layers (see Figure 2-6). Before notches are placed at or near the point loads, care should taken to ensure the notches will not generate extensive stress concentrations that cause premature failure of the beam.

- The friction between the layers of a built up beam can be ignored for analysis purposes. Even when layers were clamped tightly together before being screwed together, slippage of the layers occurred before any extensive amount of frictional forces could be developed. Dynamic friction forces also appear to be negligible.

- The efficiency of built-up beams using more than three plies is quite low, and does not lend itself to practical use. Parallel chord trusses or other framing options should be investigated for use in place of keyed beams requiring more than three layers.

- Double-threaded screws used as clamping connectors ensure tight bearing of the mating slippage planes. However, the varying pitch on the threaded portions that pulls the members together does not appear to substantially affect the axial stiffness of the clamping connector.

- The efficiency of built-up beams carrying transverse loads is directly related to the stiffness of the connecting shear keys. While wood increases in stiffness as it dries, it also shrinks. Any shrinkage in the shear keys or in the timbers will negatively impact the capacity and stiffness of the beam. Therefore, kiln-dried key stock should be used, along with well dried timbers, whenever possible.

9.3 Future Research

Several areas requiring additional study became apparent during the development of this research and are listed in below.

- Additional full scale physical testing of keyed beams using various timber species and key materials, along with different loading configurations and key grain orientations, are critical. Additional tests will further verify the interlayer slip and shear key stiffness model's ability to model the behavior of built up beams. More testing will also allow for meaningful statistical analyses to be made, which are required for determining the reliability of this type of building system.

- While solutions to the interlayer slip model were developed for several common loading configurations, developing a less computationally intensive method of predicting beam efficiency is important for continued

use by design professionals. Developing a simplified procedure should be conducted in conjunction with, or after, additional full scale testing, to lend statistical significance to the procedure.

- Inclined white oak and Parallam PSL shear keys were used in this research, which proved to be easy to fabricate and install. To further examine the breadth of applicability of the shear key stiffness model, testing should be conducted using different materials and key configurations. The effectiveness of shear keys installed square to the timber (see Figure 2-7a) at resisting two way slippage (due to reversal of beam loading) should also be investigated.

- The use of larger shear keys, such that the individual layers of the beam are spaced some distance apart (no contact between layers), should also be investigated. While larger (thicker) shear keys increase the clamping capacity required to keep the keys from rotating, spacing the layers of the beams apart increases the effective depth with limited increase in material usage.

- The long term loading of wood, especially members that are subjected to drying in service, results in measurable amounts of creep. Built-up beams, in particular ones that use shear keys, can be subjected to fairly high in-

service stresses. Therefore, creep of the shear keys as well as the timbers should be investigated

- Using shear keys fabricated from a pair of opposing wedges allows for substantial adjustments to the shear key widths, which can account for fabrication tolerances in the shear key notch sizes. Prestressing and inducing positive camber into the beams by intentionally mis-aligning shear key notches, which can then be realigned by driving the shear keys, is of particular personal interest and should be investigated both from a theoretical as well as physical standpoint.

- An investigation into the appropriateness of the NDS provisions for lateral stability of a built-up beam should also be investigated. A partially-composite beam will not behave the same as a full-depth beam during lateral-torsional buckling.

- Use of the interlayer slip model to analyze a built-up beam made with specific cross sectional and material properties, along with a known key configuration, is fairly straight forward. However, designing the optimal keyed beam from scratch for a specific loading configuration requires evaluating many different beam configurations and comparing the results. An automated procedure for developing the optimal key configuration and beam parameters based on the designer's or fabricator's preference would

be extremely valuable. For example, an optimization sequence would determine if adding more shear keys to a beam is more cost efficient, from both a labor and material standpoint, than using fewer shear keys and slightly larger timber cross sections.

10 References

American Forest and Paper Association (AF&PA). (2005). "National design specification for wood construction," AF&PA, Washington, DC.

ASTM. (2007*). 2007 Annual Book of ASTM Standards, 04.10 Wood*, Philadelphia, PA.

Benson, T. (1999). *Timberframe.* Taunton Press, Newtown, CT.

Beer, F.P. and Johnston, E.R. (1992). *Mechanics of materials,* 2nd Ed, McGraw-Hill, New York.

Bodig, J., and Jayne, B.A. (1982). *Mechanics of wood and wood composites,* Van Nostrand Reinhold Publishing, New York.

Brungraber, B. (2008). Personal communications.

Coduto, D. (2001). *Foundation design*, 2nd Ed, Prentice Hall, Upper Saddle River, NJ.

Cowper, G.R. (1966). "The shear coefficient in Timoshenko's beam theory," *ASME Journal of Applied Mechanics*, June:335-340.

Dall'Asta, A. and Zona, A. (2004). "Slip locking in finite elements for composite beams with deformable shear connection," *Finite Elements in Analysis and Design*, 40:1907-1930.

Durm, J., and Esselborn, K. (1908). *Lehrbuch des Hochbaues,* Wilhelm Engelmann, Leipzig.

Eurocode. (2004). "Eurocode 5: Design of timber structures," EN 1995-1-1:2004(E).

Faella, C., Martinelli, E., and Nigro, E. (2002). "Steel and concrete composite beams with flexible shear connection: "exact" analytical expression of the stiffness matrix and applications," *Computers and Structures*, 80:1001-1009.

Fernow, B.E. (1892). "Timber Physics," Forestry Division Bulletins 6&8, United States Department of Agriculture, Washington, DC.

Forchheimer. (1892). "Ueber zusammengesetzte Balken," *Zeitschrift des Vereines deutscher Ingenieure,* 36:100-103.

Forest Service. (1985). "Yellow poplar," FS-272, United States Department of Agriculture, Washington, DC.

Frangi, A. and Fontana, M. (2003). "Elasto-plastic model for timber-concrete composite beams with ductile connection," *Structural Engineering International*, 12(1):47-57

Forest Products Laboratory. (1935). *Wood handbook: basic information on wood as a material of construction with data for its use in design and specifications,* USDA Forest Service, Madison, WI.

Forest Products Laboratory. (1999). *Wood handbook,* FPL-GTR-113, Madison, WI.

Goldstein, E.W. (1999). *Timber construction for architects and builders,* McGraw-Hill, New York.

Goodman, J.R. (1967). "Layered wood systems with interlayer slip," Ph.D. Dissertation. University of California, Berkley.

Goodman, J.R. and Popov, E.P. (1968). "Layered beam systems with interlayer slip," *Journal of the Structural Division*, ASCE, Nov:2535-2547

Granholm, H. (1949). "Om sammansatta balkar och pelare med sarskild hansyn till spikade trakonstrucktioner," *Transactions,* Chalmers Tekniska Hogskolas Handlingar, No. 88. Gottenburg, Sweden.

Gromala, D.W. (1985). "Determination of modulus of rigidity by ASTM D 198 flexural methods," *ASTM Journal of Testing and Evaluation*, 13(5):353-355.

International Code Council (ICC). (2006). *2006 International Building Code,* ICC. Falls Church, VA.

International Code Council Evaluation Service (ICC-ES). (2007). "Structural composite lumber," ESR-1387, Whittier, CA.

Jacoby, H. (1909). *Structural details or elements of design in heavy framing,* John Wiley and Sons, New York.

Karlsen, G.G. (1967). *Wooden structures,* Goodman, W.L., trans. Mir Publishers, Moscow.

Karlsen, G., & Slitsskouhov, Y. (1989). *Wooden and plastic structures,* Kuznetsov, A.B., trans. Mir Publishers, Moscow.

Kidwell, E. (1898). "The efficiency of built-up wooden beams," *Transactions,* American Institute of Mining Engineers, 2/97-7/97:732-818, 977-993.

Leupold, J. (1726). "Theatrum pontificiale: oder Schauplatz der Bruecken und Bruecken-Baues," Leipzig.

Mahan, D.H. (1886). *A treatise of civil engineering*, John Wiley & Sons, New York.

Maple (2007). Maple Software, vs 11.02.330022. Maplesoft, Waterloo, ON.

Newmark, N.M., Siess, C.P., and Viest, I.. M., (1951). "Tests and analysis of composute beams with incomplete interaction," *Proceedings*, Society for Experimental Stress Analysis, Vol 9., No. 1.

Newmark, N.M. (1959). "A method of computation for structural dynamics," *Journal of the Engineering Mechanics Division*, ASCE, Vol. 85:67-94.

Pleshkov, P.F. (1952). "Teoriia rascheta dereviannykh sostavnnykh sterzhnei," Moscow.

Rankine, W.J.M. (1889). *A manual of civil engineering,* 17th Edition. Charles Griffin & Company, London.

Ranzi, G. and Bradford, M.A. (2006). "Time-dependent analysis of composite beams with partial interaction using the direct stiffness approach," UNICIV Report R-423, University of New South Wales, Australia.

Ranzi, G. and Bradford, M.A. (2007). "Direct stiffness analysis of a composite beam-column element with partial interaction," *Computers and Structures,* 85:1206-1214.

Ranzi, G., Gara, F., and Ansourian, P. (2006). "General method of analysis for composite beams with longitudinal and transverse partial interaction," *Computers and Structures*, 84:2373-2384.

Schnabl, S., Saje, M., Turk, G., and Planinc, I. (2007). "Analytical solution of two-layer beam taking into account interlayer slip and shear deformation," *Journal of Structural Engineering*, 133(6):886-894.

Snow, C.H. (1903). *The principal species of wood: their characteristic properties*. John Wiley & Sons, New York.

Snow, J.P. (1895). "Wooden bridge construction on the Boston and Maine railroad," *Journal of the Association of Engineering Societies*, 14:500-512.

Strukel, M. (1900). *Der Brückenbau,* O.W. Backman, Kuopio, Finland.

Timber Frame Business Council (TFBC). (2009). Retrieved March 17, 2009, from TFBC Website: http://www.timberframe.org/

Trautwine J.C. (1862). *Civil engineer's pocket book,* John Wiley & Sons, New York.

Tredgold, T. (1820). *Elementary principles of carpentry,* E&F.N. Spon, London.

Thelandersson, S. and Larsen, H.J. (2003). *Timber engineering,* John Wiley & Sons, West Sussex, England

Wangaard, F.F. (1981). *Wood: Its structure and properties*, Penn State University, University Park, PA.

Wang, Y.C. (1998). "Deflection of steel-concrete composite beams with partial shear interaction," *Journal of Structural Engineering* 124(10):1159-1165

Warren, W.H. (1910). "Engineering construction in steel and timber," 2nd Edition, Vol 1. Longmans, Green, and Co., London.

Wheat, D.L. and Calixto, J.M. (1994). "Nonlinear analysis of two-layered wood members with interlayer slip," *Journal of Structural Engineering,* 120(6):1909-1929.

Appendix A – Solution for Two-Layer Beam with a Uniformly Distributed Load

Shear Flow:

$$q(x) = \frac{C_M w}{C_F^{\frac{3}{2}}}\left(\sinh\left(\sqrt{C_F}x\right) + \frac{\cosh\left(\sqrt{C_F}x\right)}{\sinh\left(\sqrt{C_F}L\right)}\left(1-\cosh\left(\sqrt{C_F}L\right)\right)\right) + \frac{C_M w}{2C_F}(L-x)$$

Deflection:

$$\Delta(x) = -\frac{w}{2C_F^{\,2}\sinh\left(\sqrt{C_F}L\right)(E_B I_B + E_T I_T)}\left(\frac{C_M(h_B+h_T)\sinh\left(\sqrt{C_F}L-\sqrt{C_F}x\right)}{C_F} + \sinh\left(\sqrt{C_F}L\right)\right.$$
$$*\left(\frac{C_M(h_B+h_T)\left(C_F\left(\frac{Lx^3}{6}-\frac{x^4}{12}\right)-x^2\right)}{2} - C_F^{\,2}\left(\frac{Lx^3}{6}-\frac{x^4}{12}\right)\right)$$
$$\left.+\frac{C_M(h_B+h_T)\sinh\left(\sqrt{C_F}x\right)}{C_F}\right)$$
$$+\frac{wLx\left(L^2C_FC_M(h_B+h_T)-12C_M(h_B+h_T)-2L^2C_F^{\,2}\right)}{48C_F^{\,2}(E_BI_B+E_TI_T)} + \frac{wC_M(h_B+h_T)}{2C_F^{\,3}(E_BI_B+E_TI_T)}$$

Appendix B – Solution for Two-Layer Beam with Point Load at any Point

For a simply supported beam subjected to a point load, there will be a discontinuity in the moment diagram, requiring two moment equations to describe the moment about the length. If the first point load is at a distance a from the starting (e.g. left) end on a beam with length L, the moment equations are

$$M_L(x = 0..a) = P\left(1 - \frac{a}{L}\right)x$$

$$M_R(x = a..L) = P\left(1 - \frac{a}{L}\right)x - P\left(x - a\right) \tag{B-1}$$

We will also have two governing differential equations that we will need to solve in order to find the axial force at any point along the length which are

$$\frac{d^2F_R(x)}{dx^2} - C_F F_R(x) = -C_M M_R(x)$$

$$\frac{d^2F_L(x)}{dx^2} - C_F F_L(x) = -C_M M_L(x) \tag{B-2}$$

Solving the above system of equations will yield four integration constants (two per equation). We know the axial force in the layers at the start and end must be zero so

$$F_L(0) = 0$$

$$F_R(L) = 0 \tag{B-3}$$

We also know the axial force just to the left and right of the point load needs to be the same, such that

$$F_L(a) = F_R(a) \tag{B-4}$$

Likewise, the rate of change of axial force to the left and right of the point load also needs to be the same, which means

$$\frac{dF_L(a)}{dx} = \frac{dF_R(a)}{dx} \tag{B-5}$$

Thus we have found boundary which allows us to solve for the four integration constants.

Source code for Maple 11 (Maple, 2007)

```
> Ml := x -> P*(1 - a/L)*x : Mr := x -> P*(1 - a/L)*x - P*(x - a) :
> ODEl := diff(Fl(x), x$2) - Fl(x)*C_F = -Ml(x)*C_M :
> ODEr := diff(Fr(x), x$2) - Fr(x)*C_F = -Mr(x)*C_M :
> soll := dsolve(ODEl) : solr := dsolve(ODEr) :
> Le := subs( {_C2 = C_1, _C1 = C_2}, soll) : Ri := subs( {_C2 = C_3, _C1 = C_4}, solr) :
>
  eq1 := subs({Fl(x) = 0, x = 0}, Le) :
  eq2 := subs({Fr(x) = 0, x = L}, Ri) :
  eq3 := subs({x = a}, rhs(Le) = rhs(Ri)) :
  eq4 := subs({x = a}, diff(rhs(Le), x) = diff(rhs(Ri), x)) :
> assign(simplify(solve({eq1, eq2, eq3, eq4}, {C_1, C_2, C_3, C_4})));
> Le; Ri;
```

$$Fl(x) = -\frac{1}{2}\,\frac{e^{\sqrt{C_F}\,x}\,C_M\,P\left(e^{-\sqrt{C_F}\,(-L+a)} - e^{\sqrt{C_F}\,(-L+a)}\right)}{C_F^{(3/2)}\left(e^{\sqrt{C_F}\,L} - e^{-\sqrt{C_F}\,L}\right)} + \frac{1}{2}\,\frac{e^{-\sqrt{C_F}\,x}\,C_M\,P\left(e^{-\sqrt{C_F}\,(-L+a)} - e^{\sqrt{C_F}\,(-L+a)}\right)}{C_F^{(3/2)}\left(e^{\sqrt{C_F}\,L} - e^{-\sqrt{C_F}\,L}\right)} - \frac{P\,C_M\,(-L+a)\,x}{C_F\,L}$$

$$Fr(x) = \frac{1}{2}\,\frac{e^{\sqrt{C_F}\,x}\,e^{-\sqrt{C_F}\,L}\,P\,C_M\left(e^{\sqrt{C_F}\,a} - e^{-\sqrt{C_F}\,a}\right)}{C_F^{(3/2)}\left(e^{\sqrt{C_F}\,L} - e^{-\sqrt{C_F}\,L}\right)} - \frac{1}{2}\,\frac{e^{-\sqrt{C_F}\,x}\,e^{\sqrt{C_F}\,L}\,P\,C_M\left(e^{\sqrt{C_F}\,a} - e^{-\sqrt{C_F}\,a}\right)}{C_F^{(3/2)}\left(e^{\sqrt{C_F}\,L} - e^{-\sqrt{C_F}\,L}\right)} - \frac{P\,a\,(x-L)\,C_M}{C_F\,L}$$

Recognizing the trigonometric functions cosh(x) and sinh(x) we can write these as

> *expand* (*convert* (*Le*, *trig*)); *expand* (*convert* (*Ri*, *trig*));

$$Fl(x) = \frac{C_M P \sinh\left(\sqrt{C_F}\, x\right) \sinh\left(\sqrt{C_F}\, a\right) \cosh\left(\sqrt{C_F}\, L\right)}{C_F^{(3/2)} \sinh\left(\sqrt{C_F}\, L\right)} - \frac{C_M P \sinh\left(\sqrt{C_F}\, x\right) \cosh\left(\sqrt{C_F}\, a\right)}{C_F^{(3/2)}} + \frac{P\, C_M\, x}{C_F} - \frac{P\, C_M\, x\, a}{C_F L}$$

$$Fr(x) = -\frac{P\, C_M \sinh\left(\sqrt{C_F}\, a\right) \cosh\left(\sqrt{C_F}\, x\right)}{C_F^{(3/2)}} + \frac{C_M P \sinh\left(\sqrt{C_F}\, x\right) \sinh\left(\sqrt{C_F}\, a\right) \cosh\left(\sqrt{C_F}\, L\right)}{C_F^{(3/2)} \sinh\left(\sqrt{C_F}\, L\right)} - \frac{P\, C_M\, x\, a}{C_F L} + \frac{P\, C_M\, a}{C_F}$$

Solutions for the shear flow at any point can be found by differentiating the force equations with respect to their position along the length

> *qleft* := *expand* (*convert* (*diff* (*rhs* (*Le*), *x*), *trig*));
> *qright* := *expand* (*convert* (*diff* (*rhs* (*Ri*), *x*), *trig*));

$$qleft := \frac{C_M P \cosh\left(\sqrt{C_F}\, x\right) \sinh\left(\sqrt{C_F}\, a\right) \cosh\left(\sqrt{C_F}\, L\right)}{C_F \sinh\left(\sqrt{C_F}\, L\right)} - \frac{C_M P \cosh\left(\sqrt{C_F}\, x\right) \cosh\left(\sqrt{C_F}\, a\right)}{C_F} + \frac{P\, C_M}{C_F} - \frac{P\, C_M\, a}{C_F L}$$

$$qright := \frac{C_M P \cosh\left(\sqrt{C_F}\, x\right) \sinh\left(\sqrt{C_F}\, a\right) \cosh\left(\sqrt{C_F}\, L\right)}{C_F \sinh\left(\sqrt{C_F}\, L\right)} - \frac{P\, C_M \sinh\left(\sqrt{C_F}\, a\right) \sinh\left(\sqrt{C_F}\, x\right)}{C_F} - \frac{P\, C_M\, a}{C_F L}$$

The deflection at any point can be found by solving the equations

$$\frac{d^2\Delta_L(x)}{dx^2} = \frac{M_L(x) - F_L(x)\left(\frac{h_B}{2} + \frac{h_T}{2}\right)}{E_B I_B + E_T I_T}$$
$$\frac{d^2\Delta_R(x)}{dx^2} = \frac{M_R(x) - F_R(x)\left(\frac{h_B}{2} + \frac{h_T}{2}\right)}{E_B I_B + E_T I_T} \quad \text{(B-6)}$$

with the boundary conditions

$$\Delta_L(0) = 0$$

$$\Delta_R(L) = 0$$

$$\Delta_L(L-a) = \Delta_R(L-a)$$

$$\frac{d}{dx}\Delta_L(L-a) = \frac{d}{dx}\Delta_R(L-a) \quad \text{(B-7)}$$

The solution for the axial forces at any point is bounded on the low end with no axial force, which is consistent with a simple stacked beam. On the upper end, they are bounded by the case of a solid full depth beam. Reducing the force equations above is not a simple task, so compatibility with the lower and upper bound requirements is done by example.

The axial force at any point can be calculated for a full depth beam as the volume of the stress block in the compression (or tension) zone, with the compression and tension zones being equal in magnitude. The compression force in top half of a full depth beam, the total compression force C can be calculated as

$$C = \frac{F_b h b}{2} \quad \text{(B-8)}$$

where F_b is the extreme fiber bending stress, b is the beam breadth, and h is the depth from the extreme fiber in compression to the neutral axis. The extreme fiber bending

stress can be calculated as

$$F_b = \frac{Mh}{\left(\frac{b(2h)^3}{12}\right)} \tag{B-9}$$

where M is the applied moment. For a point load P at the midspan of a beam with length L, we can combine equations B-8 and B-9 as

$$C = T = \frac{3PL}{16h} \tag{B-10}$$

For a beam with the parameters:

$$L = 100$$
$$a = 50$$
$$P = 10000$$
$$h_T = h_B = 10$$

the compression (or tension) in the top and bottom portions of the beams is 18,750 lb.

Recalling the equations (2-18) and (2-19) for C_F and C_M respectively, they can be rewritten with the above beam parameters as

$$C_F = \frac{2k}{25} \tag{B-11}$$

$$C_M = \frac{3k}{500} \tag{B-12}$$

where k is the total stiffness of the shear keys, assuming s (shear key spacing) and E (modulus of elasticity) are constant.

Using our interlayer slip solution above, we can apply very small and very large k values to account for a condition with no interlayer stiffness and for full interlayer stiffness, and calculate the corresponding forces in each layer. These calculated forces

correspond exactly with the simple stacked condition (no axial force) and the full depth condition (18,750-lb).

```
> k := 10^-10 :
>
```

$$evalf\left(subs\left(\left\{C_F = \frac{2\cdot k}{25}, C_M = \frac{3}{500}\,k, P = 10000, L = 100, a = 50, x = 0\right\}, Le\right)\right);$$
$$evalf\left(subs\left(\left\{C_F = \frac{2\cdot k}{25}, C_M = \frac{3}{500}\,k, P = 10000, L = 100, a = 50, x = 25\right\}, Le\right)\right);$$
$$evalf\left(subs\left(\left\{C_F = \frac{2\cdot k}{25}, C_M = \frac{3}{500}\,k, P = 10000, L = 100, a = 50, x = 50\right\}, \{Le, Ri\}\right)\right);$$
$$evalf\left(subs\left(\left\{C_F = \frac{2\cdot k}{25}, C_M = \frac{3}{500}\,k, P = 10000, L = 100, a = 50, x = 75\right\}, Ri\right)\right);$$
$$evalf\left(subs\left(\left\{C_F = \frac{2\cdot k}{25}, C_M = \frac{3}{500}\,k, P = 10000, L = 100, a = 50, x = 100\right\}, Ri\right)\right);$$

$$Fl(0) = 0.$$
$$Fl(25) = 0.04$$
$$\{Fr(50) = -0.04, Fl(50) = 0.07\}$$
$$Fr(75) = 0.08$$
$$Fr(100) = 0.$$

```
> k := 10^10 :
>
```

$$evalf\left(subs\left(\left\{C_F = \frac{2\cdot k}{25}, C_M = \frac{3}{500}\,k, P = 10000, L = 100, a = 50, x = 0\right\}, Le\right)\right);$$
$$evalf\left(subs\left(\left\{C_F = \frac{2\cdot k}{25}, C_M = \frac{3}{500}\,k, P = 10000, L = 100, a = 50, x = 25\right\}, Le\right)\right);$$
$$evalf\left(subs\left(\left\{C_F = \frac{2\cdot k}{25}, C_M = \frac{3}{500}\,k, P = 10000, L = 100, a = 50, x = 50\right\}, \{Le, Ri\}\right)\right);$$
$$evalf\left(subs\left(\left\{C_F = \frac{2\cdot k}{25}, C_M = \frac{3}{500}\,k, P = 10000, L = 100, a = 50, x = 75\right\}, Ri\right)\right);$$
$$evalf\left(subs\left(\left\{C_F = \frac{2\cdot k}{25}, C_M = \frac{3}{500}\,k, P = 10000, L = 100, a = 50, x = 100\right\}, Ri\right)\right);$$

$$Fl(0) = 0.$$
$$Fl(25) = 9375.$$
$$\{Fl(50) = 18749.98675, Fr(50) = 18749.98674\}$$
$$Fr(75) = 9375.$$
$$Fr(100) = 0.$$

Appendix C – Solution for Two-Layer Beam with Symmetrically Placed Point Loads

For a beam with two point loads, there will be two discontinuities in the moment diagram, requiring three moment equations to describe the moment about the length. If the first point load is at a distance a from the starting end, the second point will thusly be $L - a$ away from the starting end for a beam with length L. The moment equations are

$$M1(x = 0..a) = Px$$

$$M2(x = a..L - a) = Pa$$

$$M3(x = L - a..L) = Pa - P(x - L + a) \tag{C-1}$$

We will also have three governing differential equations that we will need to solve in order to find the axial force at any point along the length which are

$$\frac{d^2F_i(x)}{dx^2} - C_F F_i(x) = -C_M M_i(x) \tag{C-2}$$

where $i = 1,2,3$. Solving the above equation will yield six integration constants (two per equation). We know the axial force in the layers at the start and end must be zero so

$$F_1(0) = 0$$

$$F_3(L) = 0 \tag{C-3 \& 4}$$

W also know the axial force just to the left and right of each point load needs to be the same, such that

$$F_1(a) = F_2(a)$$

$$F_2(L - a) = F_3(L - a) \tag{C-5 \& 6}$$

Likewise, the rate of change of axial force to the left and right of each point load also needs to be the same, which means

$$\frac{dF_1(a)}{dx} = \frac{dF_2(a)}{dx}$$

$$\frac{dF_2(L-a)}{dx} = \frac{dF_3(L-a)}{dx} \qquad \text{(C-7 \& 8)}$$

Thus we have six boundary conditions without invoking symmetry of the structure, which allows us to solve for the six integration constants.

Source code for Maple 11 (Maple, 2007)

```
> M1 := x→P·x :
> M2 := x → P·a :
> M3 := x → P·a − P·(x − L + a) :
> ODE1 := diff(F1(x), x$2) − F1(x)·Cf = −M1(x)·Cm :
> ODE2 := diff(F2(x), x$2) − F2(x)·Cf = −M2(x)·Cm :
> ODE3 := diff(F3(x), x$2) − F3(x)·Cf = −M3(x)·Cm :
> sol1 := dsolve(ODE1) :
> sol2 := dsolve(ODE2) :
> sol3 := dsolve(ODE3) :
>
  Eq1 := subs({_C2 = C1, _C1 = C2}, sol1);
  Eq2 := subs({_C2 = C3, _C1 = C4}, sol2);
  Eq3 := subs({_C2 = C5, _C1 = C6}, sol3);
```

$$Eq1 := F1(x) = e^{\sqrt{Cf}\,x} C_1 + e^{-\sqrt{Cf}\,x} C_2 + \frac{P\,Cm\,x}{Cf}$$

$$Eq2 := F2(x) = e^{\sqrt{Cf}\,x} C_3 + e^{-\sqrt{Cf}\,x} C_4 + \frac{P\,a\,Cm}{Cf}$$

$$Eq3 := F3(x) = e^{\sqrt{Cf}\,x} C_5 + e^{-\sqrt{Cf}\,x} C_6 - \frac{P\,Cm\,(x-L)}{Cf}$$

>

$$bc1 := subs(\{F1(x) = 0, x = 0\}, Eq1);$$
$$bc2 := subs(\{F3(x) = 0, x = L\}, Eq3);$$
$$bc3 := \mathrm{subs}(\mathrm{x = a, rhs(Eq1)}) = subs(x = a, rhs(Eq2));$$
$$bc4 := \mathrm{subs}(\mathrm{x = L - a, rhs(Eq2)}) = subs(x = L - a, rhs(Eq3));$$
$$bc5 := \mathrm{subs}\left(\mathrm{x = a}, \frac{d}{dx}\, rhs(Eq1)\right) = subs\left(x = a, \frac{d}{dx}\, rhs(Eq2)\right);$$
$$\mathrm{bc6} := \mathrm{subs}\left(\mathrm{x = L - a}, \frac{d}{dx}\, rhs(Eq2)\right) = subs\left(x = L - a, \frac{d}{dx}\, rhs(Eq3)\right);$$

$$bc1 := 0 = e^{0} C_1 + e^{0} C_2$$

$$bc2 := 0 = e^{\sqrt{Cf}\, L} C_5 + e^{-\sqrt{Cf}\, L} C_6$$

$$bc3 := e^{\sqrt{Cf}\, a} C_1 + e^{-\sqrt{Cf}\, a} C_2 + \frac{P\, a\, Cm}{Cf} = e^{\sqrt{Cf}\, a} C_3 + e^{-\sqrt{Cf}\, a} C_4 + \frac{P\, a\, Cm}{Cf}$$

$$bc4 := e^{\sqrt{Cf}\, (L - a)} C_3 + e^{-\sqrt{Cf}\, (L - a)} C_4 + \frac{P\, a\, Cm}{Cf} = e^{\sqrt{Cf}\, (L - a)} C_5 + e^{-\sqrt{Cf}\, (L - a)} C_6 + \frac{P\, a\, Cm}{Cf}$$

$$bc5 := \sqrt{Cf}\, e^{\sqrt{Cf}\, a} C_1 - \sqrt{Cf}\, e^{-\sqrt{Cf}\, a} C_2 + \frac{P\, Cm}{Cf} = \sqrt{Cf}\, e^{\sqrt{Cf}\, a} C_3 - \sqrt{Cf}\, e^{-\sqrt{Cf}\, a} C_4$$

$$bc6 := \sqrt{Cf}\, e^{\sqrt{Cf}\, (L - a)} C_3 - \sqrt{Cf}\, e^{-\sqrt{Cf}\, (L - a)} C_4 = \sqrt{Cf}\, e^{\sqrt{Cf}\, (L - a)} C_5 - \sqrt{Cf}\, e^{-\sqrt{Cf}\, (L - a)} C_6 - \frac{P\, Cm}{Cf}$$

> $assign\left(simplify\left(solve\left(\{bc1, bc2, bc3, bc4, bc5, bc6\}, \{C_1, C_2, C_3, C_4, C_5, C_6\}\right)\right)\right);$

> $Eq1; Eq2; Eq3;$

$$F1(x) = \frac{1}{2}\, \frac{e^{\sqrt{Cf}\, x} P\, Cm \left(-e^{\sqrt{Cf}\, (-L + a)} - e^{-\sqrt{Cf}\, a} + e^{-\sqrt{Cf}\, (-L + a)} + e^{\sqrt{Cf}\, a}\right)}{Cf^{3/2} \left(e^{-\sqrt{Cf}\, L} - e^{\sqrt{Cf}\, L}\right)} - \frac{1}{2}\, \frac{e^{-\sqrt{Cf}\, x} P\, Cm \left(-e^{\sqrt{Cf}\, (-L + a)} - e^{-\sqrt{Cf}\, a} + e^{-\sqrt{Cf}\, (-L + a)} + e^{\sqrt{Cf}\, a}\right)}{Cf^{3/2} \left(e^{-\sqrt{Cf}\, L} - e^{\sqrt{Cf}\, L}\right)} + \frac{P\, Cm\, x}{Cf}$$

$$F2(x) = \frac{1}{2}\,\frac{e^{\sqrt{Cf}\,x}\,P\,Cm\left(-e^{-\sqrt{Cf}\,a} - e^{\sqrt{Cf}\,(-L+a)} + e^{\sqrt{Cf}\,a} + e^{-\sqrt{Cf}\,(a+L)}\right)}{Cf^{3/2}\left(e^{-\sqrt{Cf}\,L} - e^{\sqrt{Cf}\,L}\right)}$$
$$- \frac{1}{2}\,\frac{e^{-\sqrt{Cf}\,x}\,P\,Cm\left(-e^{\sqrt{Cf}\,(a+L)} - e^{-\sqrt{Cf}\,a} + e^{-\sqrt{Cf}\,(-L+a)} + e^{\sqrt{Cf}\,a}\right)}{Cf^{3/2}\left(e^{-\sqrt{Cf}\,L} - e^{\sqrt{Cf}\,L}\right)}$$
$$+ \frac{P\,a\,Cm}{Cf}$$

$$F3(x) =$$
$$-\frac{1}{2}\,\frac{e^{\sqrt{Cf}\,x}\,e^{-\sqrt{Cf}\,L}\,P\,Cm\left(-e^{\sqrt{Cf}\,(-L+a)} - e^{-\sqrt{Cf}\,a} + e^{-\sqrt{Cf}\,(-L+a)} + e^{\sqrt{Cf}\,a}\right)}{Cf^{3/2}\left(e^{-\sqrt{Cf}\,L} - e^{\sqrt{Cf}\,L}\right)}$$
$$+ \frac{1}{2}\,\frac{e^{-\sqrt{Cf}\,x}\,e^{\sqrt{Cf}\,L}\,P\,Cm\left(-e^{\sqrt{Cf}\,(-L+a)} - e^{-\sqrt{Cf}\,a} + e^{-\sqrt{Cf}\,(-L+a)} + e^{\sqrt{Cf}\,a}\right)}{Cf^{3/2}\left(e^{-\sqrt{Cf}\,L} - e^{\sqrt{Cf}\,L}\right)}$$
$$- \frac{P\,Cm\,(x-L)}{Cf}$$

Solutions for the shear flow and deflection at any point can be found by using the equations

$$q_i(x) = \frac{dF_i(x)}{dx} \tag{C-9}$$

$$\frac{d^2\Delta_i(x)}{dx^2} = \frac{M_i(x) - F_i(x)\left(\frac{h_B}{2} + \frac{h_T}{2}\right)}{E_B I_B + E_T I_T} \tag{C-10}$$

The solution for the axial forces at any point is bounded on the low end with no axial force, which is consistent with a simple stacked beam. On the upper end, they are bounded by the case of a solid full depth beam. Reducing the force equations above is not a simple task, so compatibility with the lower and upper bound requirements is done by example.

For a beam with the parameters:

$$L = 100$$
$$a = 25$$
$$P = 10000$$
$$h_T = h_B = 10$$

The axial compressive or tensile force in a full depth beam anywhere in the constant moment (middle span) region as

$$C = T = \frac{3Pa}{4h} = 18{,}750\ lb \tag{C-11}$$

Using the relationships for C_F and C_M outlined in equations B-11 and B-12 respectively, we can evaluate the interlayer slip model, which yields identical forces in each layer.

```
> k := 0.00000001:
>
```

$$evalf\left(subs\left(\left\{Cm = \frac{3\cdot k}{500}, Cf = \frac{2\cdot k}{25}, L = 100, a = 25, x = 0, P = 10000\right\}, Eq1\right)\right);$$
$$evalf\left(subs\left(\left\{Cm = \frac{3\cdot k}{500}, Cf = \frac{2\cdot k}{25}, L = 100, a = 25, x = 25, P = 10000\right\}, \{Eq1, Eq2\}\right)\right);$$
$$evalf\left(subs\left(\left\{Cm = \frac{3\cdot k}{500}, Cf = \frac{2\cdot k}{25}, L = 100, a = 25, x = 50, P = 10000\right\}, Eq2\right)\right);$$
$$evalf\left(subs\left(\left\{Cm = \frac{3\cdot k}{500}, Cf = \frac{2\cdot k}{25}, L = 100, a = 25, x = 75, P = 10000\right\}, \{Eq2, Eq3\}\right)\right);$$
$$evalf\left(subs\left(\left\{Cm = \frac{3\cdot k}{500}, Cf = \frac{2\cdot k}{25}, L = 100, a = 25, x = 100, P = 10000\right\}, Eq3\right)\right);$$

$$F1(0) = 0.$$
$$\{F1(25) = 0.01000, F2(25) = 1.44449\}$$
$$F2(50) = 1.4480($$
$$\{F2(75) = 1.44213, F3(75) = 0.01000\}$$
$$F3(100) = 0.$$

> $k := 100000000$:

>

$$evalf\left(subs\left(\left\{Cm = \frac{3\cdot k}{500}, Cf = \frac{2\cdot k}{25}, L = 100, a = 25, x = 0, P = 10000\right\}, Eq1\right)\right);$$

$$evalf\left(subs\left(\left\{Cm = \frac{3\cdot k}{500}, Cf = \frac{2\cdot k}{25}, L = 100, a = 25, x = 25, P = 10000\right\}, \{Eq1, Eq2\}\right)\right);$$

$$evalf\left(subs\left(\left\{Cm = \frac{3\cdot k}{500}, Cf = \frac{2\cdot k}{25}, L = 100, a = 25, x = 50, P = 10000\right\}, Eq2\right)\right);$$

$$evalf\left(subs\left(\left\{Cm = \frac{3\cdot k}{500}, Cf = \frac{2\cdot k}{25}, L = 100, a = 25, x = 75, P = 10000\right\}, \{Eq2, Eq3\}\right)\right);$$

$$evalf\left(subs\left(\left\{Cm = \frac{3\cdot k}{500}, Cf = \frac{2\cdot k}{25}, L = 100, a = 25, x = 100, P = 10000\right\}, Eq3\right)\right);$$

$$F1(0) = 0.$$

$$\{F1(25) = 18749.86741, F2(25) = 18749.86742\}$$

$$F2(50) = 18750.$$

$$\{F2(75) = 18749.86741, F3(75) = 18749.86742\}$$

$$F3(100) = 0.$$

Appendix D – Calculations for Quantity of Clamping Connectors

Calculations for the quantity of clamping connectors (LogHog screws) required for the physical testing were based on a 2.5-inch by 8-inch inclined white oak shear key installed in a 7.5-inch wide timber and loaded such that it is compressed perpendicular to the grain. The shear key is able to resist 16,050 lb of compressive force at the proportional limit compressive stress of 1,070 psi (FPL, 1999). Per section 3.3.2, the distance from the bearing face of the shear key to the clamping connector set as the key thickness. The dimension between the center of the bearing faces is 2.375 inch and the distance from the far bearing face to the clamping connector is 10.125 inch. These dimensions are shown in Figure D-1.

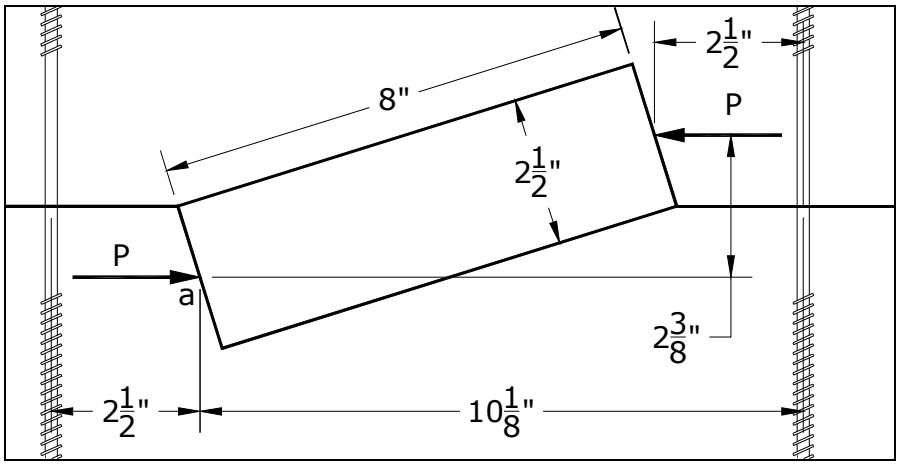

Figure D-1 Shear key and clamping connector dimensioning

The clamping force required by the screws was calculated by summing moments about point "a" shown in Figure D-1 such that

$$\sum M_a = 0 = R(10.125") - P(2.375") \tag{D-1}$$

where R is the clamping force required, and P is 16,050 lb, the shearing force being resisted. Equation (D-1) can be solved for the required clamping force of 3,765 lb.

The adjusted allowable withdrawal force W' per inch of penetration for a wood screw is

$$W = (2850G^2D)C_D \tag{D-2}$$

were D is the outside diameter of the wood screw, G is the specific gravity of the timber (0.43 for yellow poplar), and C_D is the load duration factor (AF&PA, 2005). The LogHog screws used for the testing have a thread length of 4 inches and thread diameter of 0.305 inch. Testing of the key configurations and keyed beams was anticipated to take approximately 10-20 minutes, which corresponds to a load duration factor of 1.6. The total withdrawal capacity of a LogHog screw was calculated to be 1,029 lb using equation (D-2). The total number of screws required is

$$\frac{3{,}765 lb}{1{,}029 lb / screw} = 3.66 \approx 4\ screws \tag{D-3}$$

per shear key.

Appendix E – Longitudinal Modulus of Elasticity and Shear Modulus in Bending Tests

E.1 Determination from Testing

A procedure is set forth in ASTM D 198 and by Gromala to calculate the longitudinal modulus of elasticity E_L and shear modulus G from basic center-point load bending test data (ASTM, 2007; Gromala, 1985). Their procedure requires not only center-point bending to be conducted, but several variations of the depth to length ratio. With the physical testing conducted in this research, a center-point loading was conducted in the small scale tests with only one depth to span ratio. In the large scale tests, third-point loading was conducted on a different depth to span ratio. The following procedure was developed to determine the longitudinal modulus of elasticity as well as shear modulus from these test results.

Using the principal of virtual work, the deflection Δ of a simply supported beam of length L subjected to a concentrated load at midspan, can be written as

$$\Delta = \int_0^L \frac{mM}{E_L I} dx + \int \frac{vV}{GA_V} dx \qquad \text{(E-1)}$$

where M and V are the actual moments and shears about the length of the beam, and m and v are the virtual moments and shears caused by a unit point load at midspan. I is the beam's moment of inertia and A_V is the beam's shear area. The shear area can be determined as

$$A_v = kA = \frac{5}{6}bd \tag{E-2}$$

where k is the shear coefficient for a rectangular cross section (Cowper, 1966). Solving equation (E-1) yields

$$\Delta = \frac{PL^3}{48E_L I} + \frac{PL}{4GA_V} \tag{E-3}$$

For a given trial, a load P is applied that results is a given deflection Δ. Recognizing $\frac{P}{\Delta}$ is the stiffness K of the member, we can rewrite the above as

$$1 = \frac{K_m {L_m}^3}{48E_L I_m} + \frac{K_m L_m}{4GA_{Vm}} \tag{E-4}$$

where the subscript m denotes center-point loading.

In a similar fashion to the center-point loading procedure above, virtual work can be used to find the deflection of a simply supported beam subjected to symmetrically placed point loads. Solving equation (E-1) for this loading configuration results in a deflection at the applied point load of

$$\Delta = \frac{Pa}{6E_L I}\left(3La - 4a^2\right) + \frac{Pa\left(L - 2a\right)}{2LGA_V} \tag{E-5}$$

which can be written in terms of stiffness as

$$1 = \frac{K_t a}{6E_L I_t}\left(3L_t a - 4a^2\right) + \frac{K_t a\left(L_t - A\right)}{2L_t GA_{Vt}} \tag{E-6}$$

where the subscript t denotes two-point loading. The average results from both the small scale center point loading tests as well as the large scale third point loading test allow us to solve equations (E-4) and (E-6) for E_L and G.

E.2 Comparison of Full Depth and Simple Stacked Beam Deflection

Based purely on beam bending, a simply supported full depth beam is twice as strong and four times as stiff as its simple stacked counterpart. However, wood has a low shear modulus, relative to other structural materials, so accounting for shear deformations can be important. The following comparison is made between a simple stacked set of 7.5in by 7.5in beams and a full depth 7.5in by 15in beam.

According to the Wood Handbook, (FPL, 1999) for yellow poplar at 12% moisture content, the modulus of elasticity is $E = 1{,}580{,}000\ psi$. This published value includes shear deformations, so the longitudinal modulus of elasticity can be found by increasing this value by 10% (FRP, 1999), such that $E_L = 1{,}738{,}000\ psi$. The shear modulus for yellow poplar can also be found from the published elastic ratios. Averaging the behavior in the radial and tangential directions yields $G = 0.071E_L = 123{,}400\ psi$.

The moment of inertia for the full depth beam is

$$I_{stacked} = 2\frac{bd^3}{12} = 2\frac{7.5^4}{12} = 527.3\ in^4$$

and for a simple stacked beam is

$$I_{full} = \frac{bd^3}{12} = \frac{(7.5)(15)^3}{12} = 2{,}109.4\ in^4$$

For the configuration used in the physical testing, the deflection of a full depth beam and simple stacked beam at the applied point load were calculated using equation (E-5) as $0.428x10^{-4}P\ in$ and $1.689x10^{-4}P\ in$ respectively. The full depth beam is 3.95x as stiff as the simple stacked beam, compared to the 4.0x as stiff that is expected using only

beam bending calculations. Although the deflection does change slightly due the inclusion of shear deformations, the difference is relatively minor. Therefore any error introduced from shear deformations in the partially composite state would also be relatively minor.

Appendix F – Adjustment of Shear Keys Test Stiffness

$d := 2.5$ Thickness of wedge

$sub := 12$

$l := 8$ Length of wedge

$E_{par12} := 1580000$ MOE of the timber @ 12%

$E_{pargreen} := 1220000$ MOE of the timber @ green

$E_{key12} := 1780000$ MOE of the key @ 12%

$E_{keygreen} := 1250000$ MOE of the key @ green

$MC_{tim} := 16.2$ MC of the timber (%)

$MC_{key} := 25$ MC of the key (%)

$b := 7.5$ Width of the timbers

$Num := 4$ Number of clamping screws

$$E_{par} := E_{par12} \cdot \left(\frac{E_{par12}}{E_{pargreen}} \right)^{\left(\frac{12 - MC_{tim}}{13} \right)} = 1453371$$

$$\theta := \operatorname{atan}\left(\frac{d}{l} \right) = 17.354 \cdot deg$$

$$E_{key} := E_{key12} \cdot \left(\frac{E_{key12}}{E_{keygreen}} \right)^{\left(\frac{12 - MC_{key}}{13} \right)} = 1250000$$

$$w := l \cdot \cos(\theta) = 7.636$$

$$t := d \cdot \cos(\theta) = 2.386$$

$$E_{\theta} := \frac{E_{par}}{sub - (sub - 1) \cdot \cos(\theta)^2} = 734527$$

$$k_t := \frac{b \cdot E_{\theta}}{2} = 2754478$$

$$k_k := \frac{b \cdot t \cdot E_{key}}{sub \cdot w} = 244141$$

$$k_{eff} := \frac{k_t \cdot k_k}{2 \cdot k_k + k_t} = 207379$$

$$k_{clamp} := \frac{Num \cdot 16435 \cdot 4}{2} = 131480$$

$$k_{key} := \frac{k_{eff} \cdot k_{clamp}}{k_{clamp} + \tan(\theta)^2 \cdot k_{eff}} = 179700$$

$2 \cdot k_{key} = 359400$ Anticipated Stiffness of test configuration (lbs / in)

Appendix G – Calculation of Slip in a Simple Stacked Beam

The mid-span deflection Δ of a simply supported beam of length L, consisting of two members of identical members stacked atop one another and subjected to symmetric point loads P, is

$$\Delta = \frac{Pa}{12EI}\left(3L^2 - 4a^2\right) \tag{G-1}$$

where a is the distance from the end of the beam to one of the point loads, E is the modulus of elasticity, and I is the moment of inertia.

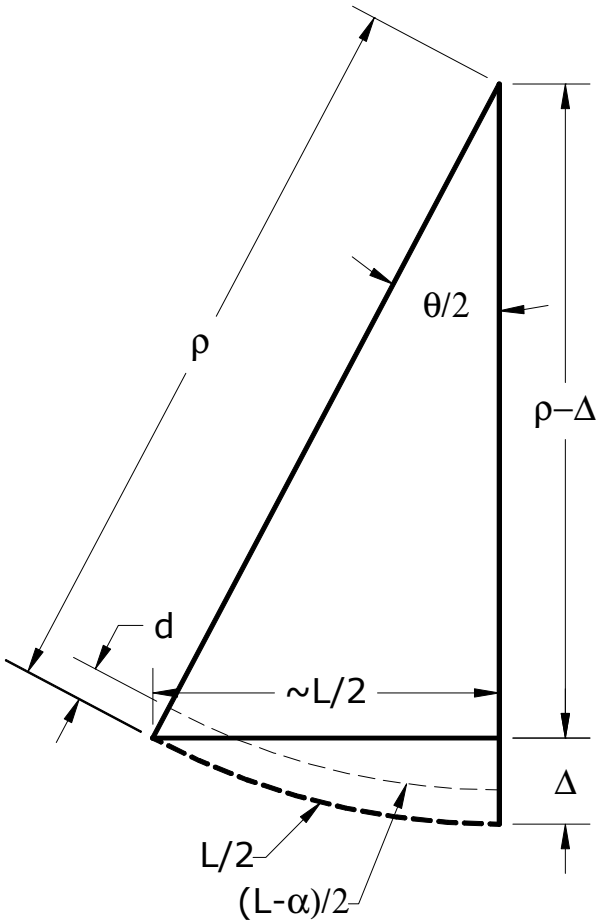

Figure G-1 Various dimensions for calculating the slip of a beam

The centerline of the displaced shape of the beam is shown as the heavy dashed line in Figure G-1, which is approximated by a chord of a circle. The radius of curvature, ρ, can be found using Pythagoreans' theorem

$$\rho = \frac{4\Delta^2 + L^2}{8\Delta} \tag{G-2}$$

The angle θ between the radius lines that pass through the supports is

$$\tan\theta = \frac{L}{\rho} = \frac{8L\Delta}{4\Delta^2 + L^2} \tag{G-3}$$

In a similar fashion, we can determine the length of the top face of the beam (shown as the light dashed line in Figure G-1) as

$$\tan\theta = \frac{L - \alpha}{\rho - d} \tag{G-4}$$

where d is the depth of a single layer of the stacked beam, and α is the change in length (shortening) of the beam. Solve the above equation for α yields

$$\alpha = \frac{8L\Delta d}{4\Delta^2 + L^2}$$

Assuming the top layer and bottom layers of the stacked beam displace equally, α is the change in length of the top layer of the bottom beam compared to the bottom layer of the top beam, which is the total slip at the ends of a simple stacked beam with no interaction between layers.

Appendix H – Interlayer Slip Calculations for Full-Scale Test Data

H.1 Analysis of Test Data from this Research

The following is Maple 11 (Maple, 2007) source code for determining the stiffness of a beam using the interlayer slip model and the two symmetrically placed point load solution shown in Appendix C. Calculations are shown for the first full-scale keyed beam test with white oak shear keys. Calculations for the other keyed beam tests use the same process, with different input parameters. The various input parameters are shown in Table 6-1.

Input Parameters

>

$L := 162:$
$a := 63:$
$bt := 7.63:$
$bb := 7.59:$
$ht := 7.49:$
$hb := 6.63:$
$Et := 1547000:$
$Eb := 1561000:$
$Ek := [1247000, 1180000, 1153000]:$
$d := [2.51, 2.47, 2.44]:$
$l := 8:$
$\phi := \frac{\pi}{2}:$

Geometry Calculations

> $At := bt \cdot ht; Ab := bb \cdot hb;$

$$At := 57.1487$$

$$Ab := 50.3217$$

> $It := \frac{bt \cdot ht^3}{12}; Ib := \frac{bb \cdot hb^3}{12};$

$$It := 267.170648$$

$$Ib := 184.332161$$

> **for** i **from** 1 **by** 1 **to** 3 **do** $\theta_i := \arctan\left(\frac{d_i}{l}\right); w_i := \cos(\theta_i) \cdot l; t_i := \cos(\theta_i) \cdot d_i;$ **end do**:

All of the shear key connections in the keyed beams used 4 LogHog screws, with an axial stiffness of 16,435-lb/in (section 4.3) and 3.5 inch of threads penetrating into each timber (see Figure 3-5).

Stiffness Terms & Calculations

$$> \quad kclamp := \frac{4 \cdot 16435 \cdot 3.5}{2} :$$

for i **from** 1 **by** 1 **to** 3 **do**

$$kt_i := \frac{\left(\frac{bb + bt}{2}\right) \cdot \left(\frac{Et + Eb}{2}\right)}{\left(12 - 11 \cdot \cos\left(\theta_i\right)^2\right) \cdot 2};$$

$$kk_i := \frac{\left(\frac{bb + bt}{2}\right) \cdot \left(Ek_i\right) \cdot t_i}{\left(12 - 11 \cdot \cos\left(\phi\right)^2\right) \cdot w_i};$$

$$keff_i := \frac{kt_i \cdot kk_i}{2 \cdot kk_i + kt_i};$$

$$keff_i := \frac{kclamp \cdot keff_i}{kclamp + keff_i \cdot \tan\left(\theta_i\right)^2};$$

$$k_i := keff_i;$$

end do:

Displacement Calculations

See Appendix C for the development of the axial force equations

>

$$F1 := x \to -\frac{1}{2}\,\frac{e^{\sqrt{Cf}\,x}\,P\,Cm\left(-e^{\sqrt{Cf}\,(-L+a)}+e^{\sqrt{Cf}\,a}-e^{-\sqrt{Cf}\,a}+e^{-\sqrt{Cf}\,(-L+a)}\right)}{Cf^{3/2}\left(-e^{-\sqrt{Cf}\,L}+e^{\sqrt{Cf}\,L}\right)} + \frac{1}{2}\,\frac{e^{-\sqrt{Cf}\,x}\,P\,Cm\left(-e^{\sqrt{Cf}\,(-L+a)}+e^{\sqrt{Cf}\,a}-e^{-\sqrt{Cf}\,a}+e^{-\sqrt{Cf}\,(-L+a)}\right)}{Cf^{3/2}\left(-e^{-\sqrt{Cf}\,L}+e^{\sqrt{Cf}\,L}\right)} + \frac{P\,Cm\,x}{Cf}:$$

$$F2 := x \to -\frac{1}{2}\,\frac{e^{\sqrt{Cf}\,x}\,P\,Cm\left(-e^{\sqrt{Cf}\,(-L+a)}+e^{\sqrt{Cf}\,a}-e^{-\sqrt{Cf}\,a}+e^{-\sqrt{Cf}\,(a+L)}\right)}{Cf^{3/2}\left(-e^{-\sqrt{Cf}\,L}+e^{\sqrt{Cf}\,L}\right)} + \frac{1}{2}\,\frac{e^{-\sqrt{Cf}\,x}\,P\,Cm\left(-e^{\sqrt{Cf}\,(a+L)}+e^{\sqrt{Cf}\,a}-e^{-\sqrt{Cf}\,a}+e^{-\sqrt{Cf}\,(-L+a)}\right)}{Cf^{3/2}\left(-e^{-\sqrt{Cf}\,L}+e^{\sqrt{Cf}\,L}\right)} + \frac{P\,a\,Cm}{Cf}:$$

$$F3 := x \to \frac{1}{2}\,\frac{e^{\sqrt{Cf}\,x}\left(-e^{\sqrt{Cf}\,(-L+a)}+e^{\sqrt{Cf}\,a}-e^{-\sqrt{Cf}\,a}+e^{-\sqrt{Cf}\,(-L+a)}\right)e^{-\sqrt{Cf}\,L}\,P\,Cm}{Cf^{3/2}\left(-e^{-\sqrt{Cf}\,L}+e^{\sqrt{Cf}\,L}\right)} - \frac{1}{2}\,\frac{e^{-\sqrt{Cf}\,x}\,e^{\sqrt{Cf}\,L}\left(-e^{\sqrt{Cf}\,(-L+a)}+e^{\sqrt{Cf}\,a}-e^{-\sqrt{Cf}\,a}+e^{-\sqrt{Cf}\,(-L+a)}\right)P\,Cm}{Cf^{3/2}\left(-e^{-\sqrt{Cf}\,L}+e^{\sqrt{Cf}\,L}\right)} - \frac{P\,Cm\,(x-L)}{Cf}:$$

The moment and deflection equations are also developed in Appendix C (equations C-1 C-10).

> $M1 := x \to P\cdot x : M2 := x \to P\cdot a : M3 := x \to P\cdot a - P\cdot(x - L + a):$

>

$$eq1 := \Delta 1(x) = int\left(int\left(\frac{M1(x) - \frac{F1(x)\cdot(hb+ht)}{2}}{Eb\cdot Ib + Et\cdot It}, x\right), x\right) + C_1\cdot x + C_2:$$

$$eq2 := \Delta 2(x) = int\left(int\left(\frac{M2(x) - \frac{F2(x)\cdot(hb+ht)}{2}}{Eb\cdot Ib + Et\cdot It}, x\right), x\right) + C_3\cdot x + C_4:$$

$$eq3 := \Delta 3(x) = int\left(int\left(\frac{M3(x) - \frac{F3(x)\cdot(hb+ht)}{2}}{Eb\cdot Ib + Et\cdot It}, x\right), x\right) + C_5\cdot x + C_6:$$

>

$$bc1 := subs\left(\{\Delta 1(x) = 0, x = 0\}, eq1\right):$$
$$bc2 := subs\left(\{\Delta 3(x) = 0, x = L\}, eq3\right):$$
$$bc3 := subs(x = a, rhs(eq1)) = subs(x = a, rhs(eq2)):$$
$$bc4 := subs(x = L - a, rhs(eq2)) = subs(x = L - a, rhs(eq3)):$$
$$bc5 := subs\left(x = a, \frac{d}{dx}\,rhs(eq1)\right) = subs\left(x = a, \frac{d}{dx}\,rhs(eq2)\right):$$
$$bc6 := subs\left(x = L - a, \frac{d}{dx}\,rhs(eq2)\right) = subs\left(x = L - a, \frac{d}{dx}\,rhs(eq3)\right):$$

> $assign\left(solve\left(\{bc1, bc2, bc3, bc4, bc5, bc6\}, \{C_1, C_2, C_3, C_4, C_5, C_6\}\right)\right);$

The stiffness constants are described in section 2 as equations (2-18) and (2-19). The keys nearest the ends of any particular beam were cut from the same piece of material, and likewise for the next keys in, and so on, such that stiffness per unit length is based on half of the keys distributed over half of the length.

Constant Terms

> $$Cf := \left(\sum_{j=1}^{3} \frac{k_j}{\left(\frac{L}{2}\right)}\right) \cdot \left(\left(\frac{1}{Ab \cdot Eb} + \frac{1}{At \cdot Et}\right) + \frac{\left(\frac{ht}{2} + \frac{hb}{2}\right)^2}{Et \cdot It + Eb \cdot Ib}\right);$$
>
> $$Cm := \left(\sum_{j=1}^{3} \frac{k_j}{\left(\frac{L}{2}\right)}\right) \cdot \left(\frac{\frac{ht}{2} + \frac{hb}{2}}{Et \cdot It + Eb \cdot Ib}\right);$$

$$Cf := 0.000610680821$$

$$Cm := 0.0000646407248$$

The displacement of the beam at the point loads can be determined by evaluating any of the above deflection equations at the point load. The results of the evaluation yield the displacement in terms of the applied point loads P. The total applied load to the beam from the hydraulic ram R is $2P$.

> $RamDefl := evalf(subs(x = a, rhs(eq1)));$
> $evalf(subs(x = a, rhs(eq2)));$
> $evalf(subs(x = L - a, rhs(eq2)));$
> $evalf(subs(x = L - a, rhs(eq3)));$

$$RamDefl := -0.0001190049792P$$

$$-0.0001190049792P$$

$$-0.0001190049792P$$

$$-0.0001190049800P$$

$$\text{RamDefl} = -0.00011900P = \frac{P}{8403} = \frac{R}{16806}$$

The above solution is for the first keyed beam using white oak keys. Additional iterations of the process were conducted using the appropriate inputs from Table 6-1. The results of those analysis are included in Table H-1.

Table H-1 Interlayer slip model analysis results

Test	Key	C_f (10^{-4})	C_m (10^{-5})	Deflection in/lb (10^{-5})	Stiffness lb/in
1	OAK	6.11	6.46	11.90	16806
2	OAK	5.87	5.90	10.40	19228
3	PSL	21.29	21.22	7.53	26558
4	PSK	20.03	20.18	6.97	28708

H.2 Analysis of Test Data from Prior Research

The process used to analyze the interlayer slip model for comparison to Kidwell's (1897) research is similar to that outlined in section H.1, with the exception that the beam was subjected to a single point load at midspan, rather than a symmetrically placed pair of point loads. The Maple 11 (Maple, 2007) code is included below.

Input Parameters

>

$L := 66:$
$a := \frac{L}{2}:$
$bt := 4.75:$
$bb := 4.75:$
$ht := 2.75:$
$hb := 2.75:$
$Et := 1100000:$
$Eb := 1100000:$
$Ek := [1780000, 1780000, 1780000, 1780000]:$
$d := [1, 1, 1, 1]:$
$l := 2:$
$\phi := \frac{\pi}{2}:$

Geometry Calculations

> $At := bt \cdot ht; Ab := bb \cdot hb;$

$$At := 13.0625$$
$$Ab := 13.0625$$

> $It := \frac{bt \cdot ht^3}{12}; Ib := \frac{bb \cdot hb^3}{12};$

$$It := 8.23209635\text{◂}$$

$$Ib := 8.23209635\text{◂}$$

> **for** i **from** 1 **by** 1 **to** 4 **do** $\theta_i := \arctan\left(\frac{d_i}{l}\right); w_i := \cos(\theta_i) \cdot l; t_i := \cos(\theta_i) \cdot d_i;$ **end do**:

Stiffness Terms & Calculations

> $kclamp := 857000:$

>

for i **from** 1 **by** 1 **to** 4 **do**

$$kt_i := \frac{\left(\frac{bb + bt}{2}\right) \cdot \left(\frac{Et + Eb}{2}\right)}{\left(12 - 11 \cdot \cos(\theta_i)^2\right) \cdot 2};$$

$$kk_i := \frac{\left(\frac{bb + bt}{2}\right) \cdot (Ek_i) \cdot t_i}{\left(12 - 11 \cdot \cos(\phi)^2\right) \cdot w_i};$$

$$keff_i := \frac{kt_i \cdot kk_i}{2 \cdot kk_i + kt_i};$$

$$keff_i := \frac{kclamp \cdot keff_i}{kclamp + keff_i \cdot \tan(\theta_i)^2};$$

$$k_i := keff_i;$$

end do:

Displacement Calculations

>

$$Fl := x \to \frac{1}{2} \frac{e^{\sqrt{C_F}\, x} P C_M \left(e^{\sqrt{C_F}\,(-L+a)} - e^{-\sqrt{C_F}\,(-L+a)}\right)}{C_F^{(3/2)} \left(-e^{-\sqrt{C_F}\, L} + e^{\sqrt{C_F}\, L}\right)}$$

$$- \frac{1}{2} \frac{e^{-\sqrt{C_F}\, x} P C_M \left(e^{\sqrt{C_F}\,(-L+a)} - e^{-\sqrt{C_F}\,(-L+a)}\right)}{C_F^{(3/2)} \left(-e^{-\sqrt{C_F}\, L} + e^{\sqrt{C_F}\, L}\right)} - \frac{P C_M (-L+a)\, x}{C_F L}:$$

$$Fr := x \to -\frac{1}{2} \frac{e^{\sqrt{C_F}\, x} e^{-\sqrt{C_F}\, L} \left(-e^{\sqrt{C_F}\, a} + e^{-\sqrt{C_F}\, a}\right) P C_M}{C_F^{(3/2)} \left(-e^{-\sqrt{C_F}\, L} + e^{\sqrt{C_F}\, L}\right)}$$

$$+ \frac{1}{2} \frac{e^{-\sqrt{C_F}\, x} e^{\sqrt{C_F}\, L} \left(-e^{\sqrt{C_F}\, a} + e^{-\sqrt{C_F}\, a}\right) P C_M}{C_F^{(3/2)} \left(-e^{-\sqrt{C_F}\, L} + e^{\sqrt{C_F}\, L}\right)} - \frac{P a\, (x - L)\, C_M}{C_F L}:$$

> $Ml := x \to P \cdot \left(1 - \frac{a}{L}\right) \cdot x: Mr := x \to P \cdot \left(1 - \frac{a}{L}\right) \cdot x - P \cdot (x - a):$

> $EqL := \Delta L(x) = int\left(int\left(\frac{Ml(x) - \frac{Fl(x)\cdot(hb + ht)}{2}}{Eb\cdot Ib + Et\cdot It}, x\right), x\right) + C_1\cdot x + C_2$:

$EqR := \Delta R(x) = int\left(int\left(\frac{Mr(x) - \frac{Fr(x)\cdot(hb + ht)}{2}}{Eb\cdot Ib + Et\cdot It}, x\right), x\right) + C_3\cdot x + C_4$:

> $bc1 := subs\left(\{\Delta L(x) = 0, x = 0\}, EqL\right)$:

$bc2 := subs\left(\{\Delta R(x) = 0, x = \mathrm{L}\}, EqR\right)$:

$bc3 := \mathrm{subs}(\mathrm{x} = \mathrm{a}, \mathrm{rhs}(\mathrm{EqL})) = subs(x = a, rhs(EqR))$:

$bc4 := \mathrm{subs}\left(\mathrm{x} = \mathrm{a}, \frac{\mathrm{d}}{\mathrm{d}\,x}\ rhs(EqL)\right) = subs\left(x = a, \frac{\mathrm{d}}{\mathrm{d}\,x}\ rhs(EqR)\right)$:

> $assign\left(solve\left(\{bc1, bc2, bc3, bc4\}, \{C_1, C_2, C_3, C_4\}\right)\right);$

Constant Terms

> $C_F := \left(\sum_{j=1}^{4} \frac{k_j}{\left(\frac{L}{2}\right)}\right)\cdot\left(\left(\frac{1}{Ab\cdot Eb} + \frac{1}{At\cdot Et}\right) + \frac{\left(\frac{ht}{2} + \frac{hb}{2}\right)^2}{Et\cdot It + Eb\cdot Ib}\right);$

$C_M := \left(\sum_{j=1}^{4} \frac{k_j}{\left(\frac{L}{2}\right)}\right)\cdot\left(\frac{\frac{ht}{2} + \frac{hb}{2}}{Et\cdot It + Eb\cdot Ib}\right);$

$$C_F := 0.0120942870$$

$$C_M := 0.00329844193$$

> $RamDefl := evalf\left(subs(x = a, rhs(EqL))\right);\ evalf\left(subs(x = a, rhs(EqR))\right);$

$$RamDefl := -0.0001236313570P$$

$$-0.0001236313569P$$

For a three-layer beam, a similar process, shown below, was used to calculate the beam stiffness.

Input Parameters

>

$L := 108$:

$a := \frac{L}{2}$:

$b := 4.5$:

$h := 2.375$:

$E := 1100000$:

$Ek := 1780000$:

$d := 1$:

$l := 2$:

$\phi := \frac{\pi}{2}$:

Geometry Calculations

> $MOI := \frac{b \cdot h^3}{12}$:

> $\theta := evalf\left(arctan\left(\frac{d}{l}\right)\right) : w := l : t := d \cdot \cos(\theta)$:

Stiffness Terms & Calculations

> $kclamp := \frac{857000000}{4}$:

>

$kt := \frac{b \cdot E}{\left(12 - 11 \cdot \cos(\theta)^2\right) \cdot 2}$:

$kk := \frac{b \cdot Ek \cdot t}{\left(12 - 11 \cdot \cos(\phi)^2\right) \cdot w}$:

$keff := \frac{kt \cdot kk}{2 \cdot kk + kt}$:

$keff2 := \frac{kclamp \cdot keff}{kclamp + keff \cdot \tan(\theta)^2}$:

$k := keff2$:

Displacement Calculations

Rather than solve the set of governing differential equations for a beam with a point load at midspan, the following equations, which were developed in Appendix B as the closed form solution for a beam with any point, were used.

$$\Delta L := x \to \frac{1}{18}\,\frac{P\,x^3}{E\,MOI} - \frac{1}{18}\,\frac{P\,x^3\,a}{E\,MOI\,L} + \frac{2}{3}\,\frac{h\,C_M\,P\cosh\left(\sqrt{C_F}\,a\right)\sinh\left(\sqrt{C_F}\,x\right)}{E\,MOI\,C_F^{(5/2)}}$$
$$- \frac{2}{3}\,\frac{h\,C_M\,P\cosh\left(\sqrt{C_F}\,L\right)\sinh\left(\sqrt{C_F}\,a\right)\sinh\left(\sqrt{C_F}\,x\right)}{E\,MOI\sinh\left(\sqrt{C_F}\,L\right)\,C_F^{(5/2)}} - \frac{1}{9}\,\frac{h\,P\,C_M\,x^3}{E\,MOI\,C_F}$$
$$+ \frac{1}{9}\,\frac{h\,P\,C_M\,x^3\,a}{E\,MOI\,C_F\,L} - \frac{1}{3}\,\frac{P\,x\,h\,C_M\,a^2}{MOI\,E\,C_F} + \frac{1}{9}\,\frac{P\,x\,h\,C_M\,a^3}{MOI\,E\,C_F\,L} + \frac{2}{9}\,\frac{P\,L\,x\,h\,a\,C_M}{MOI\,E\,C_F}$$
$$- \frac{1}{9}\,\frac{P\,L\,x\,a}{MOI\,E} + \frac{2}{3}\,\frac{P\,x\,a\,h\,C_M\cosh\left(\sqrt{C_F}\,a\right)^2}{MOI\,E\,C_F^2\,L} - \frac{2}{3}\,\frac{P\,x\,a\,h\,C_M\sinh\left(\sqrt{C_F}\,a\right)^2}{MOI\,E\,C_F^2\,L}$$
$$- \frac{1}{18}\,\frac{P\,x\,a^3}{MOI\,E\,L} - \frac{2}{3}\,\frac{P\,x\,h\,C_M\cosh\left(\sqrt{C_F}\,a\right)^2}{MOI\,E\,C_F^2} + \frac{2}{3}\,\frac{P\,x\,h\,C_M\sinh\left(\sqrt{C_F}\,a\right)^2}{MOI\,E\,C_F^2}$$
$$+ \frac{1}{6}\,\frac{P\,x\,a^2}{MOI\,E}:$$

$$\Delta R := x \to -\frac{1}{18}\,\frac{P\,x^3\,a}{E\,MOI\,L} + \frac{1}{6}\,\frac{P\,a\,x^2}{E\,MOI}$$
$$- \frac{2}{3}\,\frac{h\,C_M\,P\cosh\left(\sqrt{C_F}\,L\right)\sinh\left(\sqrt{C_F}\,a\right)\sinh\left(\sqrt{C_F}\,x\right)}{E\,MOI\sinh\left(\sqrt{C_F}\,L\right)\,C_F^{(5/2)}}$$
$$+ \frac{2}{3}\,\frac{h\,P\,C_M\sinh\left(\sqrt{C_F}\,a\right)\cosh\left(\sqrt{C_F}\,x\right)}{E\,MOI\,C_F^{(5/2)}} + \frac{1}{9}\,\frac{h\,P\,C_M\,x^3\,a}{E\,MOI\,C_F\,L} - \frac{1}{3}\,\frac{h\,P\,a\,C_M\,x^2}{E\,MOI\,C_F}$$
$$+ \frac{1}{9}\,\frac{P\,x\,h\,C_M\,a^3}{MOI\,E\,C_F\,L} + \frac{2}{9}\,\frac{P\,L\,x\,h\,a\,C_M}{MOI\,E\,C_F} - \frac{1}{9}\,\frac{P\,L\,x\,a}{MOI\,E}$$
$$+ \frac{2}{3}\,\frac{P\,x\,a\,h\,C_M\cosh\left(\sqrt{C_F}\,a\right)^2}{MOI\,E\,C_F^2\,L} - \frac{2}{3}\,\frac{P\,x\,a\,h\,C_M\sinh\left(\sqrt{C_F}\,a\right)^2}{MOI\,E\,C_F^2\,L} - \frac{1}{18}\,\frac{P\,x\,a^3}{MOI\,E\,L}$$
$$- \frac{1}{9}\,\frac{P\,h\,C_M\,a^3}{MOI\,E\,C_F} - \frac{2}{3}\,\frac{P\,a\,h\,C_M\cosh\left(\sqrt{C_F}\,a\right)^2}{MOI\,E\,C_F^2} + \frac{2}{3}\,\frac{P\,a\,h\,C_M\sinh\left(\sqrt{C_F}\,a\right)^2}{MOI\,E\,C_F^2}$$
$$+ \frac{1}{18}\,\frac{P\,a^3}{MOI\,E}:$$

Constant Terms

> $C_F := \sum_{i=1}^{8} \frac{k}{\left(\frac{L}{2}\right)} \cdot \left(\frac{9}{b \cdot h \cdot E}\right);\ C_M := \sum_{i=1}^{8} \frac{k}{\left(\frac{L}{2}\right)} \cdot \left(\frac{4}{b \cdot h^2 \cdot E}\right);$

$$C_F := 0.0191032501$$

$$C_M := 0.00357487721$$

> $\Delta L(a);\ \Delta R(a);$

$$-0.0002415638106P$$

$$-0.000241597137P$$

Appendix I – Stress Calculations

The following is Maple 11 (Maple, 2007) source code for determining the stress in the extreme fiber of a keyed beam. The inputs can be found in Table 6-1.

Input Parameters

```
>
L := 162 :
a := 63 :
bt := 7.63 :
bb := 7.59 :
ht := 7.49 :
hb := 6.63 :
Et := 1547000 :
Eb := 1561000 :
Ek := [1247000, 1180000, 1153000] :
d := [2.51, 2.47, 2.44] :
l := 8 :
ϕ := π/2 :
```

Geometry Calculations

```
> At := bt·ht; Ab := bb·hb;
```

$$At := 57.1487$$

$$Ab := 50.3217$$

```
> It := bt·ht^3/12; Ib := bb·hb^3/12;
```

$$It := 267.1706488$$

$$Ib := 184.3321612$$

```
> for i from 1 by 1 to 3 doθ_i := arctan(d_i/l); w_i := cos(θ_i)·l; t_i := cos(θ_i)·d_i; end do:
```

Stiffness Terms & Calculations

```
> kclamp := 4·16435·3.5/2 :
>
for i from 1 by 1 to 3 do
kt_i := ((bb + bt)/2)·((Et + Eb)/2) / (12 − 11·cos(θ_i)^2)·2;
kk_i := ((bb + bt)/2)·(Ek_i)·t_i / (12 − 11·cos(ϕ)^2)·w_i;
keff_i := kt_i·kk_i / 2·kk_i + kt_i;
keff_i := kclamp·keff_i / kclamp + keff_i·tan(θ_i)^2;
k_i := keff_i;
end do:
```

Force & Moment Equations

> $$F1 := x \to -\frac{1}{2}\,\frac{e^{\sqrt{Cf}\,x}\,P\,Cm\left(-e^{\sqrt{Cf}\,(-L+a)}+e^{\sqrt{Cf}\,a}-e^{-\sqrt{Cf}\,a}+e^{-\sqrt{Cf}\,(-L+a)}\right)}{Cf^{3/2}\left(-e^{-\sqrt{Cf}\,L}+e^{\sqrt{Cf}\,L}\right)} + \frac{1}{2}\,\frac{e^{-\sqrt{Cf}\,x}\,P\,Cm\left(-e^{\sqrt{Cf}\,(-L+a)}+e^{\sqrt{Cf}\,a}-e^{-\sqrt{Cf}\,a}+e^{-\sqrt{Cf}\,(-L+a)}\right)}{Cf^{3/2}\left(-e^{-\sqrt{Cf}\,L}+e^{\sqrt{Cf}\,L}\right)} + \frac{P\,Cm\,x}{Cf}:$$

> $$M1 := x \to P\cdot x:$$

Constants

> $$Cf := \left(\sum_{j=1}^{3}\frac{temp\cdot k_j}{\left(\frac{L}{2}\right)}\right)\cdot\left(\left(\frac{1}{Ab\cdot Eb}+\frac{1}{At\cdot Et}\right)+\frac{\left(\frac{ht}{2}+\frac{hb}{2}\right)^2}{Et\cdot It+Eb\cdot Ib}\right);\quad Cm := \left(\sum_{j=1}^{3}\frac{temp\cdot k_j}{\left(\frac{L}{2}\right)}\right)\cdot\left(\frac{\frac{ht}{2}+\frac{hb}{2}}{Et\cdot It+Eb\cdot Ib}\right);$$

$$Cf := 0.0006106808219\ temp$$

$$Cm := 0.00006464072481\ temp$$

> $$P := \frac{34130}{2};$$

$$P := 17065$$

Stress Calculations

> $$eq1a := \frac{\left(M1(x)-F1(\mathrm{x})\cdot\left(\frac{(ht+hb)}{2}\right)\right)\cdot Et\cdot z}{Et\cdot It+Eb\cdot Ib}-\frac{F1(\mathrm{x})}{At}:$$

The maximum stress occurs at the extreme fiber of a beam, either in the top or bottom layer of a symmetric beam. Based on the sign convention used in developing the interlayer stiffness model (see Figure 2-3), the distance to the extreme fiber on the top layer of a two ply beam is $-\frac{h_T}{2}$. As the maximum stress on the top fiber is in compression, the calculated stress is negative.

> $$evalf\left(subs\left(\left\{temp=1, x=a, z=-\frac{ht}{2}\right\}, eq1a\right)\right);$$

$$-6212.796860$$